AD-A017 458

AN INVESTIGATION OF THE STATIC THRUST AUGMENTATION CAPABILITIES OF A DIVERGENT EJECTOR-AFTERBURNER

Carl H. Steiling, Jr.

Air Force Institute of Technology
Wright-Patterson Air Force Base, Ohio

June 1975

DISTRIBUTED BY:

NTIS

National Technical Information Service
U. S. DEPARTMENT OF COMMERCE

Unclassified

SECURITY CLASSIFICATION OF THIS PAGE *(When Data Entered)*

REPORT DOCUMENTATION PAGE		READ INSTRUCTIONS BEFORE COMPLETING FORM
1. REPORT NUMBER GA/ME/75J-1	2. GOVT ACCESSION NO.	3. RECIPIENT'S CATALOG NUMBER
4. TITLE *(and Subtitle)* An Investigation of the Static Thrust Augmentation Capabilities of a Divergent Ejector-Afterburner		5. TYPE OF REPORT & PERIOD COVERED AFIT Thesis 6. PERFORMING ORG. REPORT NUMBER
7. AUTHOR(s) Carl H. Steiling, Jr. Captain USAF		8. CONTRACT OR GRANT NUMBER(s)
9. PERFORMING ORGANIZATION NAME AND ADDRESS Air Force Institute of Technology Wright-Patterson AFB, Ohio 45433		10. PROGRAM ELEMENT, PROJECT, TASK AREA & WORK UNIT NUMBERS
11. CONTROLLING OFFICE NAME AND ADDRESS		12. REPORT DATE June 1975 13. NUMBER OF PAGES 116
14. MONITORING AGENCY NAME & ADDRESS*(if different from Controlling Office)* Air Force Institute of Technology (AU) Wright-Patterson AFB, Ohio 45433		15. SECURITY CLASS. *(of this report)* 15a. DECLASSIFICATION/DOWNGRADING SCHEDULE

16. DISTRIBUTION STATEMENT *(of this Report)*

Approved for public release; distribution unlimited.

17. DISTRIBUTION STATEMENT *(of the abstract entered in Block 20, if different from Report)*

18. SUPPLEMENTARY NOTES

Approved for public release; IAW AFR/190-17

Jerry C. Hix, Capt. USAF
Director of Information

19. KEY WORDS *(Continue on reverse side if necessary and identify by block number)*

Thrust Augmentation	Static Thrust
Ejector	Rocket Thrust
Divergent Ejector	Mass Entrainment

20. ABSTRACT *(Continue on reverse side if necessary and identify by block number)*

The effects on static thrust augmentation and mass entrainment of various divergent ejector-afterburner configurations were investigated. Static tests were conducted using a gaseous oxygen/hydrogen sonic rocket as the primary gas generator. Configurations included various length mixing ducts, two different size diffusers, burn ducts, and secondary nozzles. Oxydizer-to-fuel mixture ratio was varied from .3 to 1.5 at 80 psia chamber pressure. Results indicated maximum static thrust augmentation(22%) when the

DD FORM 1 JAN 73 1473 EDITION OF 1 NOV 65 IS OBSOLETE

1a

Unclassified

SECURITY CLASSIFICATION OF THIS PAGE *(When Data Entered)*

relatively unmixed primary and secondary streams were diffused immediately after the secondary inlet and then allowed to complete mixing in a constant area duct, for a total afterburner length of about six inlet diameters. Placing the diffuser downstream of a long constant area mixing duct resulted in poor thrust augmentation due to large negative wall pressure build-ups. The diffuser increased secondary mass entrainment in all cases. The afterburning zone shifted as mixture ratio changed and its relationship to maximum thrust augmentation or mass entrainment is highly configuration dependent.

(1) 90

AN INVESTIGATION OF THE STATIC THRUST AUGMENTATION CAPABILITIES OF A DIVERGENT EJECTOR-AFTERBURNER

THESIS

GA/ME/75J-1

Carl H. Steiling, Jr.
Captain USAF

DDC
NOV
RECEIVED

Approved for public release; distribution unlimited.

GA/ME/75J-1

AN INVESTIGATION OF THE STATIC THRUST AUGMENTATION CAPABILITIES OF A DIVERGENT EJECTOR-AFTERBURNER

THESIS

Presented to the Faculty of the School of Engineering
of the Air Force Institute of Technology
Air University
in Partial Fulfillment of the
Requirements for the Degree of
Master of Science

by

Carl H. Steiling, Jr., B.S. Engr. Sci.
Captain USAF
Graduate Astronautics

June 1975

Approved for public release; distribution unlimited.

ic

Preface

This study was undertaken to explore the static thrust augmentation of the divergent ejector-afterburner. The potential advantages of this type system applied to a rocket engine or VSTOL aircraft powerplant include weight-saving, increased thrust, and fuel economy. I varied configurations of the afterburner in search of performance trends and optimum augmentation. Since there are such a large number of parameters affecting ejector operation, I attempted to keep many of these constant in order that configuration influence be emphasized. It is hoped that the results will prove useful in directing future efforts in this area, as well as laying groundwork for practical applications.

There were a number of individuals who aided me in this study and to whom I offer my sincere thanks. Dr. William C. Elrod, my advisor, provided timely support, suggestions, and guidance. Capt. Paul M. Bevilaqua of the Aerospace Research Laboratory offered constructive criticism of this manuscript and much insight into the problem. Mr. John Parks ably assisted me throughout the experimental work. Mr. M.L. Wolf and his shop personnel provided excellent workmanship in the manufacture of the apparatus. Mr. Tom Loudermilk of the Air Force Aero Propulsion Laboratory willingly helped in obtaining electronic equipment. Finally, a special thanks to my wife, Dena, for patience and encouragement throughout.

Carl H. Steiling, Jr.

Contents

	Page
Preface	ii
List of Figures	v
List of Tables	vii
List of Symbols	viii
Abstract	x
I. Introduction	1
Background	2
Problem and Scope	3
II. Description of Apparatus	5
Rocket Engine	5
Ejector-Afterburner	5
General	5
Design	6
Equipment Mounting	9
Ignition System	11
Instrumentation	11
III. Experimental Procedure	14
Phase I - Base-Line Tests	14
Phase II - Ejector-Afterburner Tests	14
Phase III - Verification and Repeatability Tests	15
IV. Results and Discussion	17
Variation of Mixing Duct Length	20
Constant Area Duct	20
Small Diffuser	20
Large Diffuser	21
Diffuser Effectiveness	22
Small Diffuser	22
Large Diffuser	23
Comparison of Large Diffuser, Small Diffuser and Dump Configurations	23
Burn Duct Effectiveness	25
Small Burn Duct	25
Large Burn Duct	26

Page

IV. Results and Discussion (contd)

Secondary Nozzle Effectiveness 26
Small Secondary Nozzle 26
Large Secondary Nozzle 29
Wall Pressure Profiles 30
General 30
Long Configuration 30
Short Configuration 33
Dump Configuration 35
Verification Testing 37

V. Conclusions and Recommendations 39

Conclusions 39
Recommendations 40

Bibliography 41

Appendix A: Ejector-Afterburner Performance Graphs . 44

Appendix B: Data Reduction 70

Appendix C: Rocket Performance 78

Appendix D: Tabulated Performance Data 87

Vita 101

List of Figures

Figure		Page
1	Schematic of Inlet and Mixing Ducts	7
2	Schematic of Diffusers, Burn Ducts, and Secondary Nozzles	8
3	Schematic Side View of Equipment Mounting . . .	10
4	Ejector-Afterburner Alignment	15
5	Duct Wall Pressure Profiles of a Long Configuration (L/D = 11.03)	31
6	Duct Wall Pressure Profiles of a Short Configuration (L/D = 5.77)	34
7	Duct Wall Pressure Profiles of a Dump Configuration	36
8	Verification of Experimental Repeatability . .	38
9	Effect of Mixing Duct Length on Constant Area Duct Performance	45
10	Effect of Mixing Duct Length on Small Diffuser Performance	46
11	Effect of Mixing Duct Length on Large Diffuser Performance	47
12	Small Diffuser Effectiveness (L_m = 23.25) . . .	48
13	Small Diffuser Effectiveness (L_m = 15.75) . . .	49
14	Small Diffuser Effectiveness (L_m = 8.25) . . .	50
15	Large Diffuser Effectiveness (L_m = 15.75) . . .	51
16	Large Diffuser Effectiveness (L_m = 8.25) . . .	52
17	Performance of Large Diffuser, Small Diffuser and Dump Configurations (L_m = 8.25)	53
18	Performance of Large Diffuser, Small Diffuser and Dump Configurations (L_m = 15.75)	54
19	Performance of Large Diffuser and Small Diffuser (L_m = 0.75)	55

Figure		Page
20	Small Burn Duct Effectiveness (L_m = 23.25) . .	56
21	Small Burn Duct Effectiveness (L_m = 15.75) . .	57
22	Small Burn Duct Effectiveness (L_m = 8.25) . . .	58
23	Small Burn Duct Effectiveness (L_m = 0.75) . . .	59
24	Large Burn Duct Effectiveness (L_m = 15.75) . .	60
25	Large Burn Duct Effectiveness (L_m = 8.25) . . .	61
26	Large Burn Duct Effectiveness (L_m = 0.75) . . .	62
27	Small Secondary Nozzle Effectiveness (L_m = 23.25)	63
28	Small Secondary Nozzle Effectiveness (L_m = 15.75)	64
29	Small Secondary Nozzle Effectiveness (L_m = 8.25)	65
30	Small Secondary Nozzle Effectiveness (L_m = 0.75)	66
31	Large Secondary Nozzle Effectiveness (L_m = 15.75)	67
32	Large Secondary Nozzle Effectiveness (L_m = 8.25)	68
33	Large Secondary Nozzle Effectiveness (L_m = 0.75)	69
34	Thrust Performance Map of Rocket Only	73
35	Theoretical and Experimental Primary Mass Flow Rates	79
36	Theoretical and Experimental Characteristic Exhaust Velocity	81
37	Theoretical and Experimental Specific Impulse .	83
38	Theoretical and Experimental Thrust Coefficient	84
39	Theoretical Chamber and Primary Nozzle Exit Temperatures	86

List of Tables

Table		Page
I	Configuration and Performance Summary	18
II	Theoretical and Experimental Performance Equations	71
III	Measurement Capability Error Summary	76
IV	Performance Data	88

List of Symbols

A	cross sectional area, sq in.
AR	mass entrainment ratio ($\dot{m}_s/\dot{m}_p$)
C_f	thrust coefficient
C^*	characteristic exhaust velocity, ft/sec
D	diameter, in. (without subscript: initial ejector-afterburner duct diameter)
F	thrust, lbf
g_c	gravitational constant, 32.2 lbm-ft/lbf-sec^2
ΔH_{ec}	enthalpy difference between rocket chamber and exit, kcal/mole
I_{sp}	specific impulse, lbf-sec/lbm
k	ratio of specific heats
L	axial length, in. (without subscript: total axial ejector-afterburner duct length)
L^*	characteristic chamber length, in.
M	Mach number
$\dot{m}$	mass flow rate, lbm/sec
$\mathcal{M}$	average molecular weight of primary exhaust gases, lbm/mole
MR	mixture ratio ($\dot{m}_{O_2}/\dot{m}_{H_2}$)
P	pressure, psia
R	gas constant for air, 53.4 ft-lbf/mole-R
$\mathcal{R}$	universal gas constant, 1545 ft-lbf/mole-R
T	temperature, R
V	velocity, ft/sec
X	axial distance from secondary inlet to pressure tap, in.

Subscripts

a	ambient
ab	ejector-afterburner
avg	arithmetic mean
b	burn duct
c	chamber
d	diffuser
e	primary nozzle exit
H_2	hydrogen (gas)
in	secondary inlet
m	mixing duct
n	secondary nozzle
O_2	oxygen (gas)
p	propellant or primary
r	rocket
s	secondary stream property at secondary inlet
5	ejector-afterburner duct exit

Greek Letter

ϕ	static thrust augmentation (F_{ab}/F_r)

Abstract

The effects on static thrust augmentation and mass entrainment of various divergent ejector-afterburner configurations were investigated. Static tests were conducted using a gaseous oxygen/hydrogen sonic rocket as the primary gas generator. Configurations included various length mixing ducts, two different size diffusers, burn ducts, and secondary nozzles. Oxydizer-to-fuel mixture ratio was varied from .3 to 1.5 at 80 psia chamber pressure. Results indicated maximum static thrust augmentation (22%) when the relatively unmixed primary and secondary streams were diffused immediately after the secondary inlet and then allowed to complete mixing in a constant area duct, for a total afterburner length of about six inlet diameters. Placing the diffuser downstream of a long constant area mixing duct resulted in poor thrust augmentation due to large negative wall pressure build-ups. The diffuser increased secondary mass entrainment in all cases. The afterburning zone shifted as mixture ratio changed and its relationship to maximum thrust augmentation or mass entrainment is highly configuration dependent.

AN INVESTIGATION OF THE STATIC THRUST AUGMENTATION CAPABILITIES OF A DIVERGENT EJECTOR-AFTERBURNER

I. Introduction

The idea of air augmentation of rocket and aircraft engines has long been of interest. The inherent nature of chemical propellants limits the specific impulse that a rocket engine can achieve. Various ducted rocket and rocket/ramjet systems have successfully demonstrated the ability of air augmentation to increase specific impulse, range, and payload capability of the basic rocket vehicle. Likewise, aircraft engine takeoff rated thrust has been augmented and deflected to such a degree as to permit vertical and short takeoffs and landings. The pumping action of the ejector seems ideally suited to both these applications.

The ejector augments thrust, particularly at static or low speeds, as a result of passing the primary jet through the ejector duct, entraining a secondary flow. This mass entrainment produces a negative differential pressure on the duct inlet lip. An application of the momentum equation to the system yields a net forward, thrust-producing force (Ref 1). Energy is exchanged between the primary exhaust jet and the secondary air flow. In the fuel-rich rocket exhaust, if the temperature is sufficiently high, a secondary heat release occurs (afterburning).

Background

Generally speaking, the level of thrust augmentation increases with the amount of secondary air entrained, if the static pressure in the mixing duct is constant (Ref 2). Thrust augmentation also increases with the level of primary and secondary stream mixing (Ref 3:481). Various studies have been undertaken at the Air Force Institute of Technology to determine the parameters effecting secondary flow entrainment and the means of increasing it.

A gaseous oxygen/hydrogen rocket was the primary gas generator for these studies. Yarborough designed the 65 lbf thrust rocket engine and realized a 27% augmentation of static thrust, using a constant area ejector-afterburner with a supersonic primary stream (Ref 4:41). Nidiffer, using a sonic primary nozzle, obtained 22% static thrust augmentation with a constant area ejector-afterburner (Ref 5:37). As a result of Yarborough's and Nidiffer's recommendations, Adam studied the influence of turbulators or mixing fingers to promote mixing in the secondary stream. He found secondary mass entrainment to increase by 44% at low mixture ratios with the correct placement of turbulators in a constant area ejector-afterburner (Ref 6:28). However, most turbulators were not able to withstand the high temperature exhaust gas environment. Markwardt, in a study of mixing characteristics in the constant area ejector-afterburner, found static thrust augmentation to be 1[illegible]%, citing changing mixing characteristics of the rocket injector to account for

this decrease from previous studies (Ref 7:31,33). Jahnke attempted unsuccessfully to utilize cooled heat flux probes in the ejector-afterburner environment to study turbulent mixing characteristics. Mechanical stresses caused failure of the sensors. In the course of his study, Jahnke found no thrust augmentation while using a constant area ejector-afterburner and a sonic primary nozzle (Ref 8:29).

Problem and Scope

Jahnke recommended the use of a divergent section in conjunction with the constant area ejector duct to augment thrust. Theoretical predictions indicate that diffusion of the mixed ejector flow can increase thrust performance by a factor of three, under ideal conditions and assuming an incompressible flow (Ref 9:349-350; Ref 10:282-285; Ref 11:244; Ref 12:9). Experimental evidence indicates the advantages of the divergent ejector-afterburner in simulated flight conditions (Ref 13:169). Also, the length, and consequent weight, of the ejector duct can be reduced due to the decreased mixing length required (Ref 14:315-316). The interaction of this diffusion process and the afterburning which occurs in the hot, fuel-rich exhaust products of the rocket engine pose a question as to how the net result will effect static thrust augmentation. Therefore, the problem was to investigate the static thrust augmentation capabilities of the divergent ejector-afterburner.

Experimental test firings were made to determine the basic rocket thrust performance and the performance of 26

different ejector-afterburner configurations. A sonic primary nozzle was installed for all tests. Rocket primary stream mixture ratios (oxygen-to-fuel mass flow ratio) were limited to the range .3 to 1.5. This range was optimum for thrust augmentation in past studies. Also, theoretical predictions indicated a transition from non-afterburning to afterburning in this range. Due to limitations of test equipment, rocket chamber pressure variations of $\pm$ 3 psi from 80 psia were accepted. The ejector-afterburner designs were compatible with the equipment used in past studies. The parameters of interest were the static thrust augmentation ratio (thrust with ejector-afterburner installed as compared to the thrust of the basic rocket) and mass entrainment ratio (ratio of secondary mass flow rate to primary or rocket exhaust mass flow rate).

The fundamental one-dimensional assumptions of an ideal rocket applied to analysis of the rocket gas generator (Ref 15:37-38). In addition, the secondary air inlet flow was assumed to be isentropic with test cell conditions being the stagnation conditions.

II. Description of Apparatus

The experimental apparatus consisted of the rocket engine, equipped with a sonic nozzle, and two complete ejector-afterburner ducts. Each duct incorporated a diffuser, mixing and burning sections, and a secondary nozzle. The investigation was conducted at the Rocket Engine Test Facility of the Department of Aero-Mechanical Engineering at the Air Force Institute of Technology. The description of the physical layout, propellant supply and control plumbing, and operating instructions is available in the Facility Operations Manual (Ref 16).

Rocket Engine

The primary stream gas generator used in this study was a gaseous oxygen/hydrogen rocket originally designed by Yarborough for a nominal thrust level of 65 lbf at 80 psia chamber pressure (Ref 4:79-97). The nozzle was a convergent type designed for this engine by Nidiffer to produce a nominal 40 lbf thrust at 80 psia chamber pressure (Ref 5:69-73). Chamber diameter was 2 in. and nozzle exit diameter was .821 in. Characteristic chamber length (L^*) for the engine, with convergent nozzle installed, was 40.8 in.

Ejector-Afterburner

General. The purpose of the diffuser was to increase the mass entrainment by lowering the mixing duct static pressure. This would result in a lowered differential

pressure across the inlet lip, producing a favorable thrust force, if negative pressures acting across the diffuser area ratio could be offset. After passing through the diffuser section, the primary and secondary streams are sufficiently mixed to where secondary heat release (afterburning) occurs. This takes place in a "burn duct" of constant area. As a result of the heat addition, the flow static pressure decreases. The secondary nozzle, placed downstream of the burn duct, converts the thermal energy to kinetic energy.

Two ejector-afterburner ducts were designed so as to incorporate the constant area mixing sections used in previous studies. The primary difference in these two ducts was the diffuser area ratio. Without flow separation, pressure recovery in the large diffuser would be superior. Figures 1 and 2 are schematics of the inlet, mixing ducts, diffusers, burn ducts and secondary nozzles used in this investigation.

Design. Appropriate design data was used to determine diffuser area ratios (Ref 17). Diffuser inlet diameter was constrained to 2.88 in., the diameter of the mixing sections that were previously built. The axial length of the diffuser was chosen so that the entire duct, with 7.5 in. mixing section installed, would have an L/D of 8 to 10. This range of L/D was found to be optimum in tests with the constant area ejector-afterburner (Ref 5; Ref 6; Ref 7). The diffusers were manufactured from cold-roll steel and were cadmium-plated for corrosion resistance.

The cross sectional area of the burn duct was determined

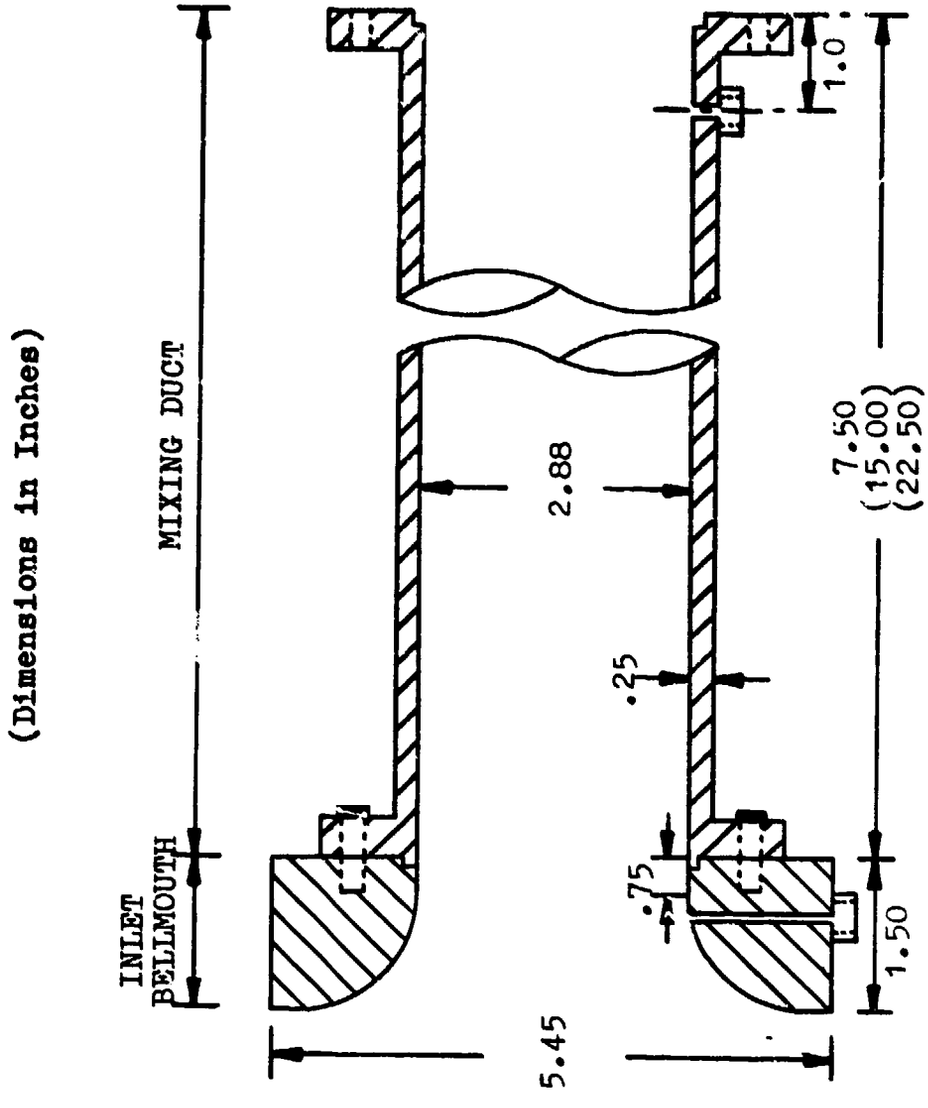

Fig. 1. Schematic of Inlet and Mixing Ducts

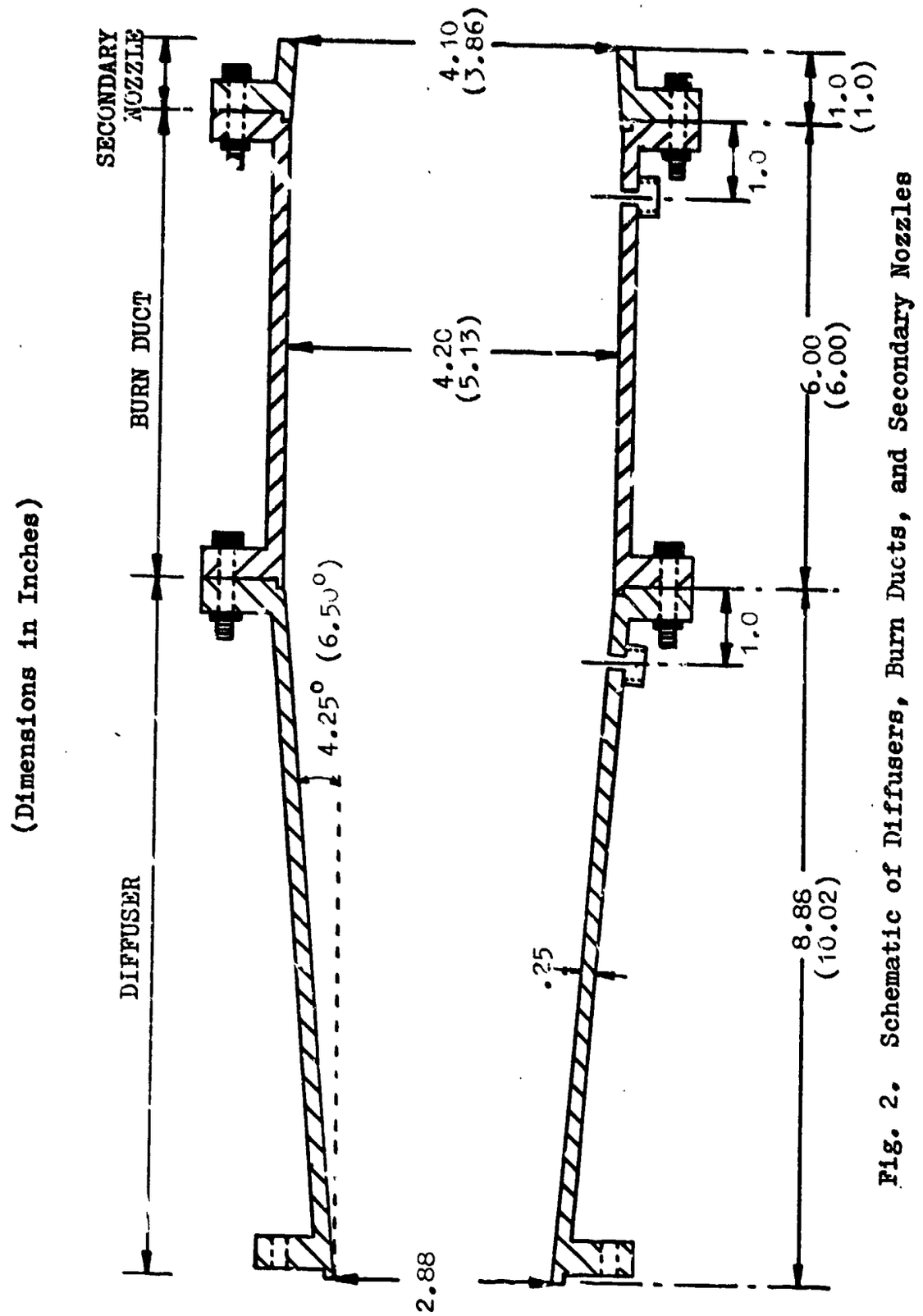

Fig. 2. Schematic of Diffusers, Burn Ducts, and Secondary Nozzles

by the respective diffuser exit area. These ducts were constant area, 6.0 in. in length, and machined from stainless steel tubing.

The secondary nozzles were designed primarily as flow regulating devices. Exit areas were determined so as to keep separation in the diffuser section to a minimum. The axial length of 1.0 in. was chosen for ease of manufacture from stainless steel.

Equipment Mounting

The rocket engine was attached horizontally to a thrust stand by means of four pendulum mounts and two engine mounts. This allowed the rocket engine assembly free movement in the axial direction. Thrust was transmitted through the engine mounts and the hollow thrust beam contact shaft to the thrust beam where two active strain gages were mounted for the reaction force measurement (Fig 3). A weight cradle was also attached by means of a cable and pulley arrangement to the thrust beam contact shaft through a hole in the thrust beam. Calibrated weights, placed in the cradle, were used for thrust calibration. A specified pre-load weight was placed in the cradle for all test firings to serve as a means of damping out rocket engine movements.

The ejector-afterburner was attached to either one or two afterburner mounts, depending on the configuration under investigation. The afterburner mounts were, in turn, attached to four steel afterburner support rods. Each afterburner support rod fit through holes drilled in each of the

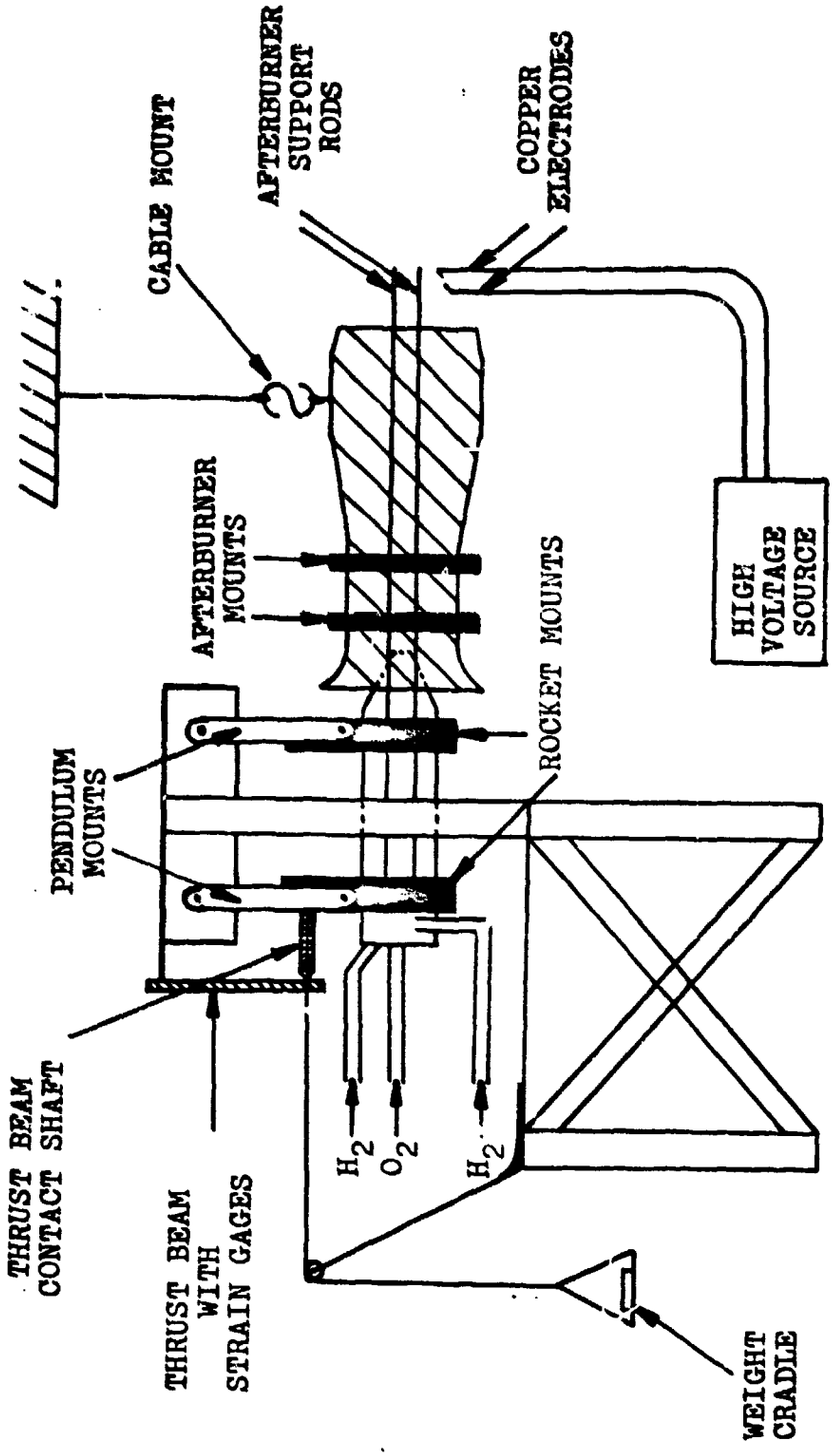

Fig. 3. Schematic Side View of Equipment Mounting

engine and afterburner mounts. Set screws in the mounts held the rods firmly in place, allowing thrust measurement to be made of the integral rocket/ejector-afterburner system. Separate set screws in the afterburner mounts were for afterburner alignment.

Due to the weight of some of the ejector-afterburner configurations examined, additional support was necessary to keep the duct aligned axially for proper thrust vector alignment. A cable mount provided this additional support. One end of the cable was attached to a beam in the ceiling of the test cell and the other end to the afterburner duct by means of an eye-bolt or safety wire, depending on the configuration. A turnbuckle in the cable allowed proper adjustment of the cable length.

Ignition System

Two copper electrodes, attached to a high voltage transformer, provided the ignition spark. The electrodes were spaced approximately ½ in. apart and placed so as to just impinge on the lower portion of the exit flow. This procedure kept electrode wear to a minimum.

Instrumentation

Data for the experimental firings was recorded on an 18-channel Consolidated Electrodynamics Corporation (CEC) recording oscillograph. Two CEC eight-channel bridge balances were used to provide excitation signal to, and condition the signal from the transducers and strain gages. Out-

put from the bridge balances was fed directly to the recorder.

Oxygen and hydrogen mass flow rates were determined by means of a Herschel venturi and thermocouple installed in each supply line. Upstream pressure and pressure drop across the venturi throat were measured by pressure transducers. These transducers were calibrated in place by measuring trace deflections on the recorder and comparing these to a precision calibrated gage reading (Ref 16:32,37). The thermocouple circuits were calibrated by placing the sensing element in a heated water bath and measuring several temperatures and correlating this with the deflection produced on the recorder. A reference cold junction standard of 32 F was used for calibration and all experimental work.

Chamber pressure was measured with a pressure transducer connected to a tap in the chamber wall located immediately prior to the nozzle section. This transducer was calibrated in place using a precision calibrated gage as the reference. The tubing used to connect the transducer to the pressure tap was disconnected after each series of runs. This permitted water, produced in the chamber reaction, to drain - thus eliminating line blockage due to the water freezing at the low ambient temperatures encountered.

Differential wall pressure readings were made at four positions along the ejector-afterburner duct. Differential pressure was transmitted through 1/8 in. tubing to the low side of four differential pressure transducers, the high

side being open to atmospheric pressure. The transducers were calibrated in place with the aid of a mercury manometer (Ref 18:481-486). All pressure transducers were mounted on a board remote from the engine test stand to eliminate the possibility of vibration causing erroneous indications.

Thrust was measured by two strain gages balanced on either side of a constant stress, cantilever-mounted, aluminum beam. Because of the importance of thrust measurement to this study, the strain gages were re-calibrated each day test firings were made and when each new ejector-afterburner configuration was installed. Calibration consisted of placing known weights in the weight cradle and measuring the trace deflection this produced on the recorder (reference Appendix B for comments relative to thrust measurement error).

III. Experimental Procedure

The experimental program consisted of 215 successful test firings. It was divided into three phases: base-line tests with the rocket only, tests with the ejector-afterburner installed, and verification and repeatability tests.

Phase I - Base-Line Tests

The purpose of this phase was to obtain data on the rocket engine without the ejector-afterburner installed. Results were compared with computer predicted ideal performance. The thrust data was used as the standard of comparison in the computation of the static thrust augmentation. The control loader settings, required to obtain values of mixture ratio and chamber pressure in the desired ranges, were also obtained. A total of 22 acceptable base-line test firings of the rocket engine only were made.

Phase II - Ejector-Afterburner Tests

The main focus of this phase was to vary ejector-afterburner configurations in an attempt to find the configuration that would produce the highest average thrust augmentation. It was decided to make a minimum of six test firings with each configuration in the range of mixture ratios under consideration (.3 to 1.5). During this phase, a total of 26 ejector-afterburner configurations were examined.

In order that all tests could be comparable on a common ground, it was necessary to establish alignment dimensions

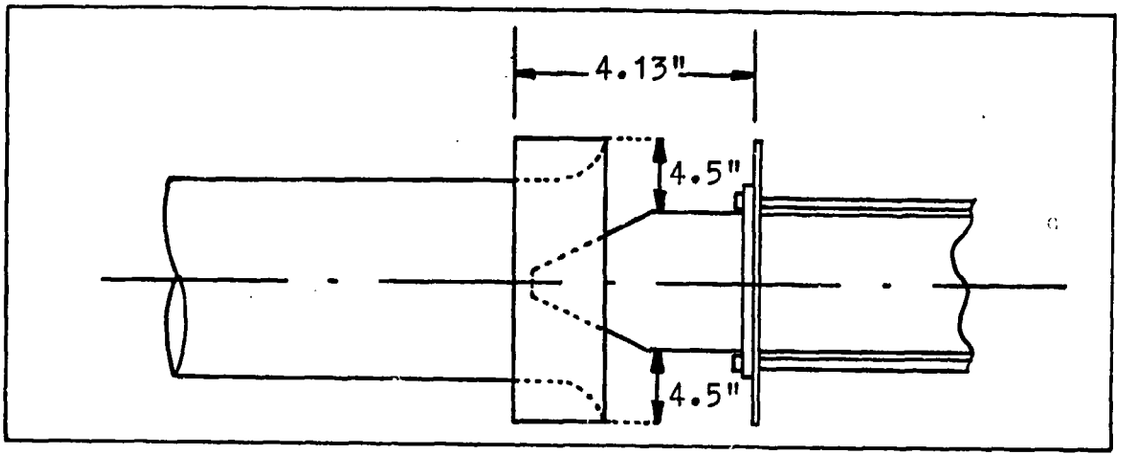

Fig. 4. Ejector-Afterburner Alignment

between the primary rocket and the bellmouth inlet of the ejector-afterburner. Figure 4 depicts the axial and radial alignment that was used on each of the 26 configurations. Therefore, secondary flow entrance area was kept at a constant value of 5.47 sq in. Periodically, throughout each test series, checks were made to insure proper afterburner alignment and level positioning.

Concurrently with this phase, plots were made of the static thrust augmentation ratio and mass entrainment ratio versus mixture ratio for each configuration. This procedure pointed up trends and enabled decisions to be made as to the best configurations to be tested.

Phase III - Verification and Repeatability Tests

To verify the accuracy and repeatability of the test procedures, it was decided to re-test the ejector-afterburner configuration which had displayed the most promising average thrust augmentation over the mixture ratio range

considered. A series of 14 acceptable tests were conducted on configuration 15. This test series was conducted 34 days after the initial tests on the configuration. In the intervening period, 11 other configurations had been tested. It was felt that this verification test would lend credibility to the test results obtained earlier.

IV. Results and Discussion

Results are presented by graphically comparing ejector-afterburner configurations in performance curves of static thrust augmentation (ϕ) and mass entrainment ratio (AR) over the mixture ratio range considered. These graphs may be found in Appendix A. The plots are meant to convey trends and lines between actual data points are not indicative of data that could be obtained in these areas, but they are included merely as an aid to distinguish the data of different configurations. The reader is cautioned to consider ordinate scale variations in comparing actual magnitudes of values from one graph to another. Data from which graphs were plotted is tabulated in Appendix D.

A summary of the configurations tested is contained in Table I. This table displays the dimensions of each of the configurations. Values of ϕ_{avg} and AR_{avg} are the arithmetic mean values of all test runs made on a given configuration. Classical ejector geometry parameters of secondary-to-primary flow exit area ratio (A_5/A_e) and length-to-diameter ratio (L/D) of the duct are also given. These parameters are important in weight and scaling considerations. Both the primary flow exit area (A_e) and secondary inlet diameter (D) were constant in this investigation.

The method of data reduction and a measurement error analysis may be found in Appendix B. The basic rocket performance is detailed in Appendix C.

Table I
Configuration and Performance Summary

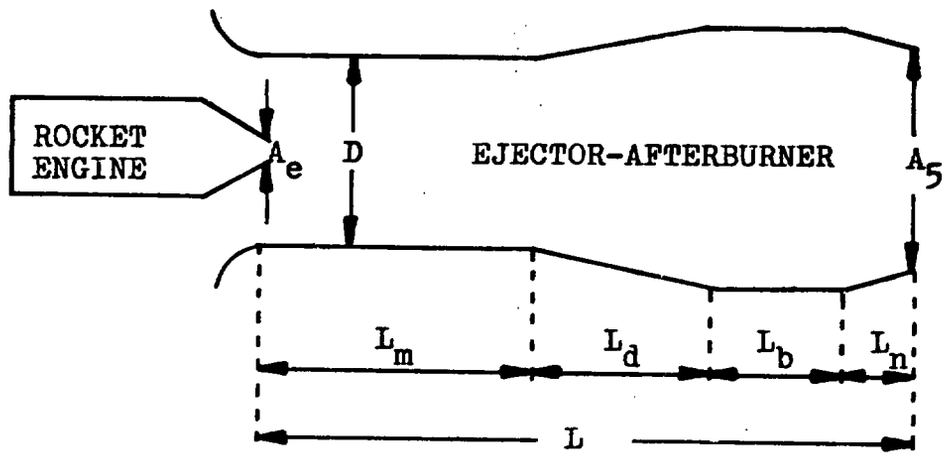

Configuration (runs)	Dimensions (inches)				L/D	A_5/A_e	AR_{avg}	ϕ_{avg}
	L_m	L_d	L_b	L_n				
1 (6)	23.25	0.00	0.00	0.00	8.07	12.31	4.01	1.10
2 (6)	23.25	8.88	0.00	0.00	11.16	26.19	6.02	1.02
3 (8)	23.25	8.88	6.00	0.00	13.24	26.19	6.09	0.91
4 (7)	23.25	8.88	6.00	1.00	13.59	24.95	6.27	0.88
5 (7)	8.25	0.00	0.00	0.00	2.86	12.31	2.84	1.03
6 (7)	8.25	8.88	0.00	0.00	5.95	26.19	4.20	1.04
7 (7)	8.25	8.88	6.00	0.00	8.03	26.19	4.34	0.96
8 (6)	8.25	8.88	6.00	1.00	8.38	24.95	4.58	0.99

- Table Continued Next Page -

Configuration (runs)	Dimensions (inches)				L/D	A_5/A_e	AR_{avg}	Φ_{avg}
	L_m	L_d	L_b	L_n				
9 (7)	8.25	10.02	0.00	0.00	6.34	39.56	3.71	0.94
10 (7)	8.25	10.02	6.00	0.00	8.43	39.56	4.30	0.86
11 (7)	8.25	10.02	6.00	1.00	8.77	22.11	3.99	0.87
12 (7)	8.25	0.00	6.00	0.00	4.95	26.19	3.37	0.94
13 (7)	0.75	8.88	0.00	0.00	3.34	26.19	2.92	1.04
14 (7)	0.75	8.88	6.00	0.00	5.43	26.19	4.17	1.05
15 (7)	0.75	8.88	6.00	1.00	5.77	24.95	4.48	1.13
15 (14)	0.75	8.88	6.00	1.00	5.77	24.95	4.00	1.11
16 (7)	0.75	10.02	0.00	0.00	3.74	39.56	3.15	0.99
17 (6)	0.75	10.02	6.00	0.00	5.82	39.56	4.33	1.03
18 (7)	0.75	10.02	6.00	1.00	6.17	24.95	3.81	0.95
19 (6)	15.75	0.00	0.00	0.00	5.47	12.31	4.09	1.10
20 (7)	15.75	8.88	0.00	0.00	8.55	26.19	5.21	0.96
21 (7)	15.75	8.88	6.00	0.00	10.64	26.19	5.71	0.93
22 (8)	15.75	8.88	6.00	1.00	10.98	24.95	6.14	0.93
23 (7)	15.75	10.02	0.00	0.00	8.95	39.56	4.84	0.88
24 (7)	15.75	10.02	6.00	0.00	11.05	39.56	5.56	0.79
25 (7)	15.75	10.02	6.00	1.00	11.38	24.95	5.25	0.92
26 (7)	15.75	0.00	6.00	0.00	7.55	26.19	4.37	0.93

Variation of Mixing Duct Length

Constant Area Duct. Figure 9 depicts a comparison of ϕ and AR for ejector-afterburner configurations 1, 5, and 19. These three configurations are constant area ducts. As L/D increases from 2.86 in configuration 5 to 5.47 in configuration 19, ϕ_{avg} and AR_{avg} tend to increase. However, it is significant to note that there is no appreciable difference in performance between configurations 19 and 1 (L/D = 8.07). This would seem to indicate that a large part of the mixing is complete in about six duct diameters. This agrees favorably with experiments conducted by the Martin Company on the Rocket Engine Nozzle Ejector (RENE) system. It was found that the single rocket RENE configuration required an L/D of about five to achieve adequate mixing (Ref 19:I-5). Jahnke's results, using the same configurations, were similar (Ref 8: 28).

Small Diffuser. The effects of diffusing the ejector-afterburner flow with the small diffuser, while varying L_m, is illustrated in Fig 10. Configuration 13 indicates the effect of immediate diffusion after the secondary inlet. Values of AR_{avg} are now clearly increasing in magnitude with increasing L/D. Increased L_m, and the corresponding decreased wall pressures, obviously aid mixing and mass entrainment with the small diffuser installed. There is no clear optimum L/D for mass entrainment, as average values increase in the range up to L/D = 11.16.

When the small diffuser is added, there is no longer a

static thrust augmentation advantage to the longer mixing duct. In fact, configuration 13 (L/D = 3.34) performs better than configuration 20 (L/D = 11.16) over the mixture ratio range studied. This would indicate a significant weight saving for better performance. An explanation of this trend lies in the comparative magnitudes of the wall pressures along the duct. Adding a diffuser onto a long mixing duct allows large negative wall pressures to act across the diffuser section, decreasing the forward thrust component. However, diffusion of the flow after a short mixing duct, has the advantage of increasing the secondary mass flow rate, but avoiding a large negative wall pressure build-up in the mixing duct. The smaller negative pressure-area force increment in the diffuser is not as detrimental to thrust.

Large Diffuser. Figure 11 shows the effects of diffusing the flow from different length mixing ducts through the large diffuser. By way of reference, diffusion occurred in configuration 16 immediately downstream of the inlet.

As was seen with the small diffuser attached, AR_{avg} tends to increase with L/D. Conversely, values of ϕ_{avg} decrease with increasing L/D. Again, the short configuration 16 (L/D = 3.74) exhibits superior static thrust augmentation to configurations 9 (L/D = 5.34) and 23 (L/D = 8.95). With the large diffuser, ϕ dependence on L/D is more pronounced than with the small diffuser. Since wall pressure magnitudes are roughly equivalent to those of the small dif-

fuser configurations, the same or similar negative pressures, acting over the larger area of the large diffuser, produce a larger decrement in thrust.

Diffuser Effectiveness

Small Diffuser. Figures 12, 13, and 14 depict the performance effects of adding the small diffuser to the constant area mixing duct. In each case, AR_{avg} was significantly increased over the constant area configuration. The improved pumping characteristics of an ejector with terminating diffuser is well established (Ref 20:13). Adding a diffuser resulted in a decrease of ϕ_{avg} in all configurations except the shortest (Fig 14); in this case, it was approximately equal.

Pressure profiles graphically illustrate the effects of adding a diffuser to the mixing duct (Fig 5). In order that the static pressure in the duct may be equal to atmospheric at the exit, and considering the rise it undergoes in the diffuser, the flow in the mixing duct readjusts itself to accomodate a lower static pressure. This lowers the inlet lip static pressure and increases mass entrainment. However, this same effect which aids mass entrainment is deleterious to static thrust augmentation. Since there is no total pressure build-up at the inlet due to the static test conditions, secondary stream static pressure is limited to a negative increment from the surrounding atmospheric pressure (again, assuming the test cell conditions as total conditions and isentropic flow in the bellmouth). While this

negative pressure, acting over the inlet lip produces a forward force, the larger negative static pressures downstream of the inlet, acting over the diffuser area, cancel this out and can, in some cases, produce a negative static thrust augmentation ($\phi < 1.00$).

Large Diffuser. Figures 15 and 16 show the effects of the addition of the large diffuser to the constant area mixing duct. In all configurations AR_{avg} increased, as evidenced with the small diffuser. ϕ_{avg} decreases - also not unexpected in light of results obtained for the small diffuser. All comments regarding these trends that were made for the small diffuser, apply to the large diffuser.

Comparison of Large Diffuser, Small Diffuser and Dump Configurations. Figures 17 and 18 compare performance of the large and small diffusers and the dump configuration for two values of L_m. The dump configurations (12 and 26) have the same area ratio as the small diffuser, but the area increase is sudden (corresponding to a diffuser divergence angle of 90 degrees).

Since magnitudes of AR_{avg} are seen to decrease in going from the small to the large diffuser, flow separation appears to occur in the large diffuser. Some separation was predicted at this divergence angle (6.5 degrees) (Ref 17). For the longer L_m of Fig 18, AR_{avg} for the large and small diffusers approach each other. This indicates less separation occuring as the mixing duct length increases and the average flow velocity decreases. The dump configurations

appear to offer no advantages for mass entrainment, as they have the lowest AR_{avg}.

The largest ϕ_{avg} occurred with the small diffuser over the mixture ratio range studied. The magnitudes of the wall pressures were equivalent for the same mixing duct length, whether the small or large diffuser was installed. It could be said that the negative differential pressure, acting over the larger area of the large diffuser, was detrimental to thrust augmentation. However, this must also be tempered with the fact that the increased mass entrainment of the small diffuser aided its thrust performance also.

The dump configurations, which were intended to stabilize the afterburning through interaction with vortices generated at the area step, showed thrust augmentation only in the lower mixture ratio range. Pressure profiles (Fig 7) indicate no burning occurring in the duct for these mixture ratios. This is likely due to the lowered primary exit temperatures caused by the large excess of fuel. This temperature was apparently too low to support afterburning in this duct. However, as the mixture ratio increased, primary exit temperatures increased and afterburning occurred. As a result, the duct wall pressures lowered and performance dropped off significantly.

Figure 19 compares large and small diffusers placed immediately after the inlet. AR_{avg} is now slightly greater for the large diffuser. Separation could be occurring in both diffusers due to the high average flow velocity in this

area. ϕ is appreciably effected by wall pressure-area forces. The average wall pressures are approximately the same in both cases, but, since they act on a larger area in the large diffuser, the resultant negative force is greater. This decreased the net thrust by a larger increment.

Burn Duct Effectiveness

Small Burn Duct. Figures 20 through 23 depict performance curves of the basic mixing duct with small diffuser attached, compared to configurations with the basic mixing duct, small diffuser, and small burn duct attached. Each of these figures represents a different L_m.

The most pronounced increase in AR_{avg} occurred at the shortest overall L/D - configurations 13 and 14 (Fig 23). This was possibly due to the fact that mixing had the greatest margin for improvement, going from an L/D of 3.34 (configuration 13) to an L/D of 5.43 (configuration 14). Simonson and Schmeer pointed out this need for ample mixing duct length in their investigation of static thrust augmentation (Ref 21:7). An equivalent change in L/D of the constant area mixing ducts of configurations 5 and 19 showed a similar increase in Fig 9. Increases in AR_{avg} are evident at longer L/D, but to a lesser degree. ϕ_{avg} tends to decrease more at long L/D (Fig 20) and remains about equal at shortest L/D (Fig 23).

When the burn duct was added, the magnitudes of the negative wall pressures also increased. Generally speaking,

this increase was greater the longer the mixing duct was. Citing previous discussions of negative wall pressures acting over the diffuser area should suffice as explanation of the trends in AR and ϕ just noted. Again, it is significant to note that these greater negative duct pressures did not have as large an effect on the ϕ of the configuration with the shortest overall length. Even though wall pressures did increase negatively by adding the burn duct to configuration 13, magnitudes were still small and increased mass entrainment was more significant.

Large Burn Duct. The effect of adding the large burn duct to the large diffuser is illustrated in the performance curves of Figs 24, 25, and 26. In all cases, AR_{avg} increased. ϕ_{avg} decreased in all but the shortest L/D configuration (Fig 26). As in the previous discussion, the additional length of the burn duct is most influential in the shortest configuration.

There appears to be a trend in Figs 24 and 25 that indicates better thrust performance at the lower mixture ratios. It is theorized that the afterburning combustion zone influences this to a great extent. The heat release effects static pressures upstream and downstream in the subsonic flow. Overall duct length and diffuser location determine how the wall pressures will influence thrust.

Secondary Nozzle Effectiveness

Small Secondary Nozzle. Figures 27 through 30 are per-

formance curves showing the effect of adding the small secondary nozzle to the small burn duct. Each figure is for a different L_m, and consequently, a different L/D.

The small secondary nozzle enhanced AR_{avg} in each case. ϕ_{avg}, which varied inversely with L/D, increased by 8% at lowest L/D (L/D = 5.77 for configuration 15) and decreased by 3% at the longest L/D (L/D = 13.59 for configuration 4).

Average wall pressures in the duct dropped slightly more negative for all configurations when the small secondary nozzle was installed. The results listed above follow the trends already noted. The larger negative wall pressure-area forces subtracted a larger increment from thrust when they acted over the diffuser, except in the shortest configuration.

Configuration 15 yielded the best ϕ_{avg} for a series of runs (1.13), as well as the highest ϕ of an individual test firing (1.22) of any configuration tested. Although its AR_{avg} was mediocre when compared to the longer configurations, it obviously combined the largest AR for the least negative wall pressures to produce this performance. Placing the diffuser immediately downstream of the inlet and diffusing the largely unmixed primary and secondary streams prevented the large build-up of negative wall pressures from acting over the diffuser area, as occurred in other configurations with longer mixing ducts. The addition of a burn duct and secondary nozzle was advantageous in that the streams had more opportunity to mix after being dif-

fused. Also, the ϕ of this short configuration is enhanced by a small positive increment in AR.

At some mixture ratios (notably in the medium range) wall pressure across the diffuser actually decreased (Fig 6), indicating an acceleration of the flow. This could have possibly been due to the turbulence generated in flow separation or to the diffuser section acting as an air-augmented primary nozzle divergent section, accelerating the flow to supersonic velocity (a further treatment of the air-augmented bypass nozzle is given in Ref 22). If separation occurred, it could not be determined, due to pressure tap location, whether the flow had remained attached at another position, creating an unsymmetric condition. Figure 30 shows that, at the mixture ratios in question, thrust performance was degraded considerably due to the larger negative wall pressures acting over the diffuser.

Configuration 4 had the largest AR_{avg} (6.27) over the mixture ratio range of any configuration studied. Configuration 22 exhibited the largest single AR (7.22) of any test firing. Both of these configurations were in the higher portion of the L/D range studied: configuration 4 had an L/D of 13.59 (longest of all configurations) and configuration 22 had an L/D of 10.98. The larger negative static pressures generated in these long mixing duct configurations and the more complete mixing of primary and secondary streams aided the mass entrainment. Unfortunately, as mentioned earlier, large negative wall pressures across the

diffuser definitely hindered the static thrust augmentation of these configurations.

Large Secondary Nozzle. The effects of adding the large secondary nozzle to the large burn duct are depicted in Figs 31, 32, and 33. L_m varies from figure to figure.

AR_{avg} decreased in all cases when the nozzle was added. ϕ_{avg} increased, except in the shortest configuration (18), where it decreased sharply. These seemingly opposite trends to the previous discussions are due to the flow regulation of the large secondary nozzle.

The configurations with the large nozzle installed were the only ones to exhibit a substantial positive increment of wall pressure at the last pressure tap in the duct. This would indicate a decrease in the average velocity at this point caused by the flow constriction of the secondary nozzle. It must be kept in mind that, even though operation was with the large secondary nozzle, the actual exit area was smaller than the secondary nozzle used with the small diffuser (see Fig 2).

This flow regulation had an effect on all duct wall pressures upstream of the diffuser exit. The pressures in this area were reduced in magnitude from 30% to 60%. Considering this, trends previously pointed out are brought into perspective: less negative duct wall pressure acting over the diffuser increased ϕ and the lowered magnitudes of mixing duct pressures decreased AR. Again, the ϕ of the shortest configuration behaved just the opposite. Whereas

negative wall pressure-area forces were less, the lower mass entrainment of this configuration influenced the direction ϕ took to a greater extent. Flow separation in the diffuser of the shortest configuration could have resulted in the thrust augmentation following the same pattern as the constant area duct where lip thrust is most important.

Wall Pressure Profiles

General. Pressure profiles of the wall pressure along the ejector-afterburner duct were plotted for each configuration. Pressure profiles from a configuration with large L/D (24), a configuration with short L/D (15), and a dump configuration (26) are presented (Figs 5-7). These are representative of all configurations. The distance of a particular pressure tap along the duct is normalized by the total axial duct length.

Long Configuration. The pressure profiles illustrated in Fig 5 were typical of long configurations. It is observed that pressure recovery in the diffuser (X/L = 0.43 to 0.78) is greater at lower mixture ratios. Also, the magnitudes of wall pressures vary as the mixture ratio changes. To explain these trends it is necessary to understand the changing flow conditions in the ejector-afterburner duct, as the primary flow mixture ratio changes.

One can consider three interdependent variables that are affected by increasing mixture ratio: exhaust gas temperature, ignition delay time, and turbulent velocity gradients. Primary stream exhaust gas temperature and velocity

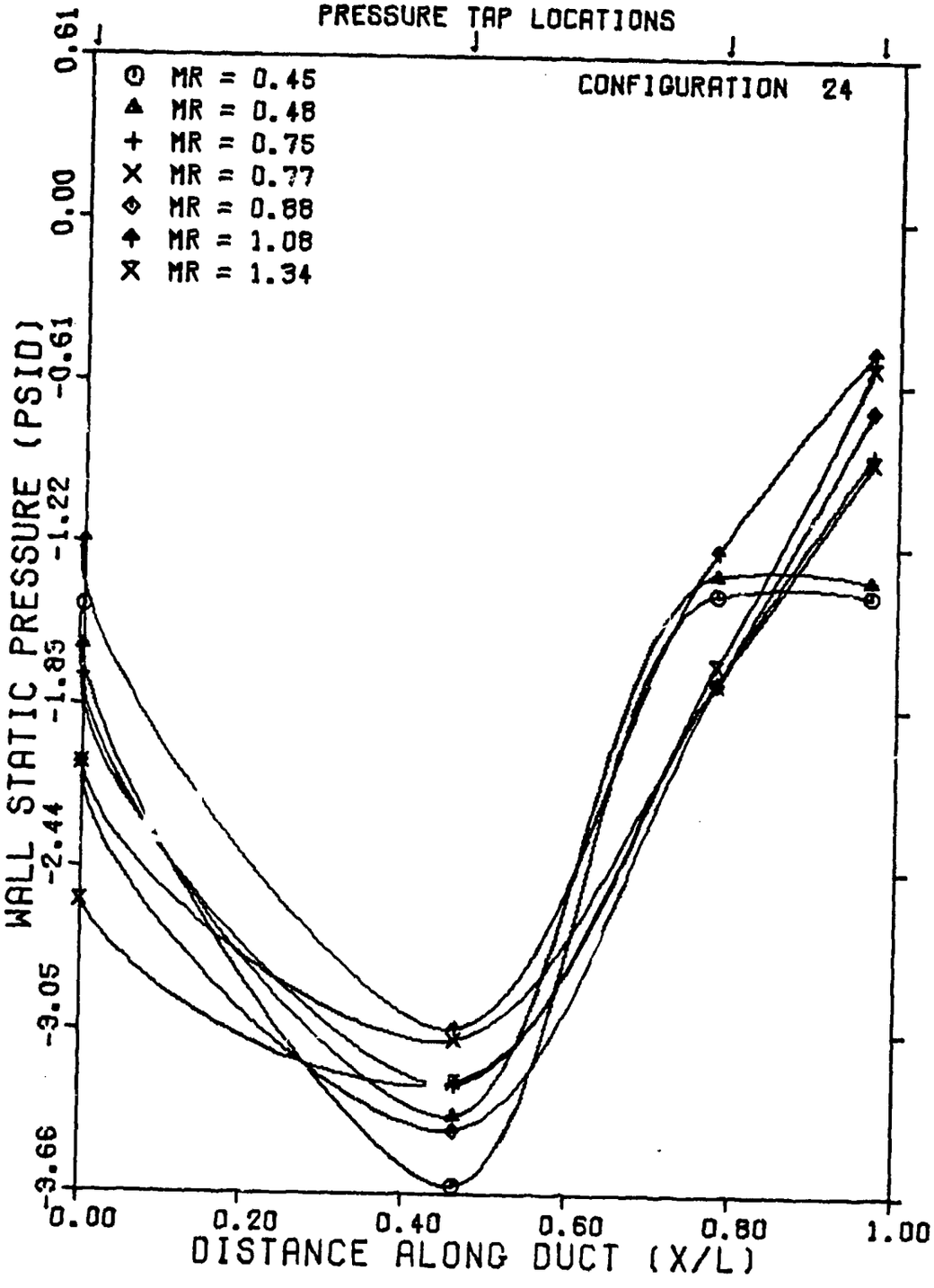

Fig. 5. Duct Wall Pressure Profiles of a Long Configuration (L/D = 11.03)

increase with mixture ratio (Fig 39). At elevated temperatures, the ignition delay time of hydrogen in air decreases (Ref 13:22-24; Ref 23; Ref 24:25-26). At higher primary stream velocities, larger shear forces exist between the primary and secondary streams, generating greater turbulence (Ref 25:1, 5-6).

The decrease in diffuser pressure recovery at higher mixture ratios can now be accounted for. Higher primary stream velocities, and the corresponding increase in average flow velocity causes some flow separation in the diffuser at higher mixture ratios. The increased turbulence generated in the mixing process may also contribute to upsetting the flow and causing separation.

The changing magnitudes of wall pressures in the duct are likely due to a variation of the afterburning combustion zone, as well as the aforementioned flow separation. As ignition delay time decreased, and turbulence and velocity increased, the combustion region probably transitioned upstream. It was observed experimentally that oscillations in the secondary inlet differential pressure occurred as mixture ratio increased (above approximately .55). It is not certain that these disturbances were generated by the combustion zone as it approached the inlet. The disturbances may be present at all mixture ratios and coupled with the flow to produce dynamic effects only as mixture ratio was increased (above the .55 value). At any rate, oscillations in the duct wall pressure readings probably do indi-

cate some relocation of the combustion zone as mixture ratio changes, causing the wall pressure magnitudes to vary.

Short Configuration. Figure 6 depicts pressure profiles, at varying mixture ratios, for configuration 15. These profiles are typical for the short configurations studied.

At lower mixture ratios (at or below .62 in the figure) wall static pressure rise through the diffuser (X/L = 0.0 to 0.5) was normal. Also, at these mixture ratios, pressure disturbances were observed at the secondary inlet, indicating duct afterburning. Because of the shorter L/D of these configurations, it is difficult to say exactly where in the duct burning was occurring, or if it was occurring after the hot gases had exited the duct.

Increasing the mixture ratio above .62 lead to a wall static pressure decrease across the diffuser. As discussed earlier, it is not clear whether this was caused by flow separation or the diffuser acting as an air-augmented primary nozzle divergent section, accelerating the flow to supersonic velocity. In the test firings in this mixture ratio range with the short configurations, the secondary inlet pressure remained comparatively steady, contrary to indications obtained with longer configurations at the same mixture ratios. If this was indication of no burning in the duct, ther it would appear that afterburning was beneficial in keeping the flow attached in the diffuser. On the other hand, if the flow had accelerated to supersonic velocity

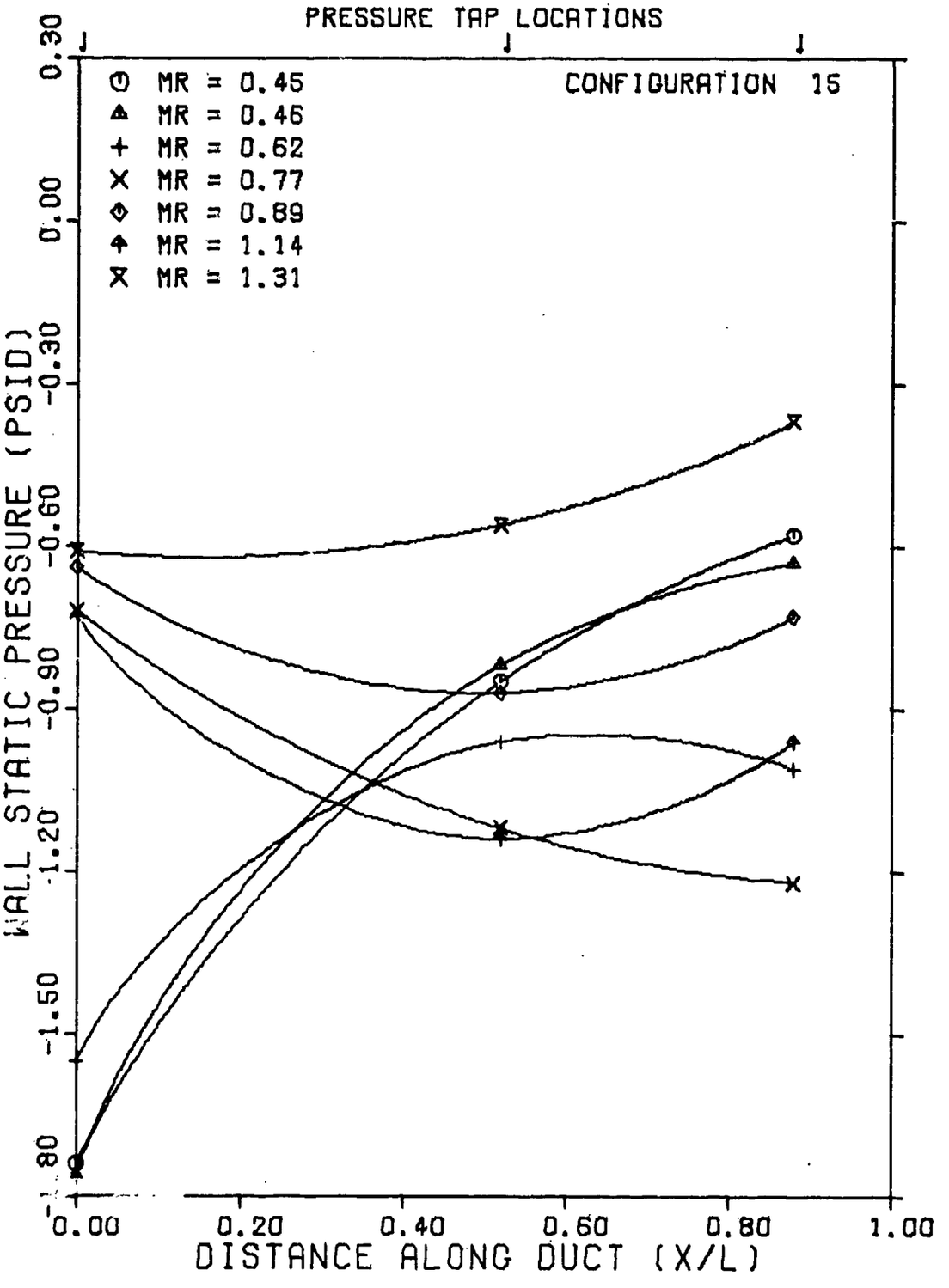

Fig. 6. Duct Wall Pressure Profiles of a Short Configuration (L/D = 5.77)

through an air-augmented divergent section, pressure disturbances from the afterburning zone further downstream in the duct would not have been sensed at the inlet. Performance curves for these configurations show significant degradation of thrust augmentation and mass entrainment in this mixture ratio range.

Dump Configuration. As Fig 7 shows, at low mixture ratios (at or below .48) there was an increase of wall static pressure in the mixing duct. This behavior, seen only at low mixture ratios with the dump configurations installed, indicates a very stable mode of operation, probably without afterburning. All oscillations of differential pressure readings along the duct were at a minimum. Static thrust augmentation was enhanced by the wall pressure being closer to atmospheric.

It is believed that the vortices generated at the area step, at low mixture ratios, were large enough to inhibit the flow along the walls in the mixing duct. This effect may have taken the form of a rapidly increasing boundary layer width. As mixture ratio increased and the afterburning flame interacted with the vortices, they were suppressed in magnitude and pressure profiles took the forms consistent with configurations with the diffuser installed. As mentioned in the previous discussion, the onset of afterburning tended to aid in flow attachment, and produced corresponding lower wall static pressures and lower thrust augmentation.

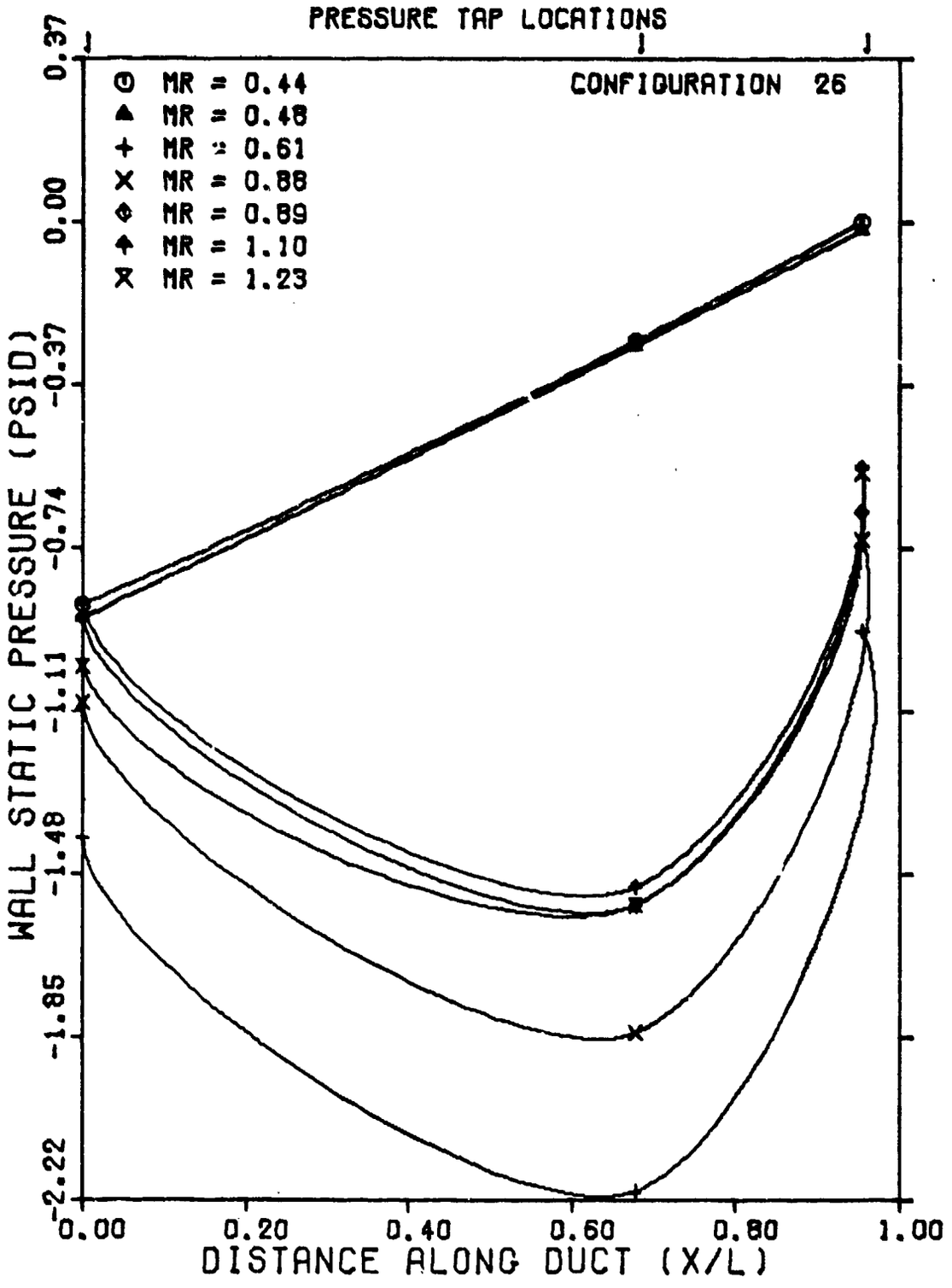

Fig. 7. Duct Wall Pressure Profiles of a Dump Configuration

Verification Testing

Figure 8 depicts a comparison of the performance between the original test series run on configuration 15 and the verification tests run on the same configuration. The verification tests were performed after configuration 15 was reassembled, over one month after the original tests. Eleven other configurations were tested during this period.

The repeatability of the experiment is evidenced by the general agreement between data obtained on these two test series. ϕ_{avg} deviation is within the measurement capability accuracy of ϕ (Table III). Values of AR_{avg} obtained from the two test series differed by .48. This is twice the predicted average error in AR due to measurement capability (Table III). The additional error was introduced in the instrumentation. Most of the error in AR seen at lower mixture ratios, vanishes above about MR = .9.

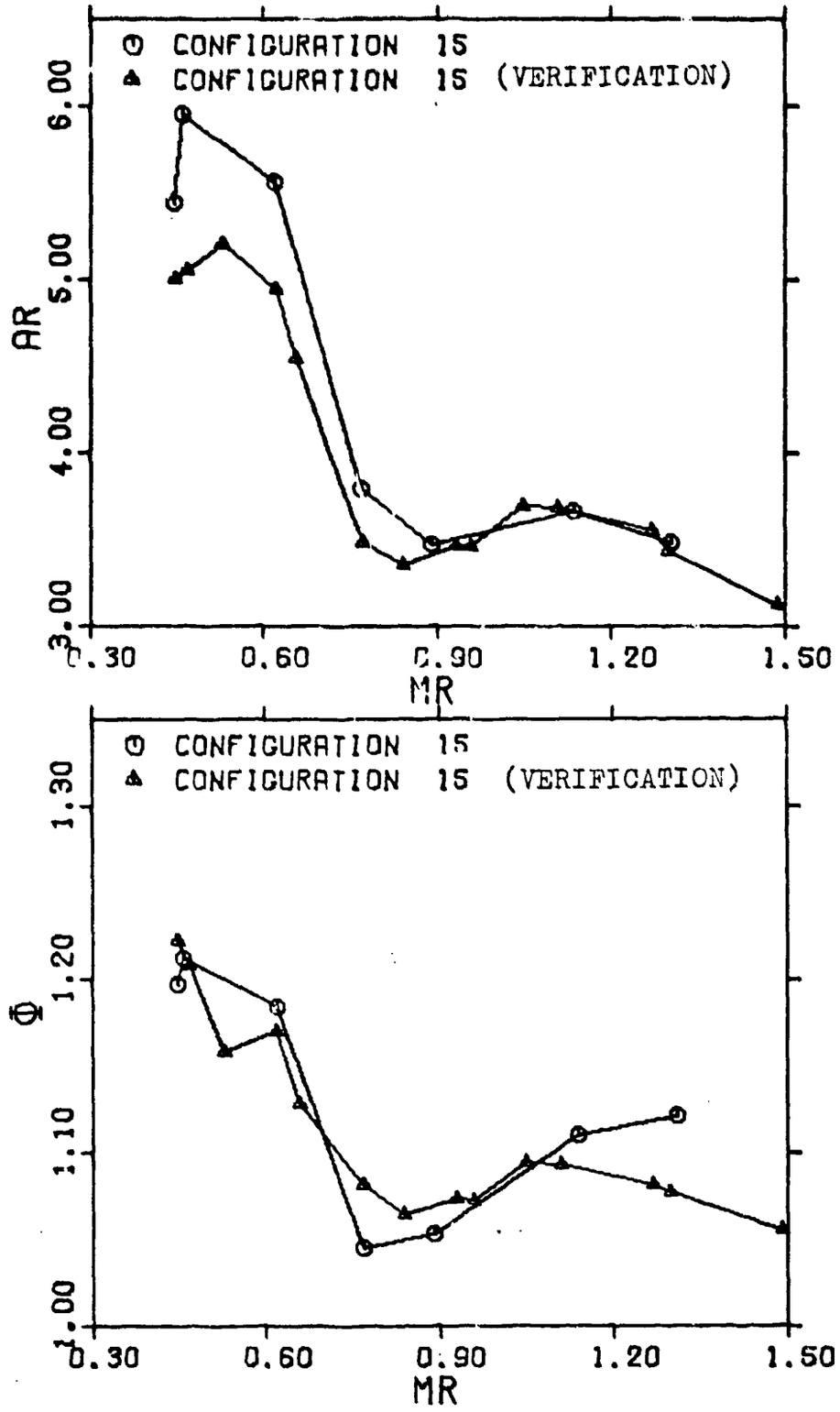

Fig. 8. Verification of Experimental Repeatability

V. Conclusions and Recommendations

Conclusions

An investigation to determine the static thrust augmentation capabilities of various divergent ejector-afterburner configurations resulted in these conclusions:

1. Static thrust is augmented to the greatest degree if the largely unmixed primary and secondary streams are diffused immediately after the secondary inlet and then allowed to mix in a constant area duct. This permits increased mass entrainment, and the corresponding increased lip thrust, without a large negative wall pressure build-up prior to the diffuser and static thrust increases with mass entrainment. Conversely, if the flow is diffused after passing through a long mixing duct, static thrust is decreased. This is due to the negative wall pressures, built up in the mixing duct, acting over the diffuser area and static thrust generally decreases with increased mass entrainment.

2. The relationship between maximum static thrust augmentation or maximum mass entrainment and the afterburning zone is highly configuration dependent.

3. In all cases, the secondary mass entrainment of a constant area duct is increased by adding a terminating diffuser.

4. For the configurations studied, the mixing of the primary and secondary streams progressed most rapidly in the first six duct diameters. At shorter lengths, mass entrain-

ment was particularly sensitive to L/D ratio; at greater lengths less sensitive.

Recommendations

The following recommendations are made for future work on the rocket/ejector-afterburner system:

1. Further explore configurations with the diffuser placed immediately downstream of the secondary inlet. More pressure taps placed circumferentially around the diffuser could be used to determine if unsymmetric flow separation is occurring. If the flow is separating, the use of secondary stream injection or splitter vanes in the diffuser might increase pressure recovery and thrust augmentation.

2. Investigate the thrust augmentation of the divergent ejector-afterburner at various induced secondary mass flow rates. This would simulate an in-flight condition.

3. Investigate the thrust augmentation of the divergent ejector-afterburner with a supersonic primary stream. Some researchers contend that the underexpanded convergent-divergent primary stream nozzle is most advantageous for ejector operation (Ref 26:9). This could be done under both static and induced secondary flow conditions.

4. Further explore the thrust augmentation of the dump ejector-afterburner. It is recommended that a range of diameter ratios and duct lengths be studied. It is possible that the area step used in this study was not large enough to effectively stabilize the afterburning combustion zone.

Bibliography

1. Von Karman, T. "Theoretical Remarks on Thrust Augmentation" in Reissner Anniversary Volume Contributions to Applied Mechanics, edited by the Department of Aeronautical Engineering and Applied Mechanics of the Polytechnic Institute of Brooklyn. Ann Arbor, Michigan: J. W. Edwards, 1949.

2. Knox, R. M. "The Optimized Ejector-Nozzle Thrust Augmentor." Journal of the Aerospace Sciences, 29:470-471 (April 1962).

3. Quinn, B. "Compact Ejector Thrust Augmentation." Journal of Aircraft, 10:481-486 (August 1973).

4. Yarborough, P. P. Investigation of the Performance of an Ejector-Afterburner for Thrust Augmentation of a Small Rocket Engine. Unpublished Thesis. Wright-Patterson Air Force Base, Ohio: Air Force Institute of Technology, March 1966.

5. Nidiffer, K. E. Investigation of the Thrust Augmentation Capability of a Sonic Ejector-Afterburner. Unpublished Thesis. Wright-Patterson Air Force Base, Ohio: Air Force Institute of Technology, June 1967.

6. Adam, W. B. An Investigation of the Effects of Secondary Stream Turbulation on the Thrust Augmentation of an Ejector-Afterburner. Unpublished Thesis. Wright-Patterson Air Force Base, Ohio: Air Force Institute of Technology, March 1968.

7. Markwardt, J. H. A Feasibility Study For Using Cooled Heat Flux Probes in Ejector-Afterburner Environments. Unpublished Thesis. Wright-Patterson Air Force Base, Ohio: Air Force Institute of Technology, March 1970.

8. Jahnke, R. E. On the Application of the Cooled Heat Flux Probe in a Sonic Ejector. Unpublished Thesis. Wright-Patterson Air Force Base, Ohio: Air Force Institute of Technology, December 1973.

9. Bevilaqua, P. M. "Evaluation of Hypermixing for Thrust Augmenting Ejectors." Journal of Aircraft, 11:348-354 (June 1974).

10. McCormick, B. W. Aerodynamics of V/STOL Flight. New York: Academic Press, Inc., 1967.

11. Fancher, R. B. "Low-Area Ratio, Thrust-Augmenting Ejectors." Journal of Aircraft, 9:243-248 (March 1972).

12. -----. Why Ejectors for Aircraft Propulsion-Lift Systems and Where We Stand. ARL 71-0140. Wright-Patterson Air Force Base, Ohio: Aerospace Research Laboratory, August 1971. AD 732842.

13. Mossman, E. A., et al. Analytical and Experimental Investigation of Air-Augmented Rockets to Determine Thrust Minus Drag. AFRPL-TR-66-31. Edwards Air Force Base, California: Air Force Rocket Propulsion Laboratory, March 1966. AD 370515.

14. Bertin, J. Les Trompes Appliquees Au Vol Vertical. Symposium on Vertical and Short Takeoff and Landing Aircraft, AGARDograph 46. Paris, France: Advisory Group for Aeronautical Research and Development, June 1960.

15. Sutton, G. P. Rocket Propulsion Elements. New York: John Wiley and Sons, Inc., 1963.

16. Keller, R. G., et al. Operations Manual for the Rocket Engine Test Facility of the Department of Mechanical Engineering. Wright-Patterson Air Force Base, Ohio: Air Force Institute of Technology. August 1961.

17. Kline, S. J., et al. "Optimum Design of Straight-Walled Diffusers." Journal of Basic Engineering, 81:321-331 (September 1959).

18. Norton, H. N. Handbook of Transducers for Electronic Measuring Systems. Englewood Cliffs, New Jersey: Prentice Hall, Inc., 1969.

19. Martin Company, Denver Division. Experimental and Theoretical Investigation of the Rocket Engine - Nozzle Ejector (RENE) Propulsion System. AFRPL-TR-65-66. Edwards Air Force Base, California: Air Force Rocket Propulsion Laboratory, April 1965. AD 359763.

20. Fabri, J. and J. Paulon. Theory and Experiments on Supersonic Air-to-Air Ejectors. NACA Technical Memorandum 1410. Washington: National Advisory Committee for Aeronautics, September 1958.

21. Simonson, A. J. and J. W. Schmeer. Static Thrust Augmentation of a Rocket - Ejector System With a Heated Supersonic Primary Jet. NASA Technical Note D-1261. Washington: National Aeronautics and Space Administration, May 1962.

22. Hardy, J. M. Possibilites Actuelles D'etude Theorique D'une Tuyere Supersonique A Double-Flux. Aerodynamics of Power Plant Installation, Part II, AGARDograph 103. Paris, France: Advisory Group for Aeronautical Research and Development, October 1965.

23. Brokaw, R. S. Analytic Solutions to the Ignition Kinetics of the Hydrogen-Oxygen Reaction. NASA Technical Note D-2542. Washington: National Aeronautics and Space Administration, December 1964.

24. Rickeard, D. "A One-Dimensional Flow Model for an Air-Augmented Rocket." Journal of the British Interplanetary Society, 26:18-27 (January 1973).

25. Vinogradov, Y. V., et al. Effect of the Intensity of Turbulence Upon the Process of Mixing Slipstreams at a Different Ratio of Velocities. Translated from: Teoriyai Praktika Szhiganiya Gaza, 5:28-33 (1972). Wright-Patterson Air Force Base, Ohio: Foreign Technology Division, April 1974. FTD-HT-23-866-74. AD 778798.

26. Kalmykov, I. and I. Mosin. Effect of Nozzle Structural Design on the Operation of the Ejector Stage with a Conical Mixing Chamber. Translated from: Kazan Aviation Institute Transactions, 114:48-57 (1970). Wright-Patterson Air Force Base, Ohio: Foreign Technology Division, June 1972. FTD-HC-23-0473-72.

Appendix A

Ejector-Afterburner Performance Graphs

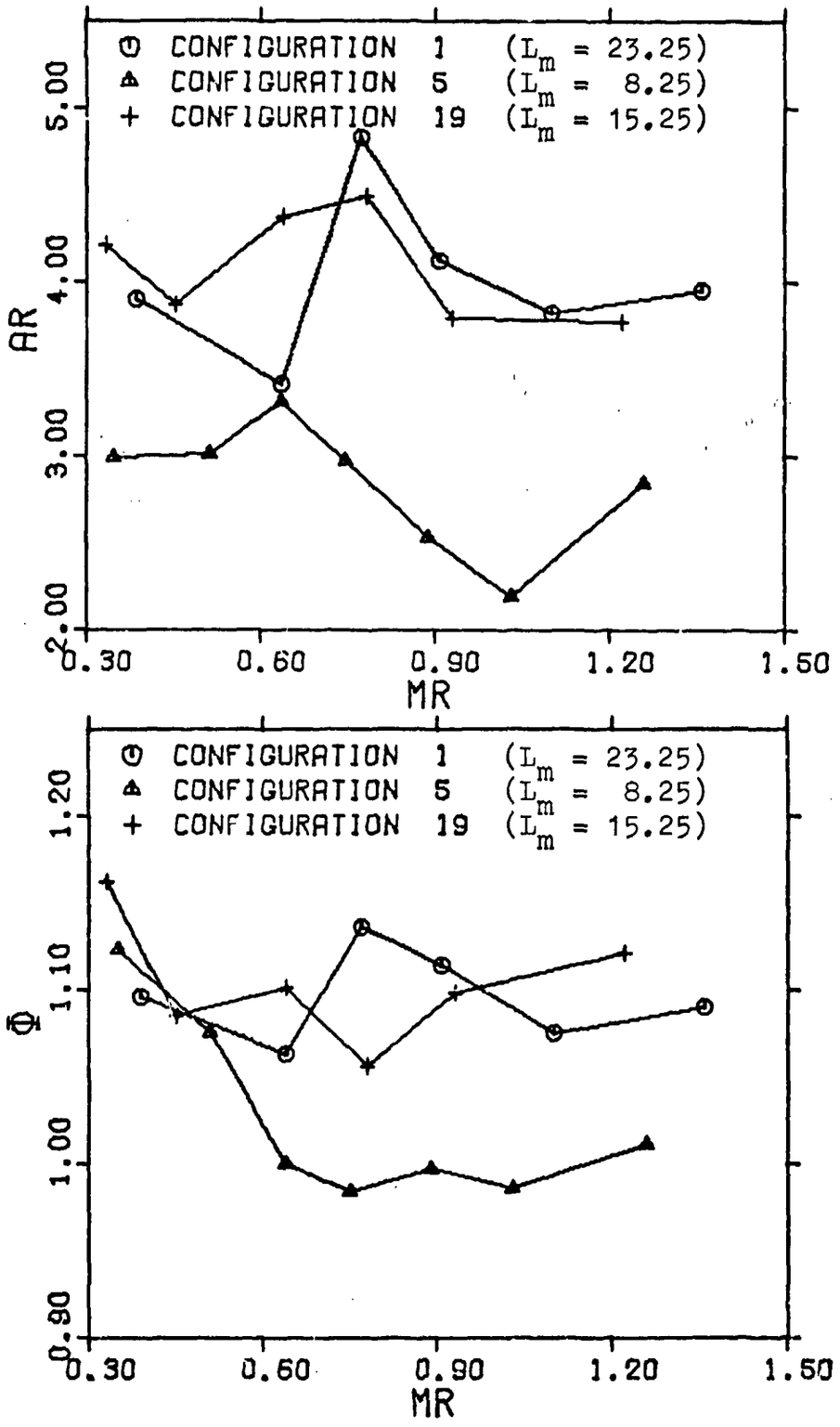

Fig. 9. Effect of Mixing Duct Length on Constant Area Duct Performance

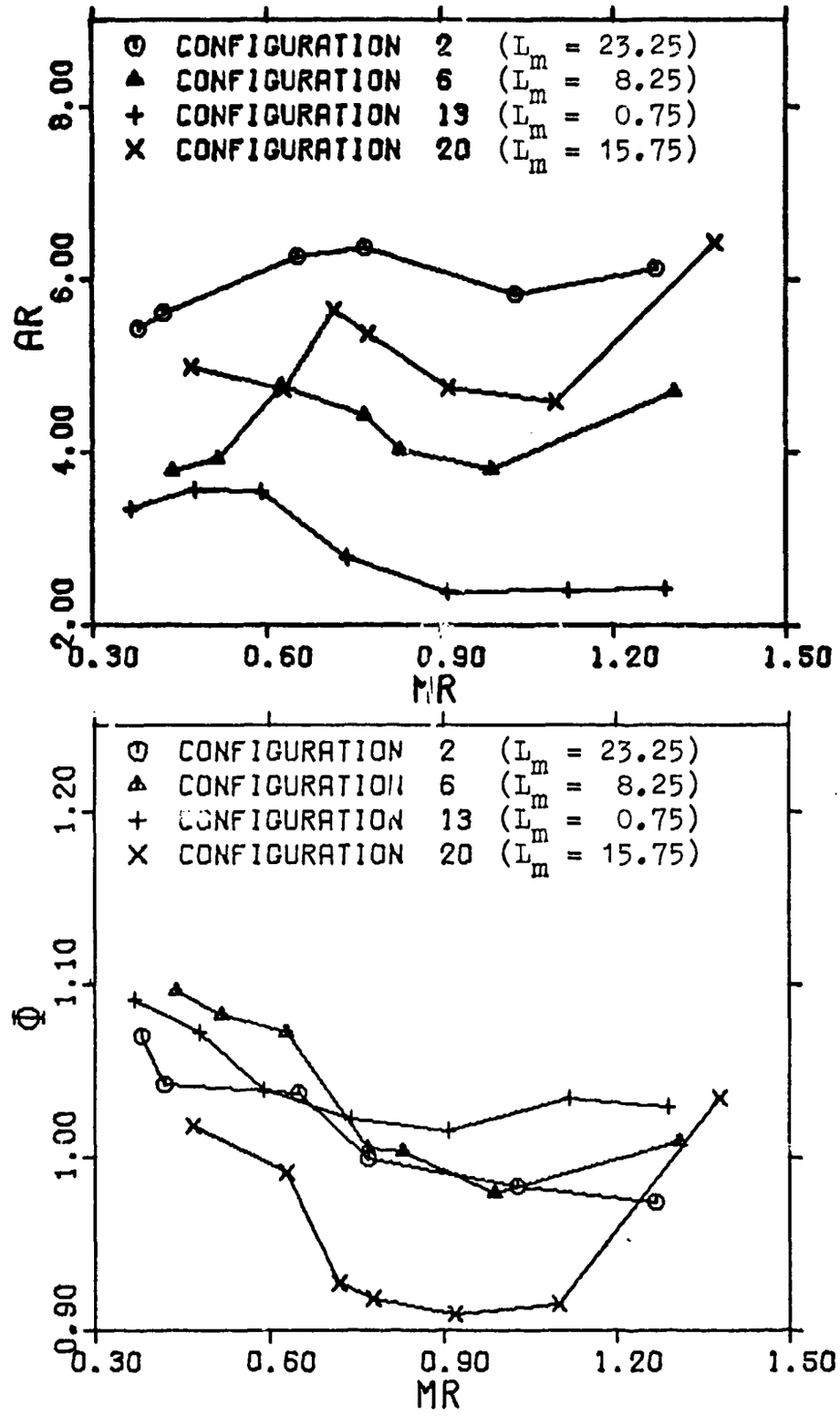

Fig. 10. Effect of Mixing Duct Length on Small Diffuser Performance

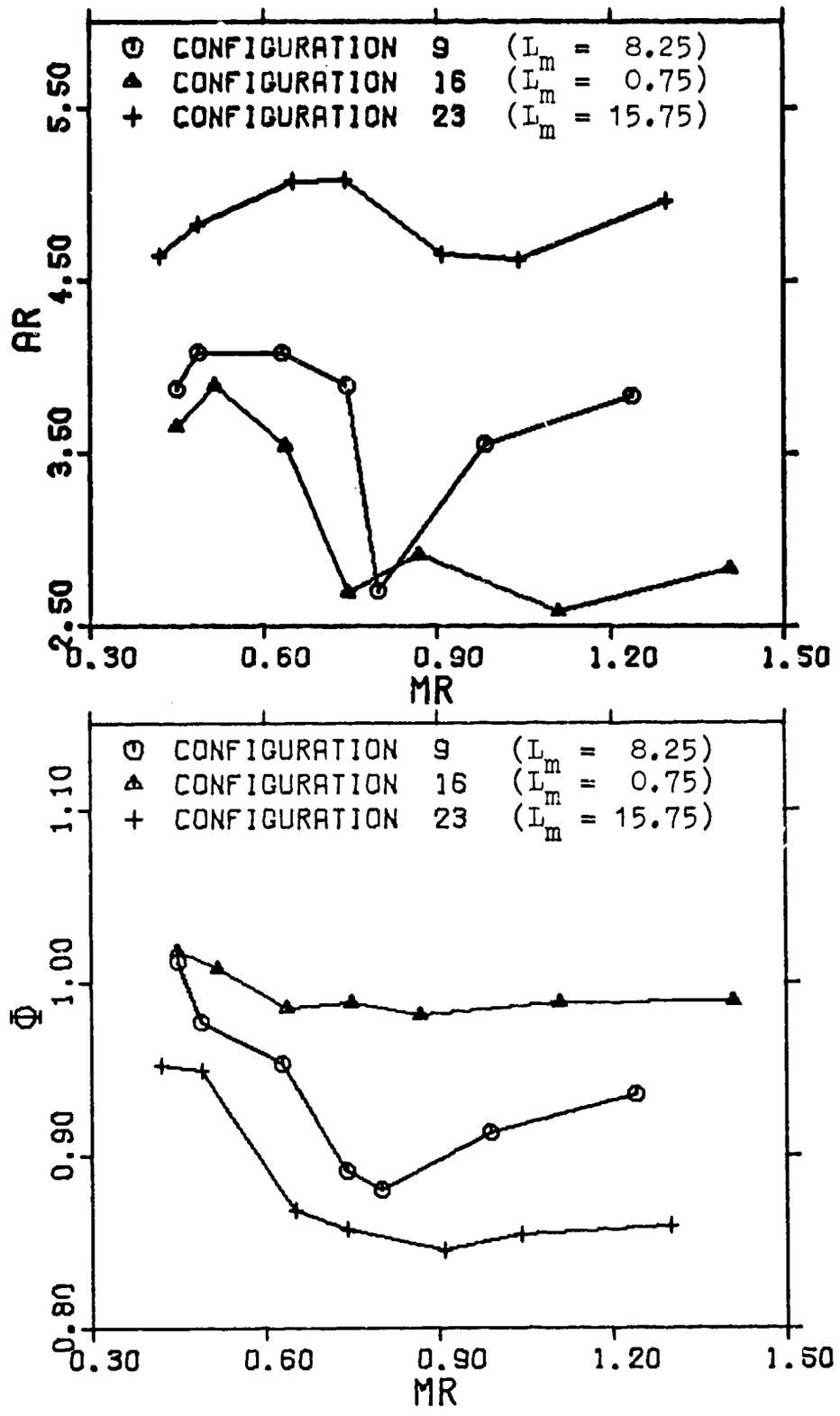

Fig. 11. Effect of Mixing Duct Length on Large Diffuser Performance

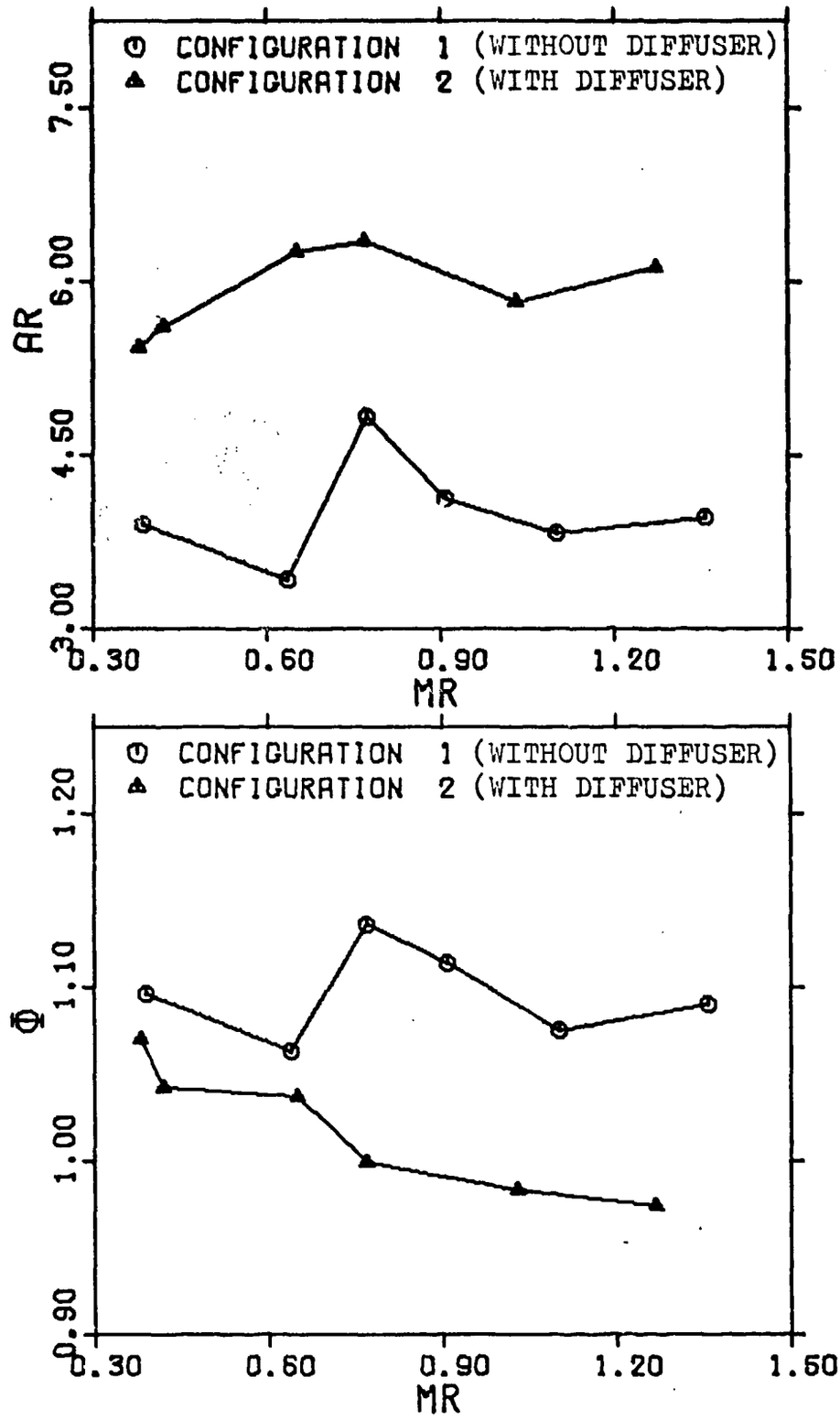

Fig. 12. Small Diffuser Effectiveness (L_m = 23.25)

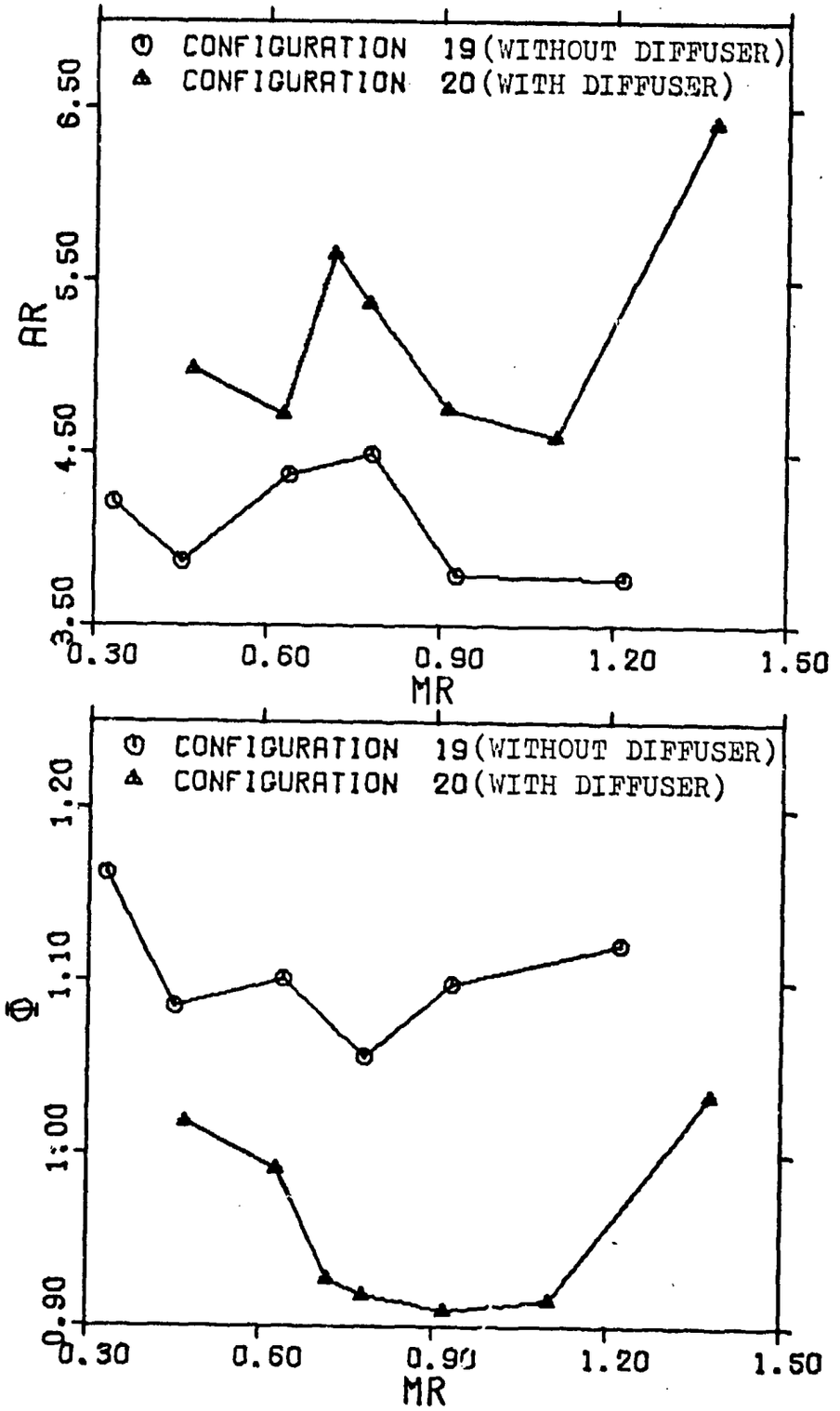

Fig. 13. Small Diffuser Effectiveness (L_m = 15.75)

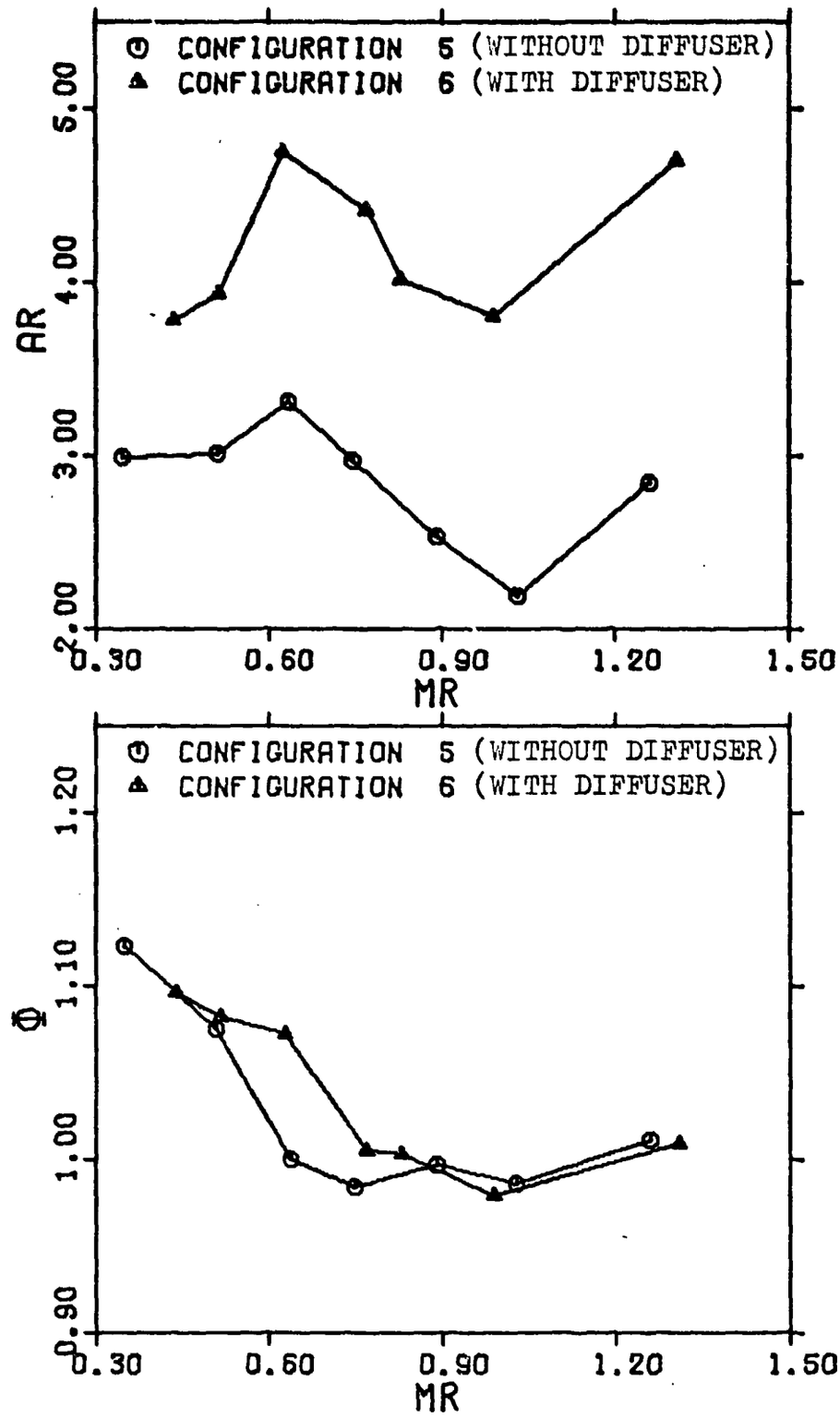

Fig. 14. Small Diffuser Effectiveness (L_m = 8.25)

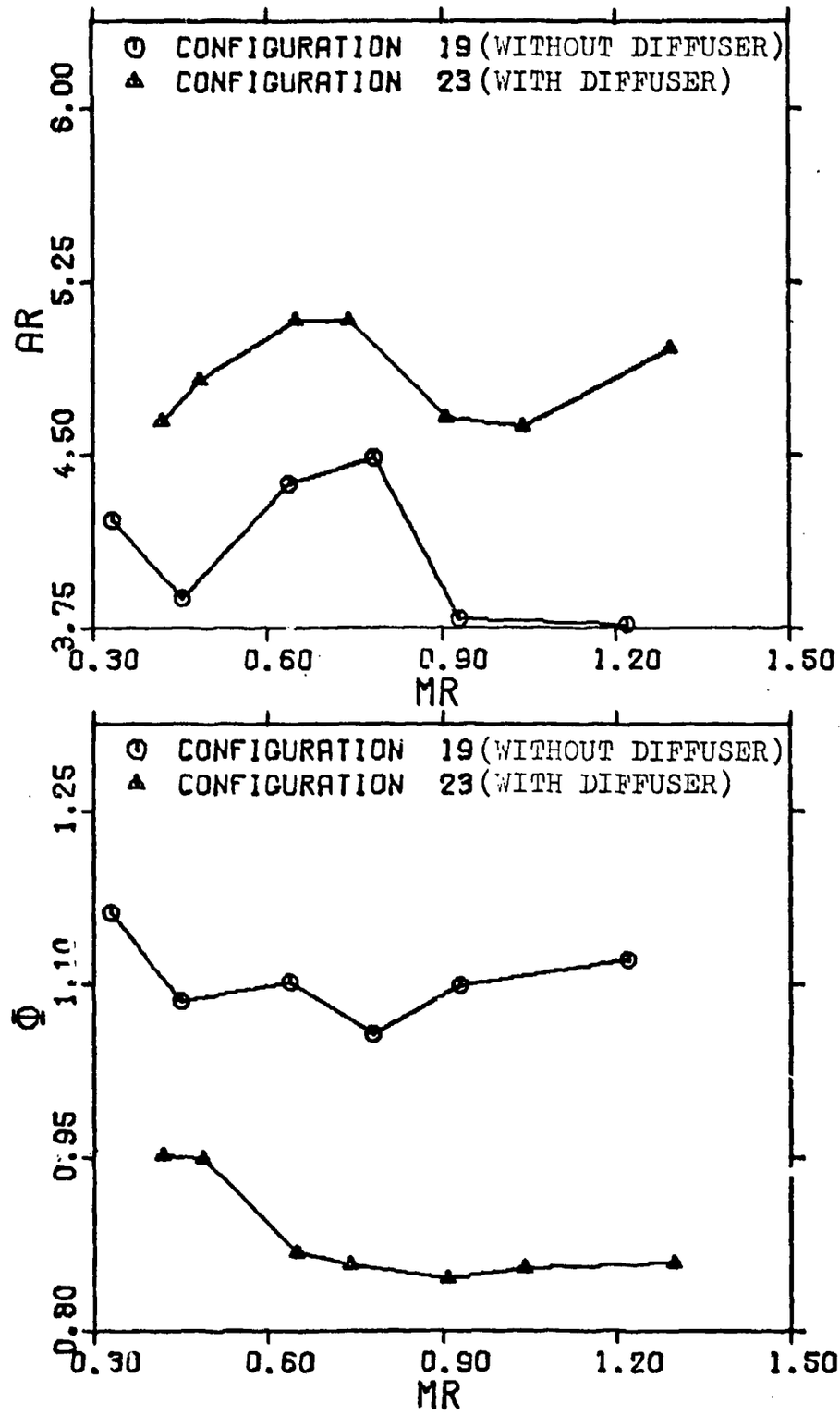

Fig. 15. Large Diffuser Effectiveness (L_m = 15.75)

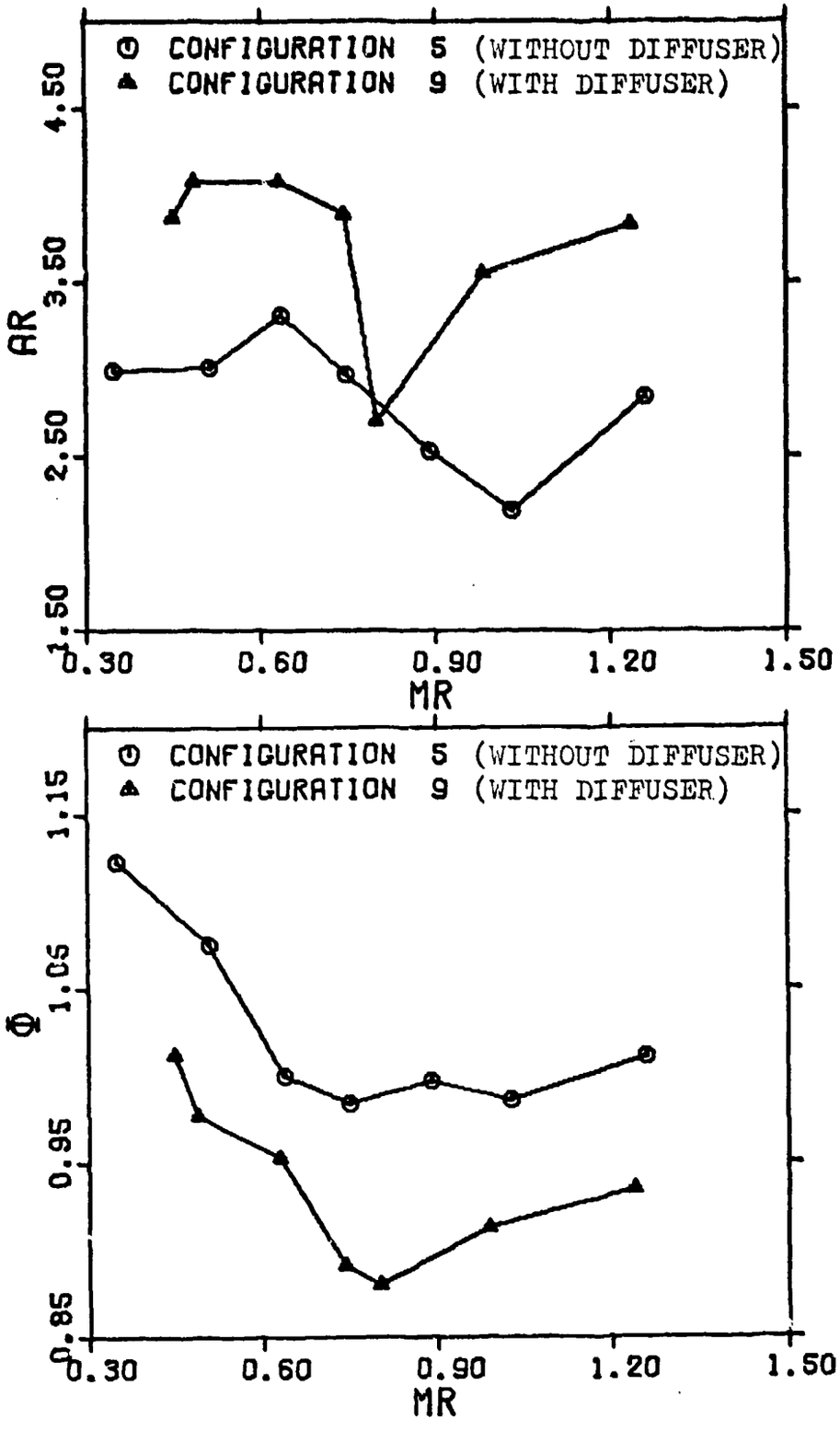

Fig. 16. Large Diffuser Effectiveness (L_m = 8.25)

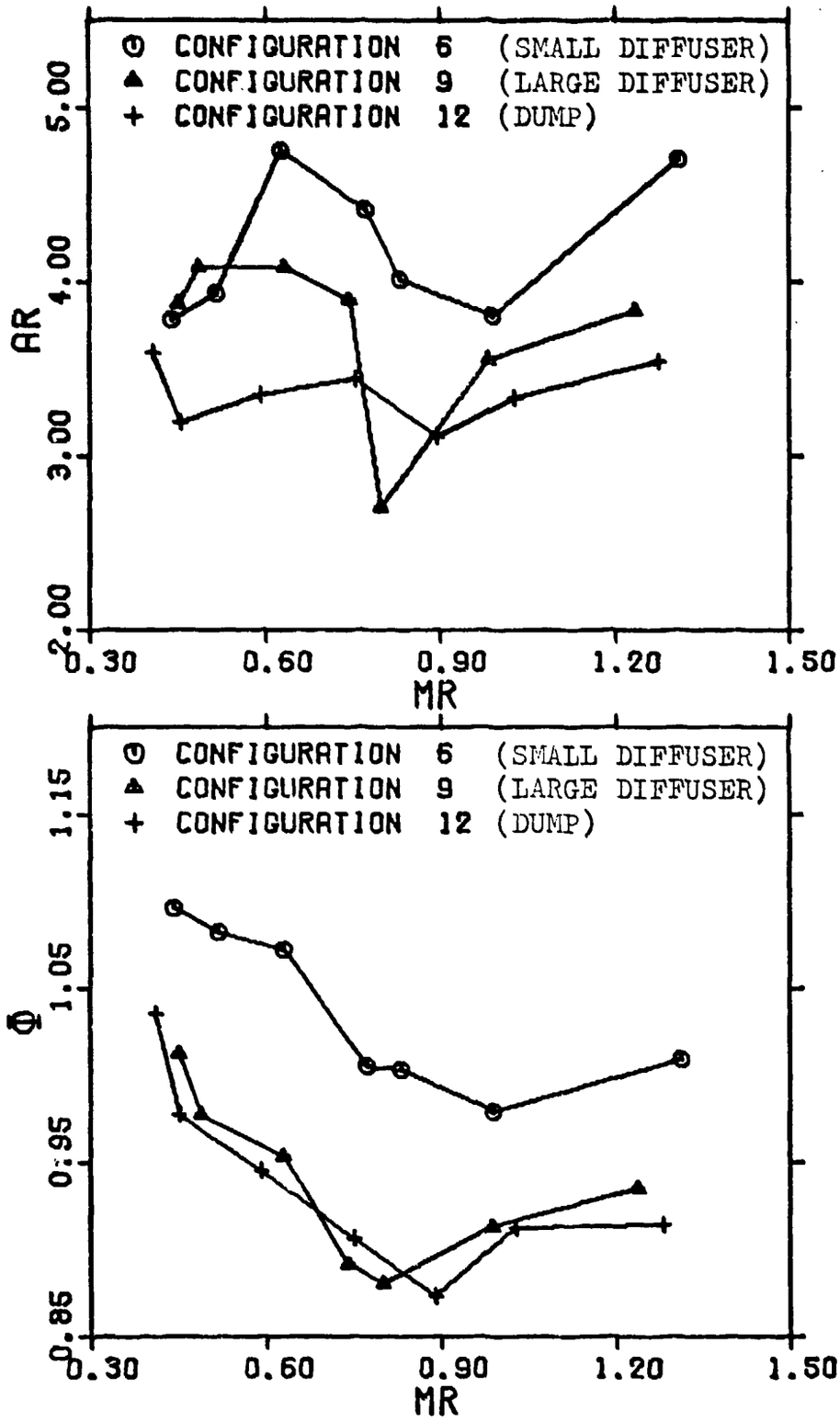

Fig. 17. Performance of Large Diffuser, Small Diffuser and Dump Configurations (L_m = 8.25)

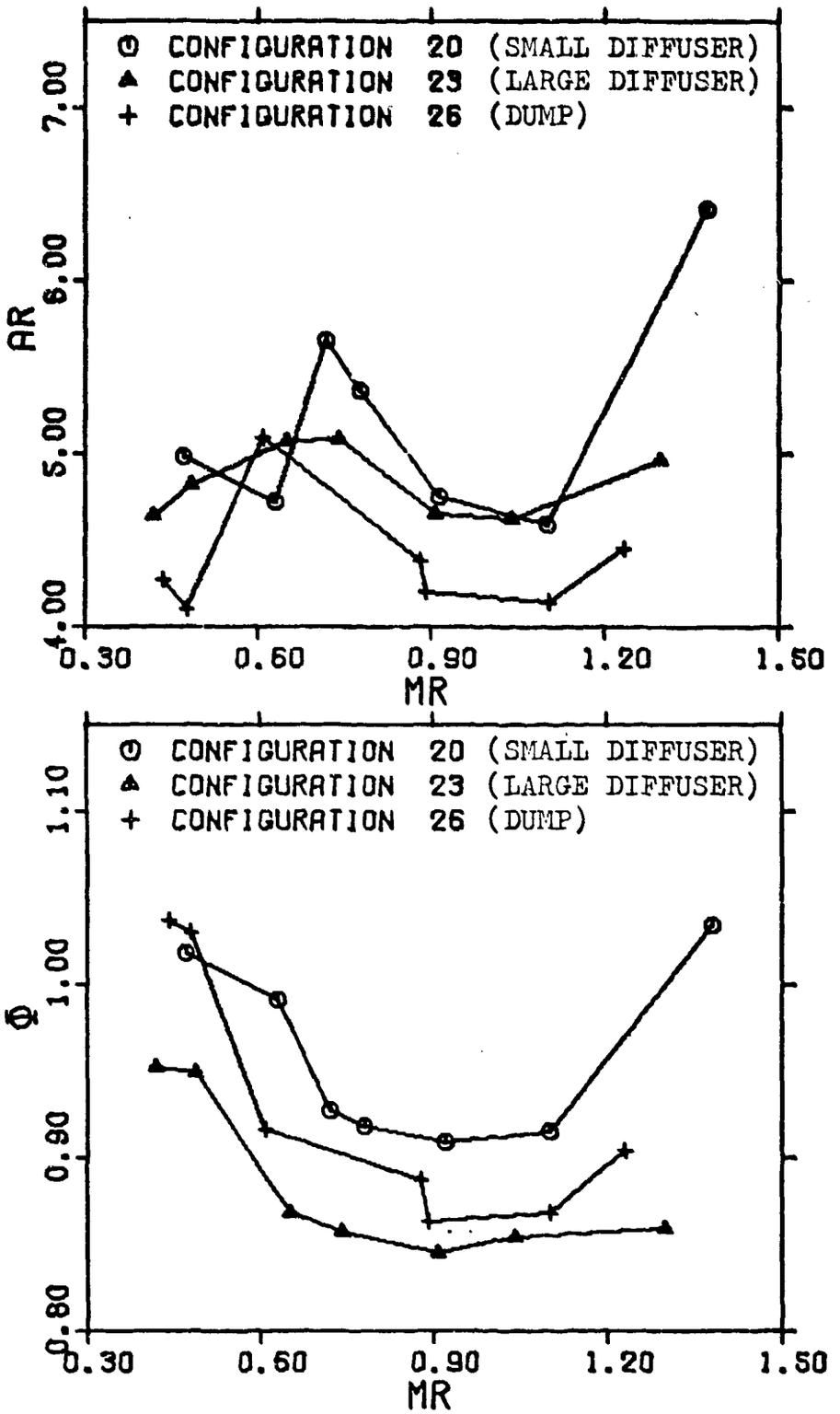

Fig. 18. Performance of Large Diffuser, Small Diffuser and Dump Configurations (L_m = 15.75)

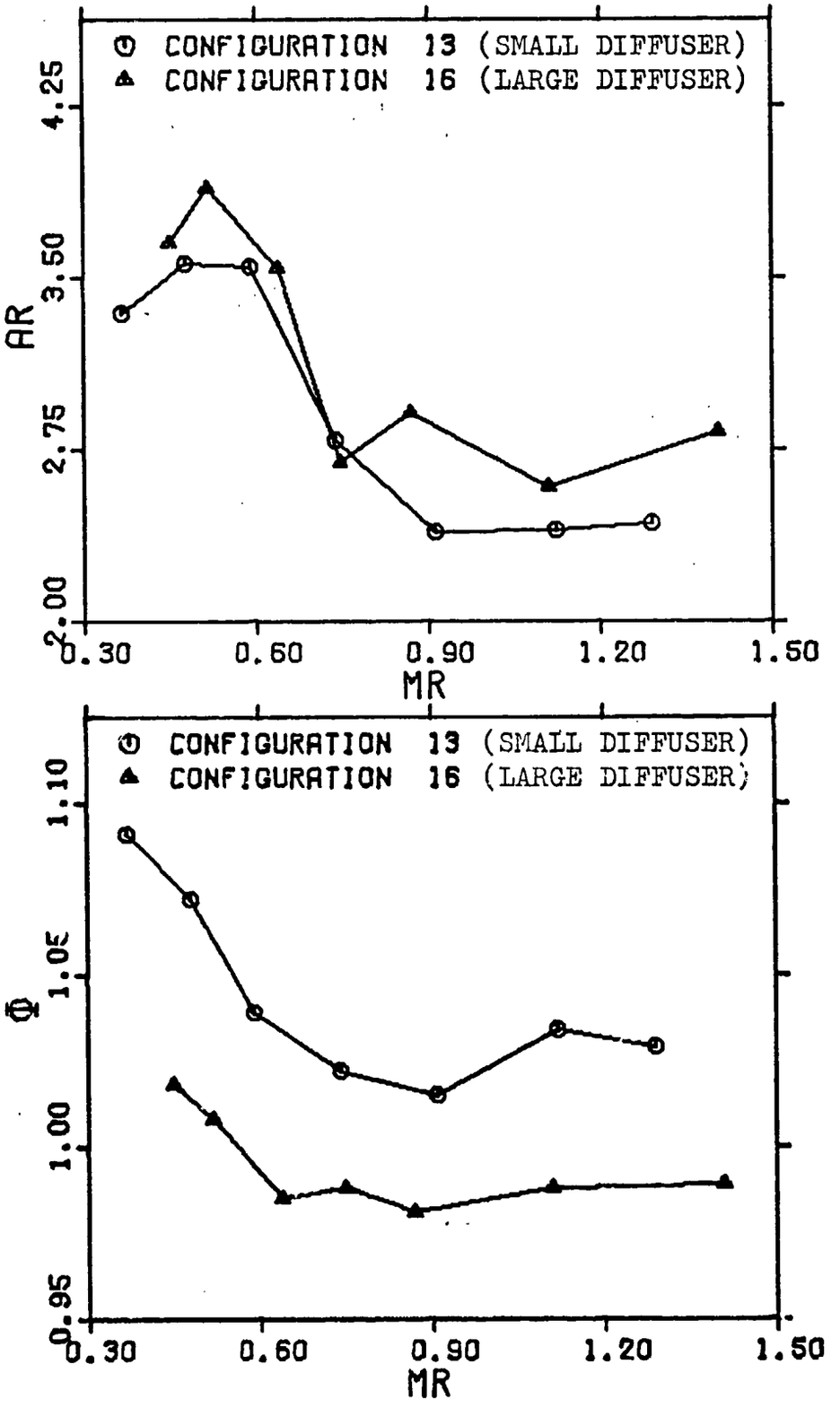

Fig. 19. Performance of Large Diffuser and Small Diffuser (L_m = 0.75)

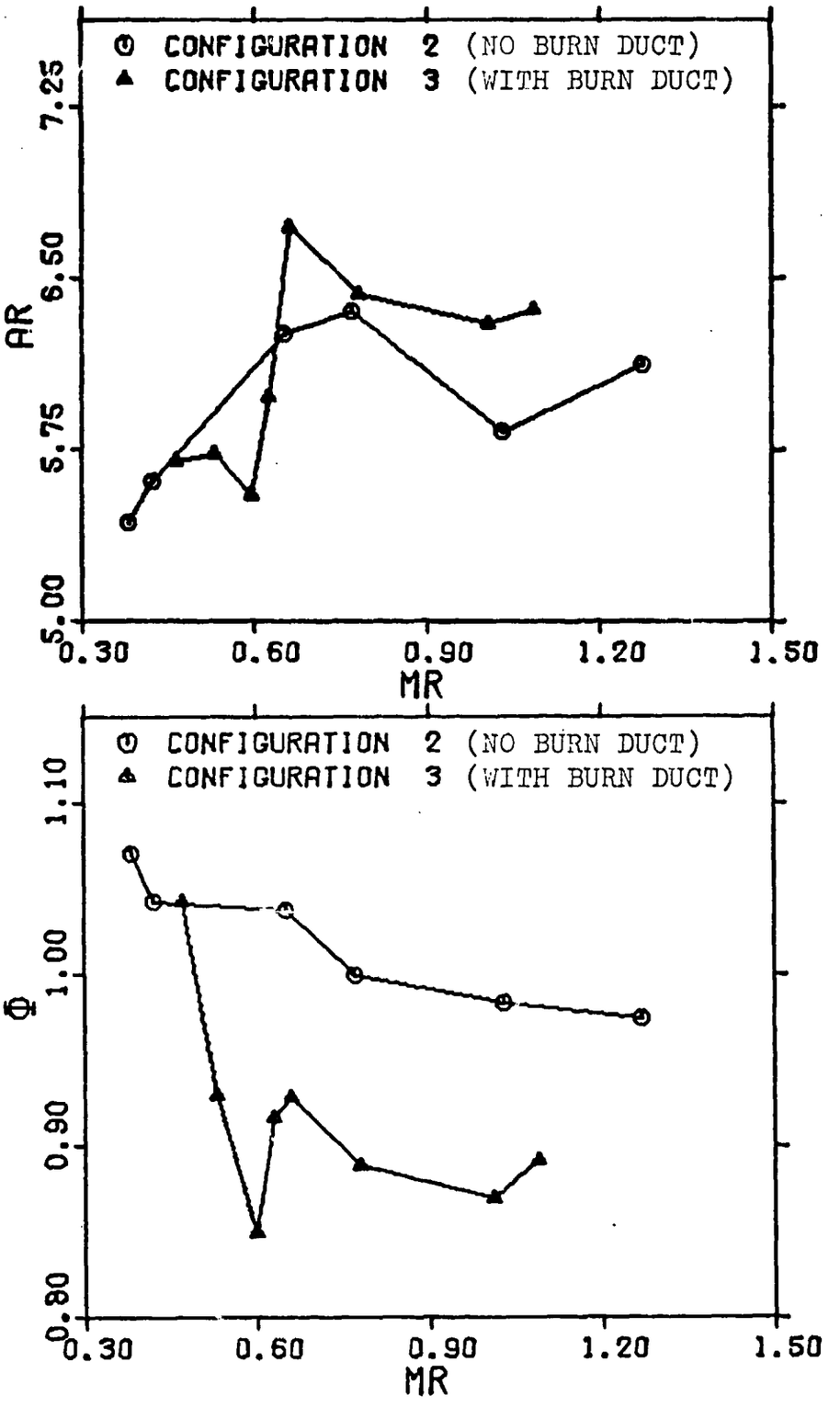

Fig. 20. Small Burn Duct Effectiveness (L_m = 23.25)

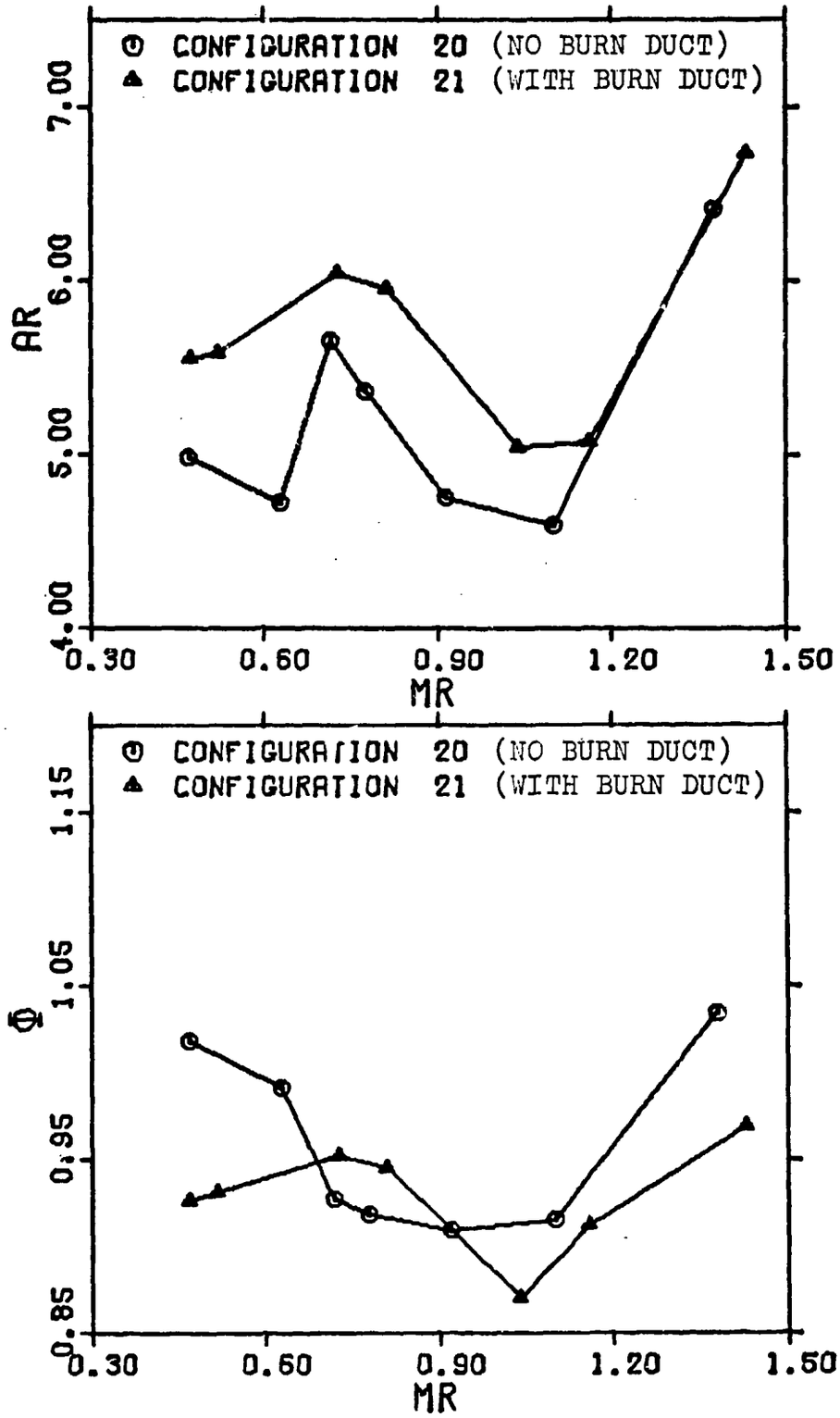

Fig. 21. Small Burn Duct Effectiveness (L_m = 15.75)

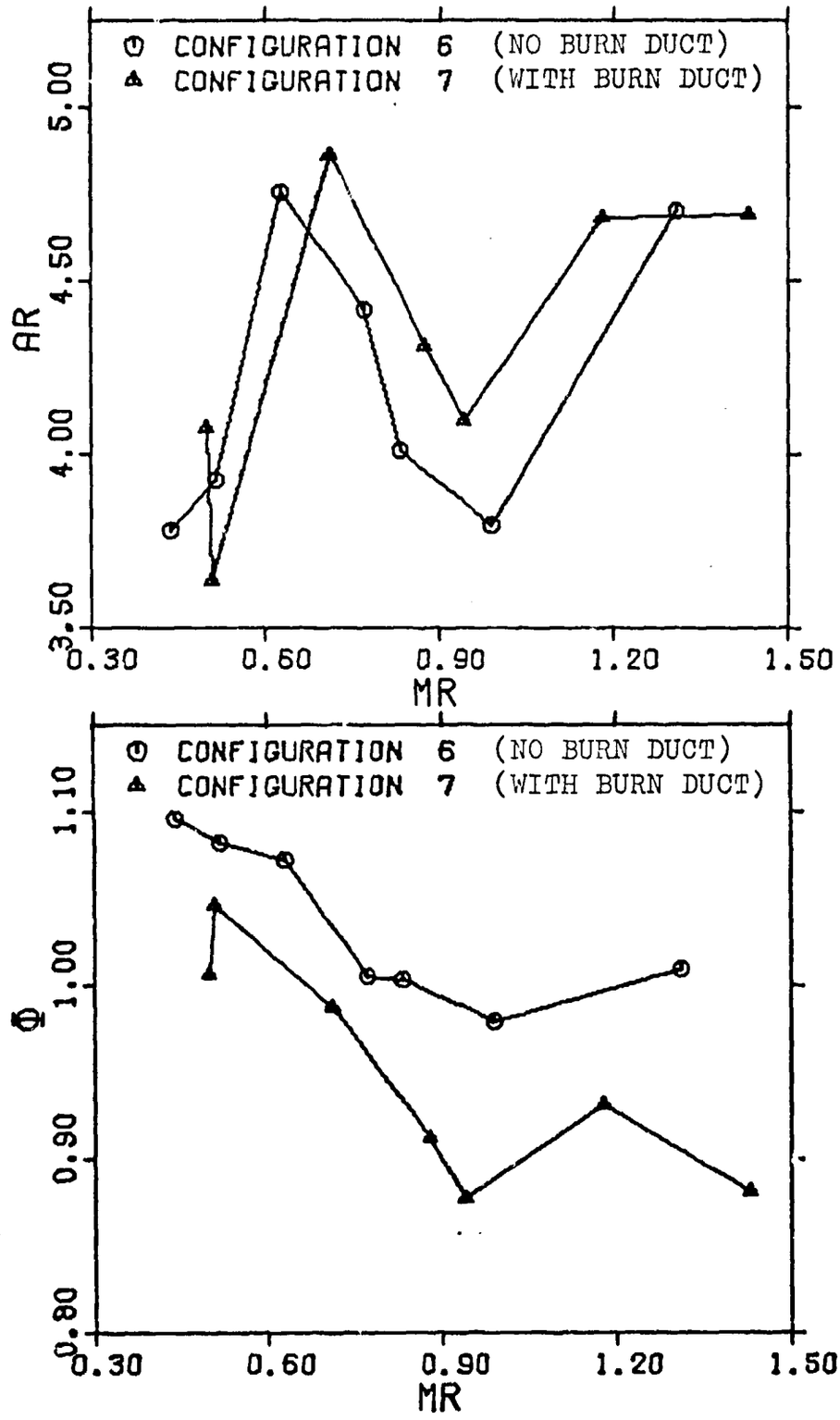

Fig. 22. Small Burn Duct Effectiveness (L_m = 8.25)

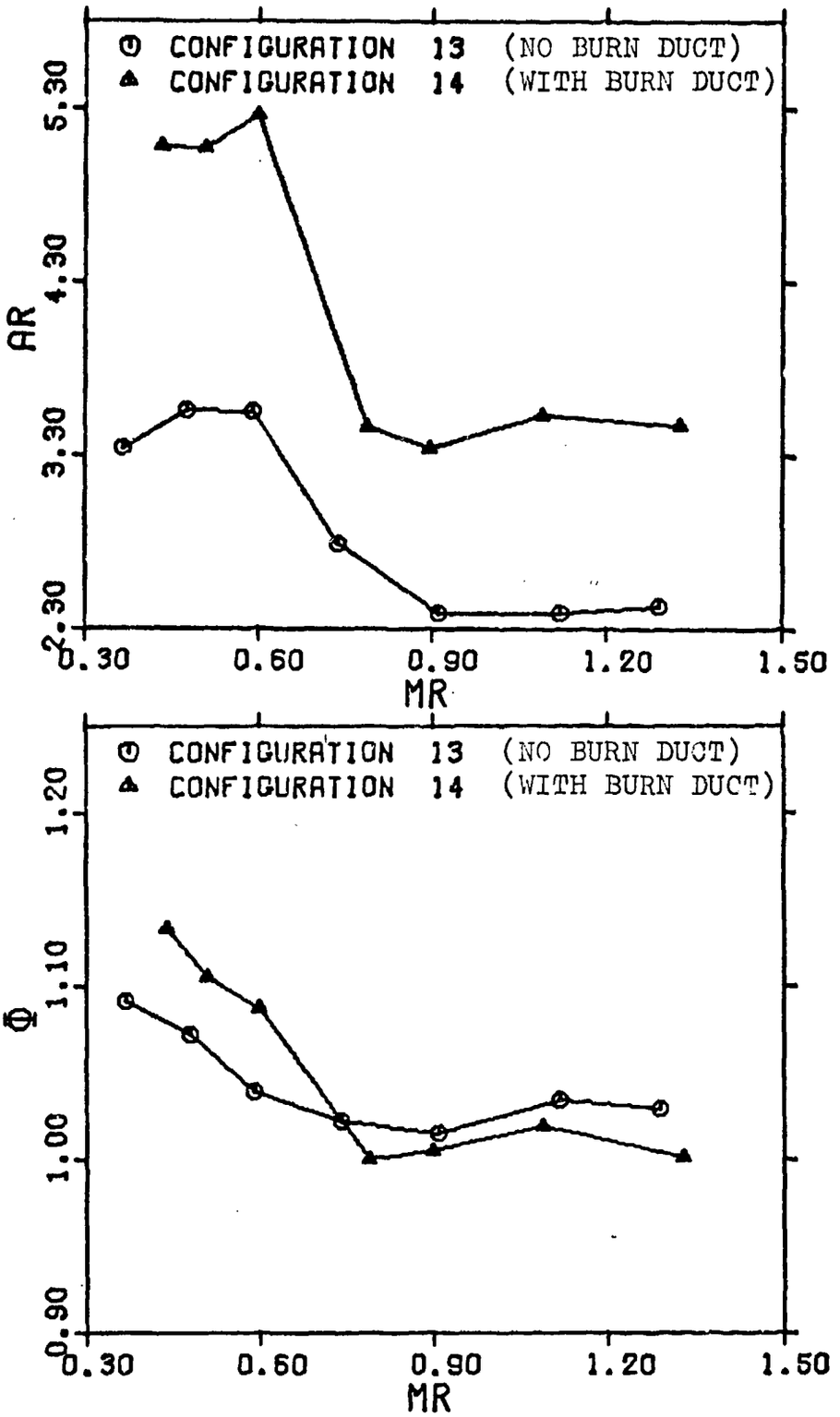

Fig. 23. Small Burn Duct Effectiveness (L_m = 0.75)

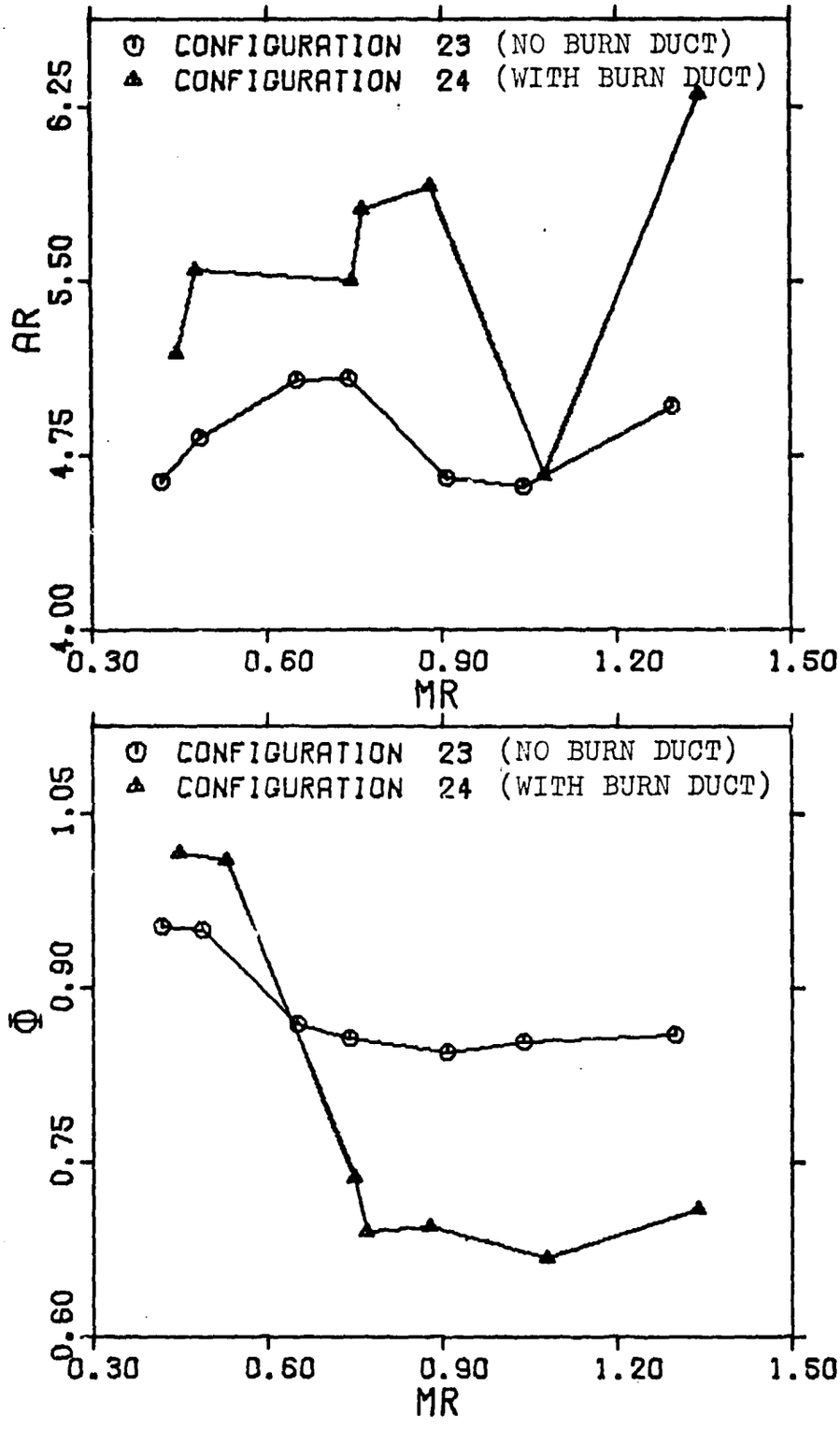

Fig. 24. Large Burn Duct Effectiveness (L_m = 15.75)

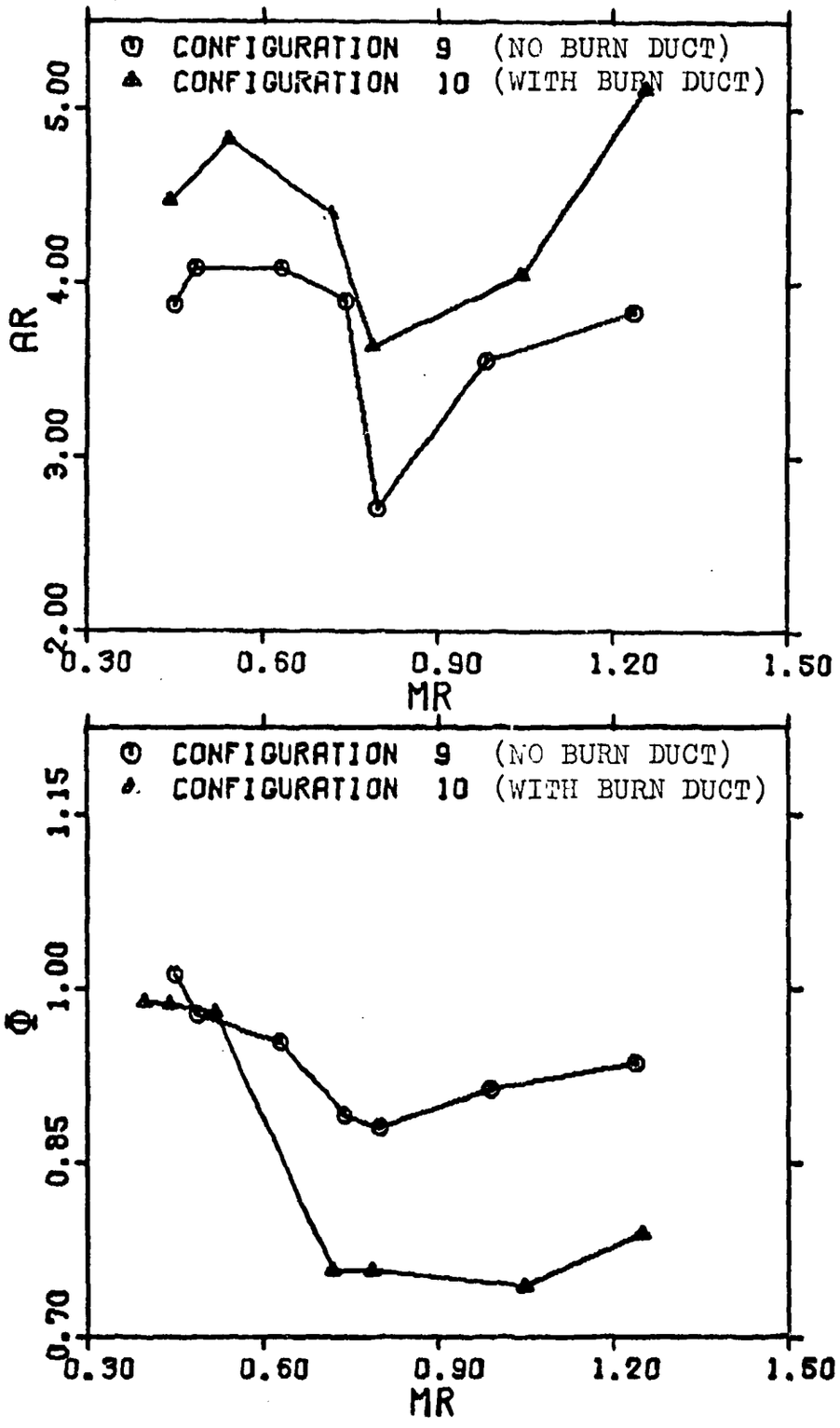

Fig. 25. Large Burn Duct Effectiveness (L_m = 8.25)

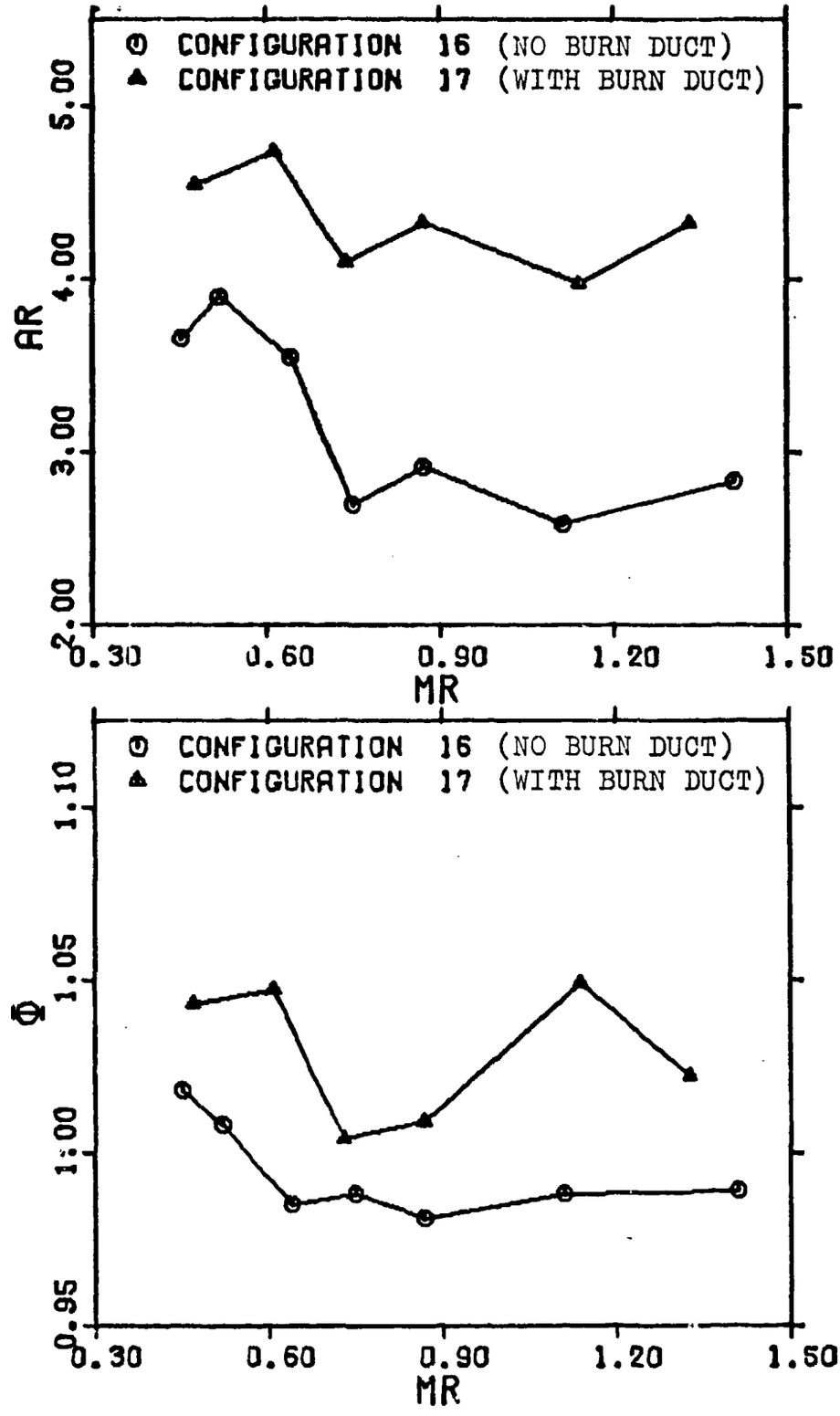

Fig. 26. Large Burn Duct Effectiveness (L_m = 0.75)

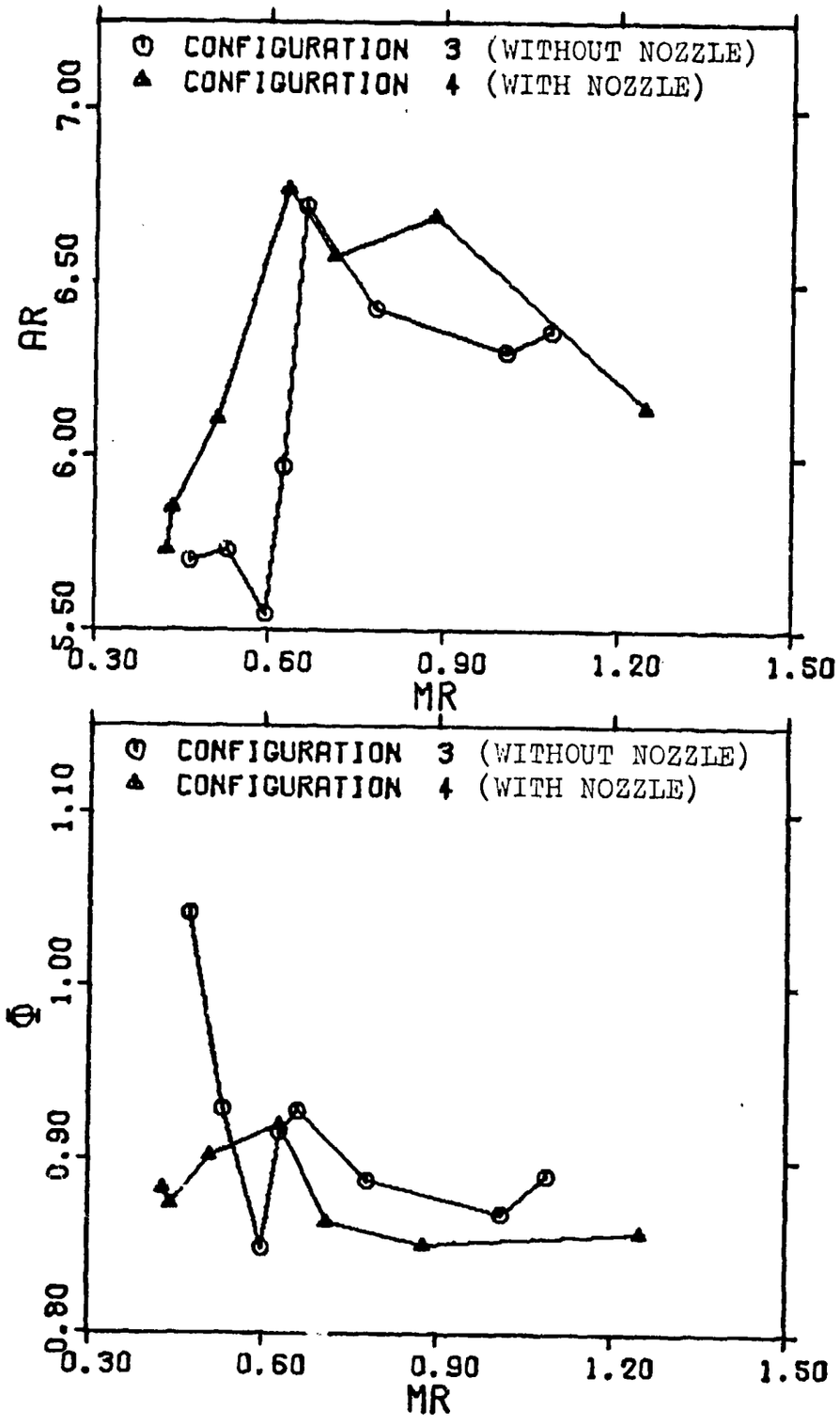

Fig. 27. Small Secondary Nozzle Effectiveness (L_m = 23.25)

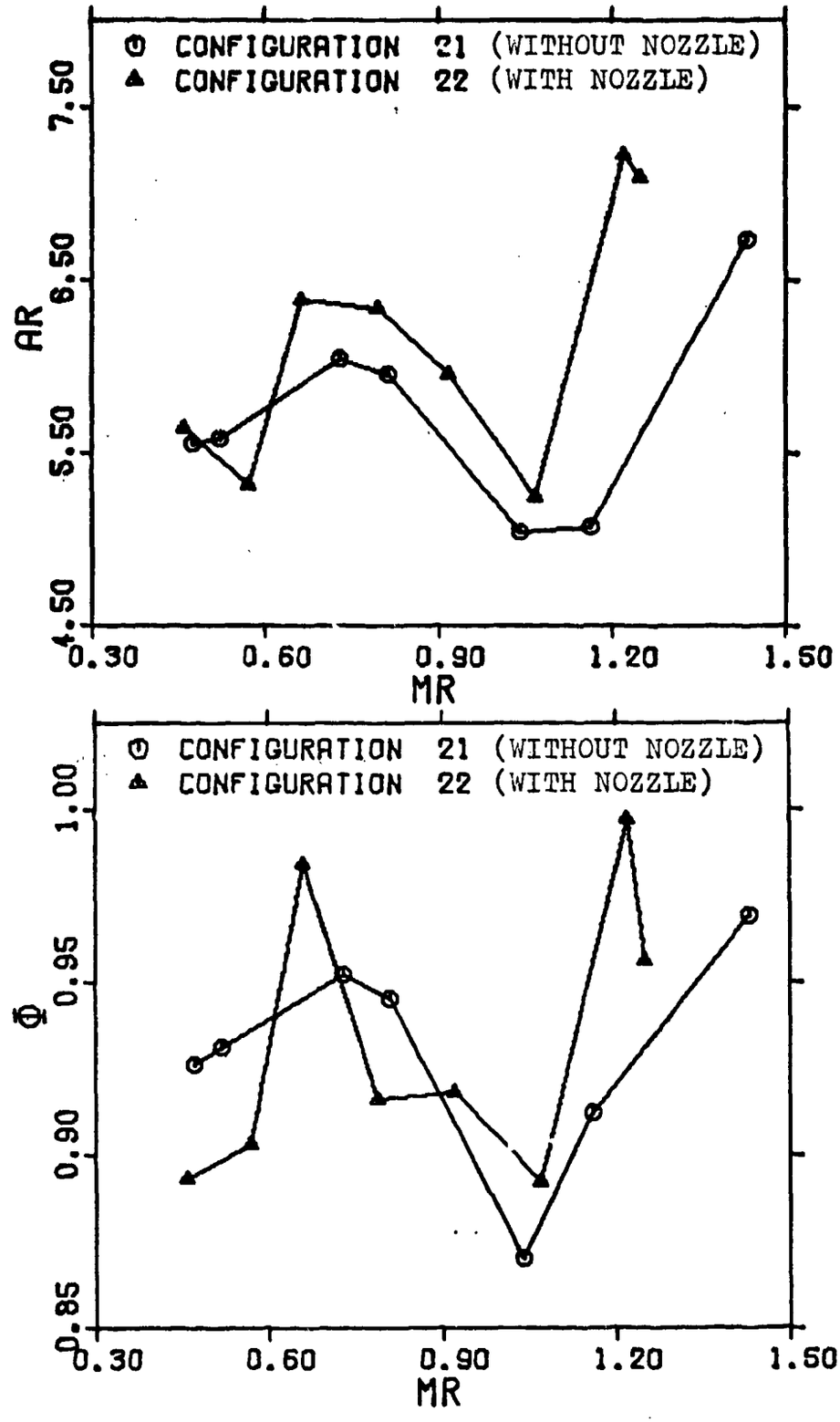

Fig. 28. Small Secondary Nozzle Effectiveness (L_m = 15.75)

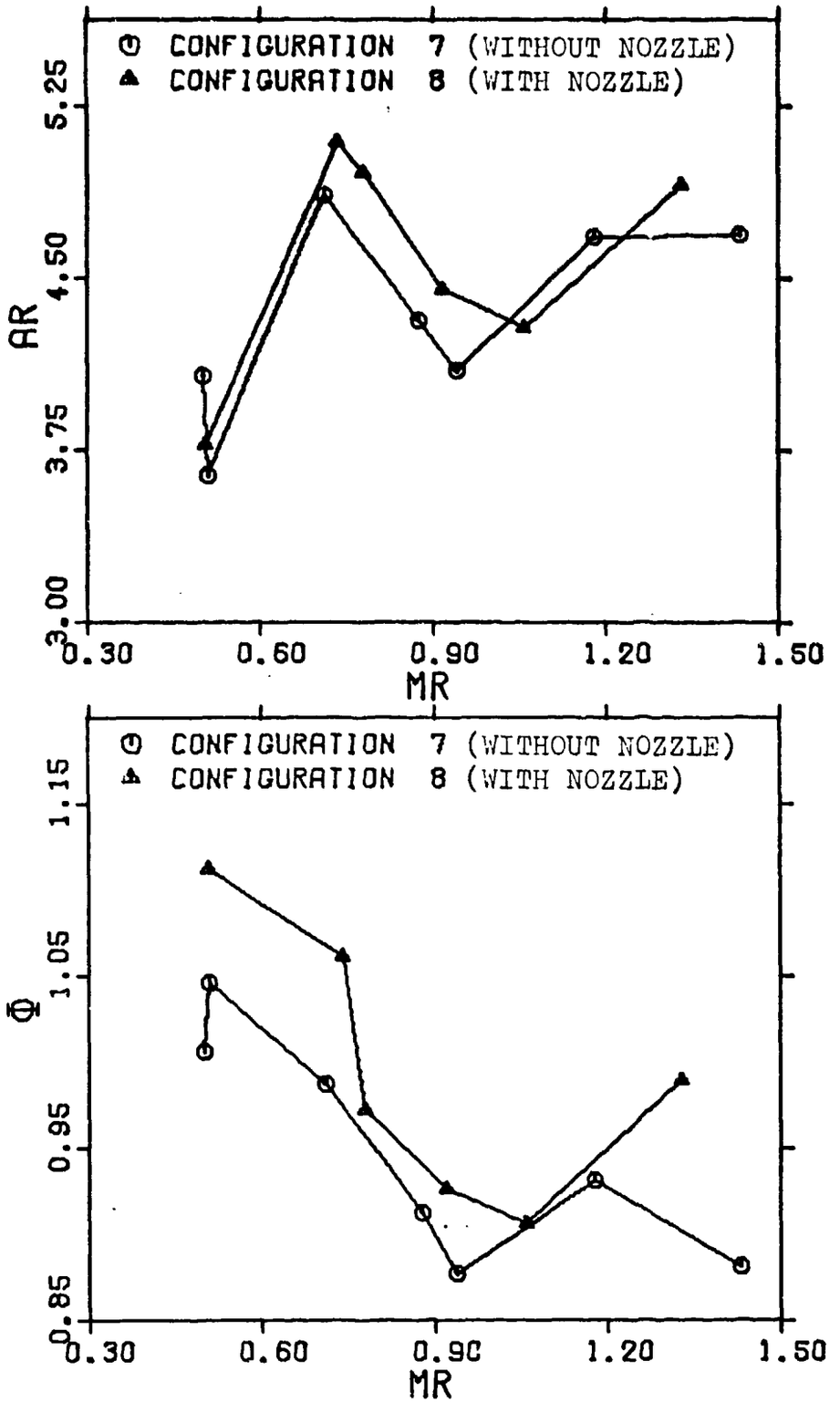

Fig. 29. Small Secondary Nozzle Effectiveness (L_m = 8.25)

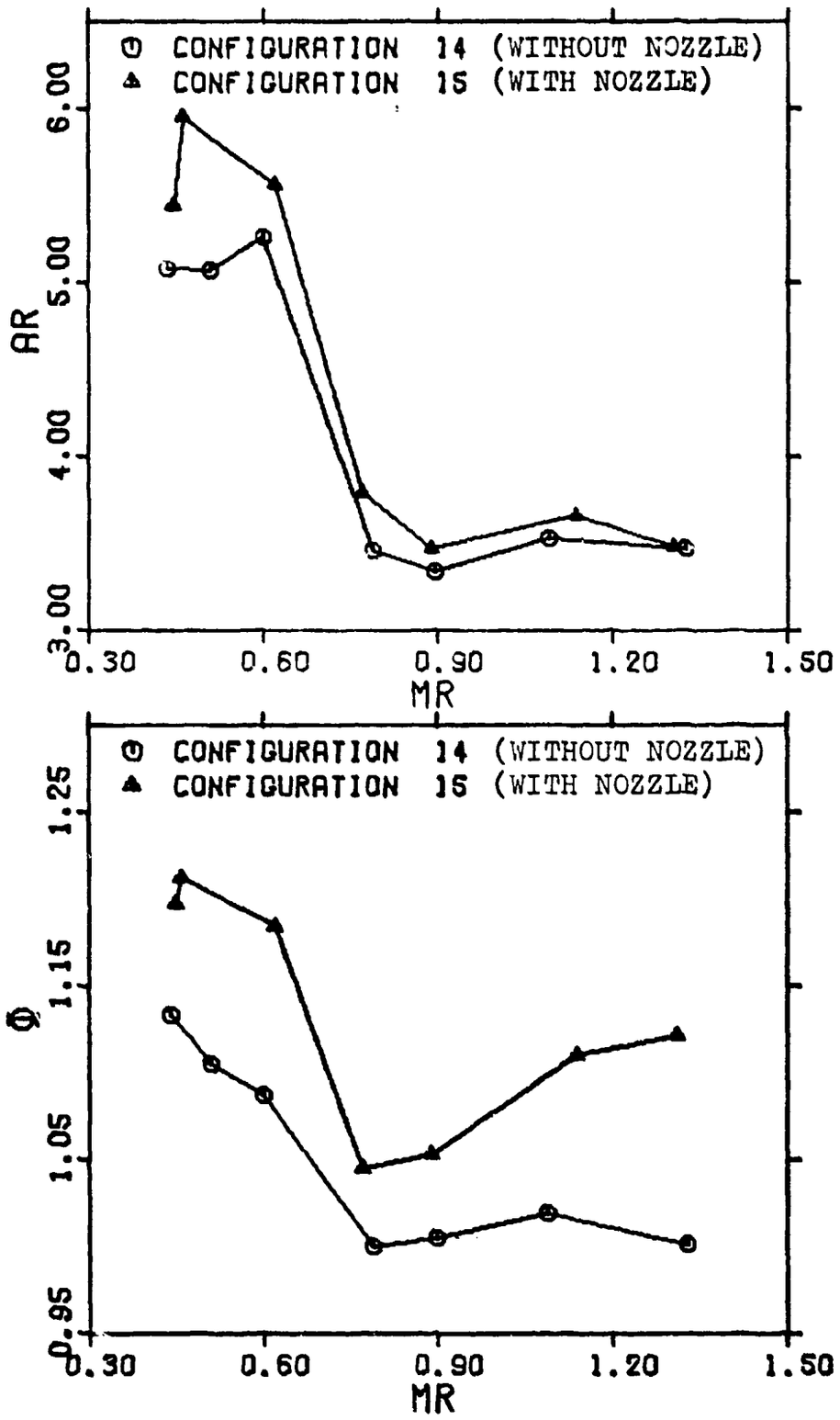

Fig. 30. Small Secondary Nozzle Effectiveness (L_m = 0.75)

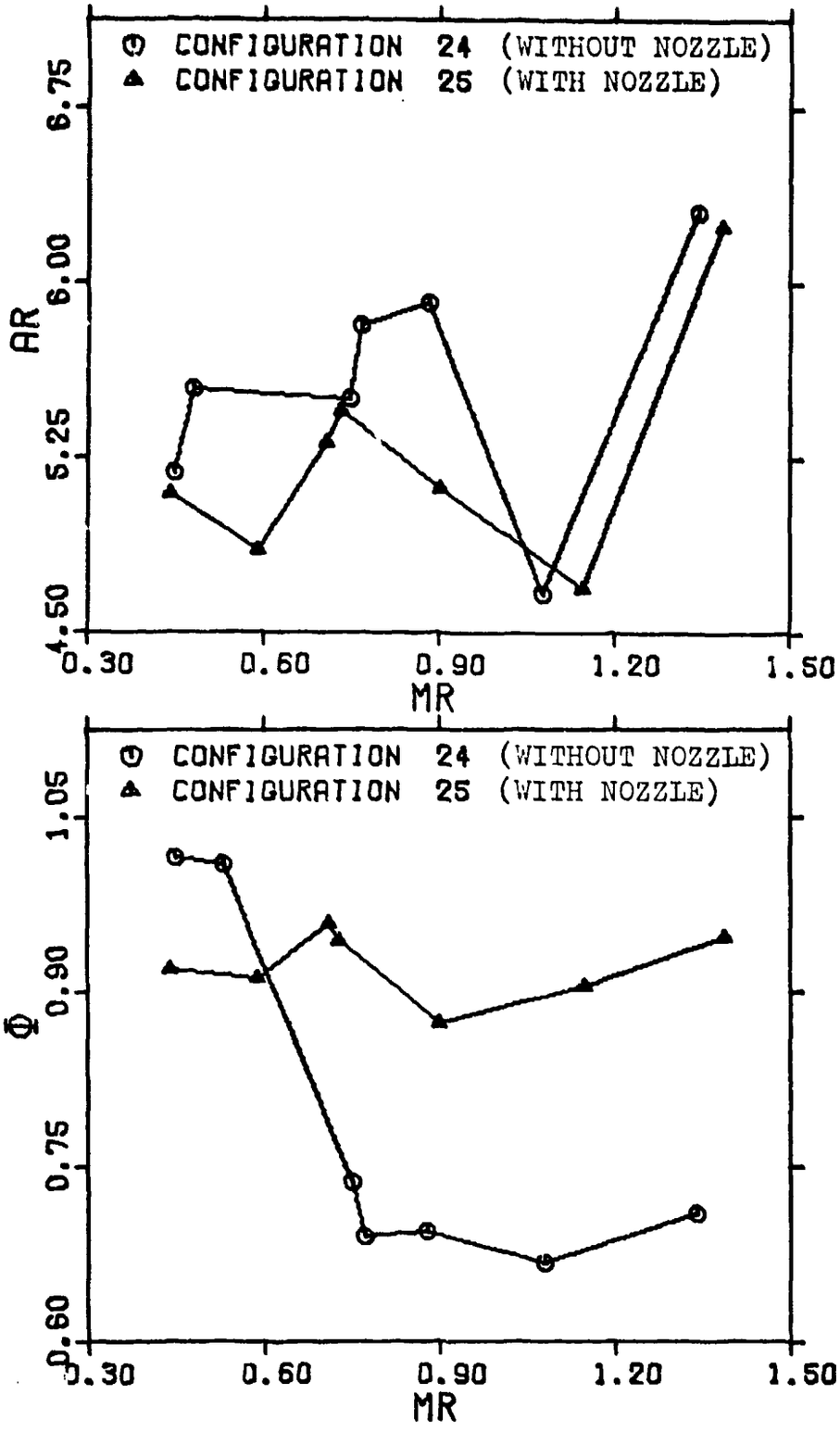

Fig. 31. Large Secondary Nozzle Effectiveness (L_m = 15.75)

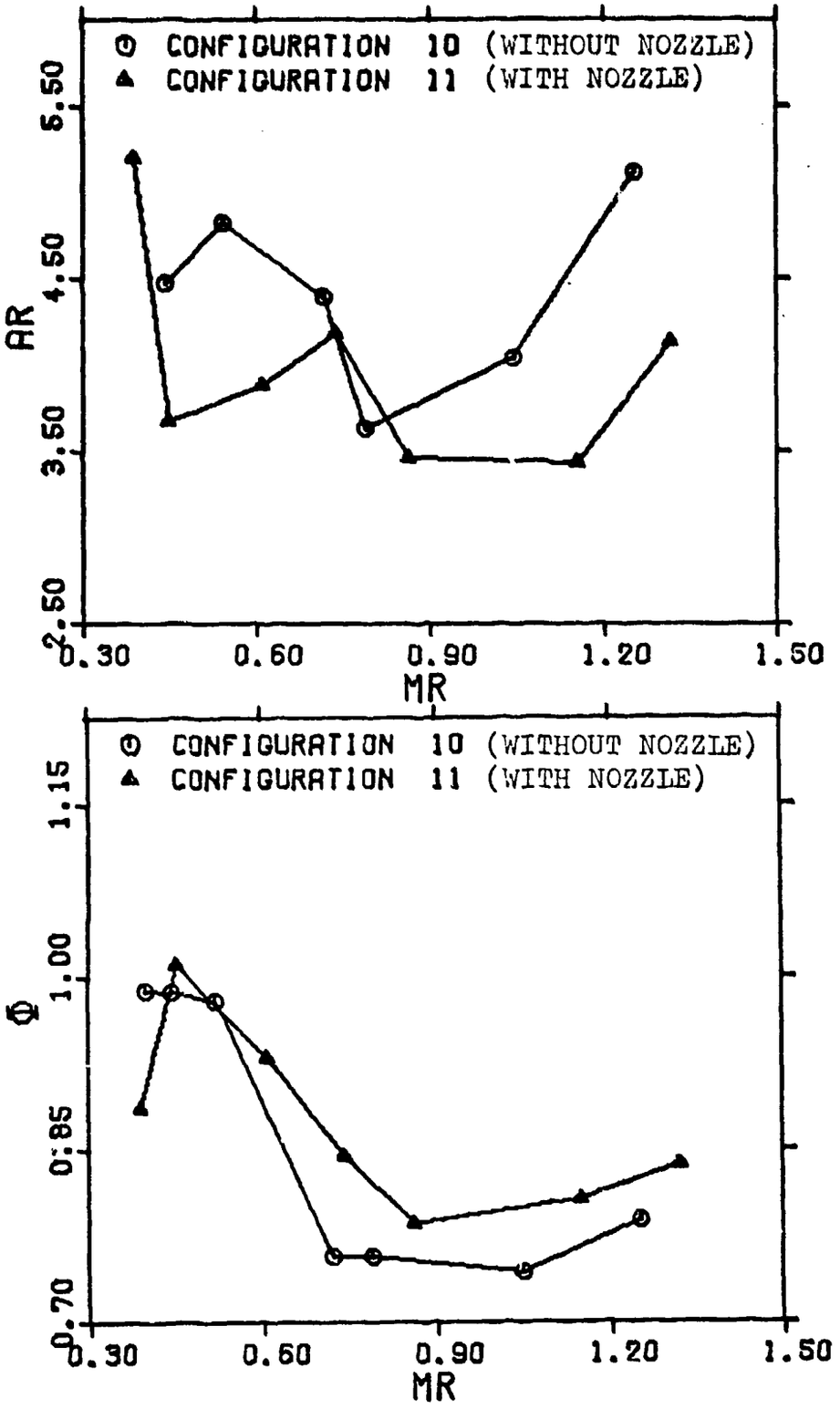

Fig. 32. Large Secondary Nozzle Effectiveness (L_m = 8.25)

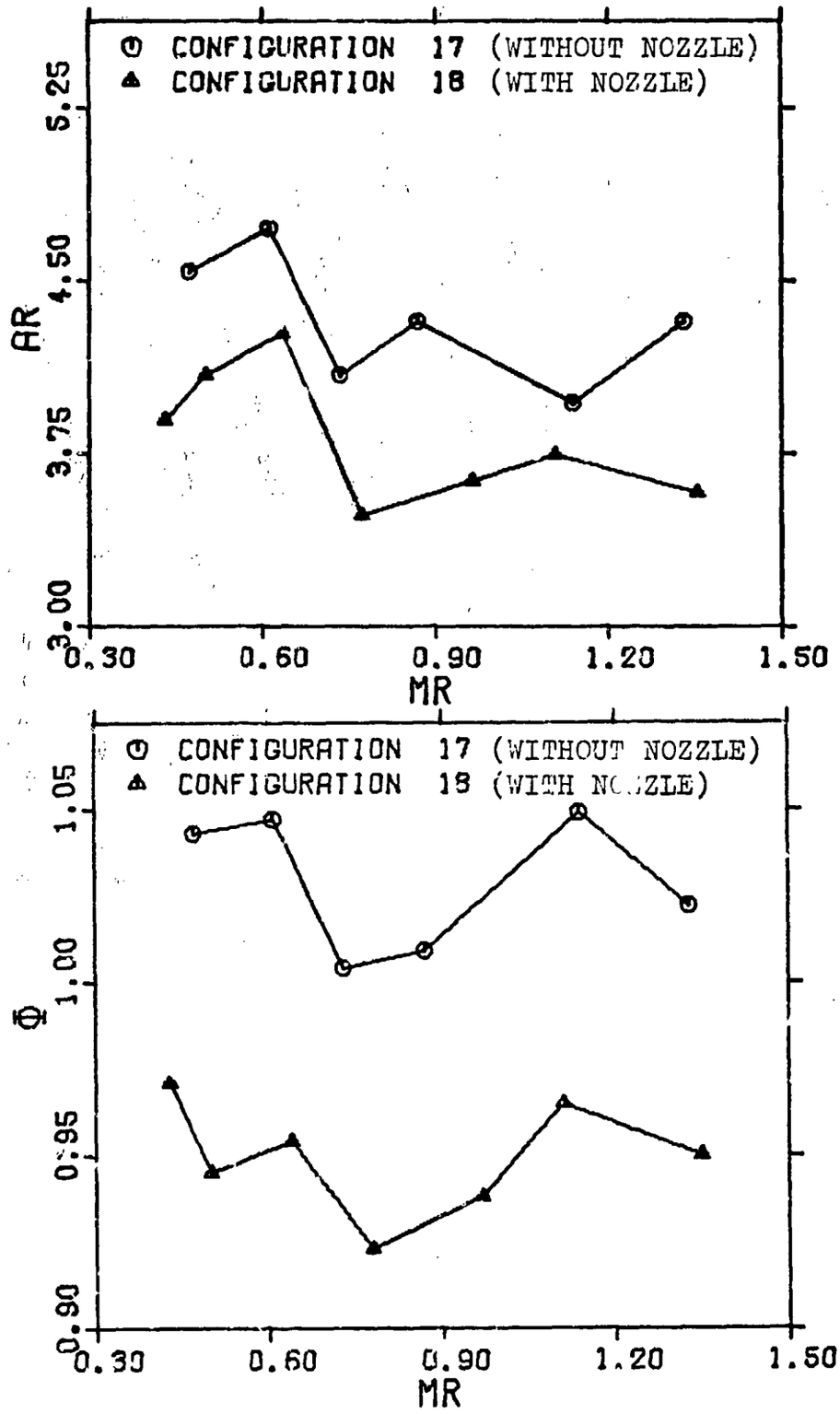

Fig. 33. Large Secondary Nozzle Effectiveness (L_m = 0.75)

Appendix B

Data Reduction

Propellant Mass Flow Rates

The oxygen mass flow rate ($\dot{m}_{O_2}$) and hydrogen mass flow rate ($\dot{m}_{H_2}$) were determined in a manner similar to previous studies (Ref 4:28-29; Ref 5:22; Ref 6:15; Ref 7:30; Ref 8:37). The mixture ratio (MR) for each run was obtained from the equation:

$$MR = \frac{\dot{m}_{O_2}}{\dot{m}_{H_2}} \qquad (1)$$

Rocket Engine Performance

Table II summarizes the equations used to calculate the theoretical and experimental engine performance. A computer program was written to calculate the adiabatic flame temperature and other theoretical rocket performance parameters. Inputs to the program were the hydrogen and oxygen mass flow rates and temperatures, chamber pressure, and necessary thermochemical data. Output included the adiabatic flame temperature (T_c), average molecular weight ($\mathcal{M}$) and ratio of specific heats (k) of the exhaust products. Theoretical values of primary nozzle exit temperature (T_e), exit velocity (V_e), thrust (F), specific impulse (I_{sp}), characteristic exhaust velocity (C^*), and thrust coefficient (C_f) were also calculated. Experimental values of I_{sp}, C^*, and C_f were obtained

Table II

Theoretical and Experimental Performance Equations

Parameter	Theoretical Equation	Experimental Equation
C^* $\left[\frac{ft}{sec}\right]$	$10^2 \times \sqrt{\frac{4.968T_c}{\mathcal{M}k}\left[\frac{k+1}{2}\right]^{(k+1)/(k-1)}}$	$\frac{P_c A_t g_c}{\dot{m}_p}$
I_{sp} $\left[\frac{lbf\text{-}sec}{lbm}\right]$	$\frac{V_e}{g_c} + \frac{C^*(P_e - P_a)}{g_c P_c}$ where $V_e = 10^3 \times \sqrt{\frac{90.04}{\mathcal{M}} \times \Delta H_{ec}}$	$\frac{F}{\dot{m}_p}$
C_f	$\frac{g_c I_{sp}}{C^*}$	$\frac{F}{P_c A_t}$
$\dot{m}_p$ $\left[\frac{lbm}{sec}\right]$	$P_c A_t \sqrt{\frac{k\, g_c}{\mathcal{R}T_c}\left[\frac{2}{k+1}\right]^{(k+1)/(k-1)}}$	References 4, 5, 6, 7, and 8

from the data reduction computer program to which experimental measurements were input.

Ejector-Afterburner Performance

Static Thrust Augmentation. Due to the nature of the test equipment and the short engine run times (approximately three seconds), it was impossible to set precise mixture ratios and chamber pressures. This presented a problem in that the static thrust augmentation ratio (ϕ) is a comparison, at the same mixture ratio and chamber pressure, of the thrust of the rocket with ejector-afterburner installed (F_{ab}) as compared to the thrust of the rocket only (F_r):

$$\phi = \frac{F_{ab}}{F_r} \qquad (2)$$

It was decided to plot a thrust performance map for the rocket in the range of mixture ratios (.3 to 1.5) and chamber pressures (80 $\pm$ 3 psia) which were acceptable. The ideal performance computer program was used to obtain the variation in thrust between P_c = 77 psia and P_c = 83 psia. This ideal variation was then applied to the experimental thrust readings for the rocket only. A third order polynomial least squares curve fit was then performed on the upper and lower limits of the rocket only thrust (Fig 34). The result of this procedure was a region of values in which the thrust of the rocket would fall at any combination of mixture ratios and chamber pressures that could be encountered.

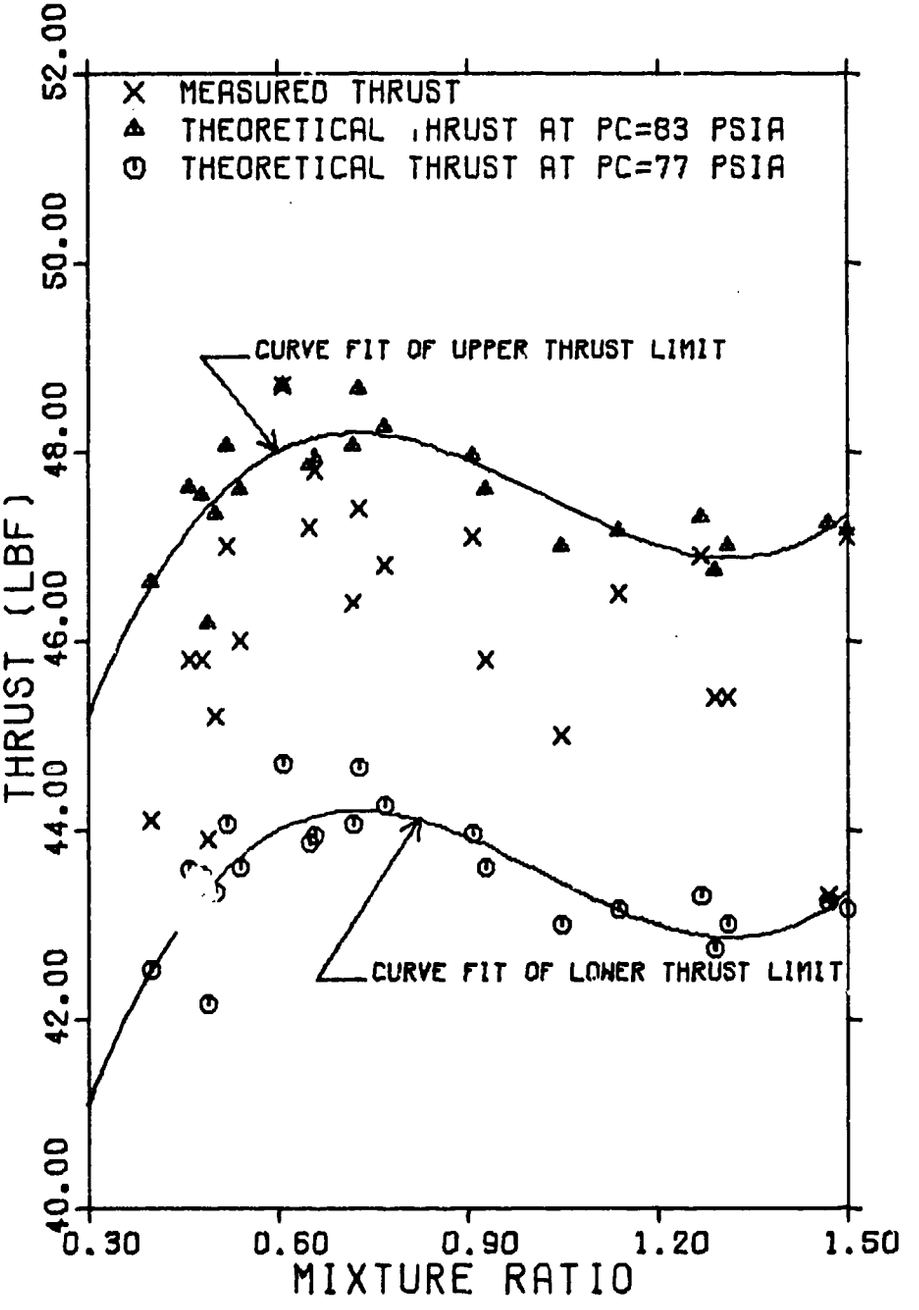

Fig. 34. Thrust Performance Map of Rocket Only

To obtain a value for ϕ, the thrust performance map was entered at the value of the mixture ratio calculated for a test firing with the ejector-afterburner installed. A linear interpolation was then performed between the curve fit for rocket thrust at P_c = 77 psia and the curve fit for rocket thrust at P_c = 83 psia, using the experimentally measured chamber pressure. This gave a unique value for F_r, which, together with the F_{ab} determined experimentally, were substituted into Eq (2) to find ϕ.

Mass Entrainment Ratio. To determine the value for mass entrainment ratio (AR), it was necessary to calculate the value for secondary mass flow rate ($\dot{m}_s$). This value was then compared with the total primary mass flow rate ($\dot{m}_{O_2} + \dot{m}_{H_2}$) to obtain the mass entrainment ratio:

$$AR = \frac{\dot{m}_s}{\dot{m}_p} \tag{3}$$

Test cell conditions were assumed to be stagnation and flow in the bellmouth inlet was assumed to be isentropic. This enabled the use of the isentropic pressure relationship:

$$P_a/P_{in} = (1 + \frac{k-1}{2} M_s^2)^{k/(k-1)} \tag{4}$$

This equation was used to obtain secondary mach number (M_s) for k = 1.4.

Another isentropic relationship was used to obtain $\dot{m}_s$:

$$\dot{m}_s/A_s = \sqrt{\frac{k}{R}} \frac{P_a}{\sqrt{T_a}} M_s (1 + \frac{k-1}{2} M_s^2)^{-(k+1)/2(k-1)} \qquad (5)$$

Substituting the appropriate values for secondary flow inlet area (A_s), k, and R, yielded:

$$\dot{m}_s = \frac{5.027 P_a M_s}{T_a (1 + .2M_s^2)^3} \qquad (6)$$

Measurement Capability Accuracy

Periodic re-calibration of pressure transducers kept experimental errors to a minimum. Considering the fact that trace deflections on the recorder could be read accurately to within ± .01 in., errors in measurements and average percentage errors in calculated experimental values were obtained. Table III summarizes the results of this work.

Of particular note is the fact that values of static thrust augmentation were accurate to within ± .02. This figure was arrived at considering the average root-mean-square error of the curves fit to the upper and lower limits of rocket-only thrust, and the errors in the chamber pressure and thrust measurement. Error due to mixture ratio variation was neglected due to the fact that, except at the lower mixture ratios studied (less than MR = .40), ideal thrust variation of the rocket only, between P_c = 77 psia and P_c = 83 psia, was constant at 4.0 lbf.

An additional precaution, taken to insure thrust measurement accuracy, was re-calibration of the thrust beam

Table III

Measurement Capability Error Summary

Parameter	Average Error (±)	Percent Error (±)
$\dot{m}_{O_2}$	.006 $\frac{lbm}{sec}$	5.8
$\dot{m}_{H_2}$	.001 $\frac{lbm}{sec}$	0.8
$\dot{m}_p$	.007 $\frac{lbm}{sec}$	3.1
$\dot{m}_s$	.018 $\frac{lbm}{sec}$	1.5
MR	.06	7.1
C^*	209. $\frac{ft}{sec}$	3.5
I_{sp}	7.1 sec	3.6
C_f	.01	0.9
AR	.240	4.6
ϕ	.02	2.0

mounted strain gages each day tests were made, or whenever a new ejector-afterburner configuration was installed. Large variations in the mass of different configurations affected the sensitivity of the strain gages to thrust measurement. This was due to the larger bearing friction which had to be overcome to produce the same strain on the thrust beam for the heavier configurations. A maximum variation of 3.4 lbf was observed for a given strain gage output in calibration curves for the basic rocket and the heavier configurations.

Appendix C

Rocket Performance

A detailed analysis of the performance of the primary gas generator is presented to complement the ejector-afterburner study. Equations used to obtain theoretical and experimental rocket parameters are outlined in Appendix B.

Primary Mass Flow Rate

Figure 35 depicts the range of primary (propellant) mass flow rate ($\dot{m}_p$) encountered experimentally on all acceptable runs, and the range of theoretical primary mass flow rates for $P_c = 80 \pm 3$ psia. Experimental values ranged from .02 to .06 lbm/sec higher than theoretically predicted, as mixture ratio increased.

Larger experimental mass flow rates are to be expected due to a number of factors. Actual density of the exhaust gases is higher than theoretical because of incomplete combustion and slight increases in molecular weight as the gases flow through the nozzle. Heat transfer in the chamber and nozzle also causes exhaust gas density to rise higher than predicted when using an adiabatic assumption (Ref 15: 68).

Figure 35 could indicate that the combustion efficiency of the engine decreased at higher mixture ratios. The more incomplete combustion would likely cause the range of theoretical-to-real mass flow rates to increase. However, higher heat transfer rates at the elevated temperatures of

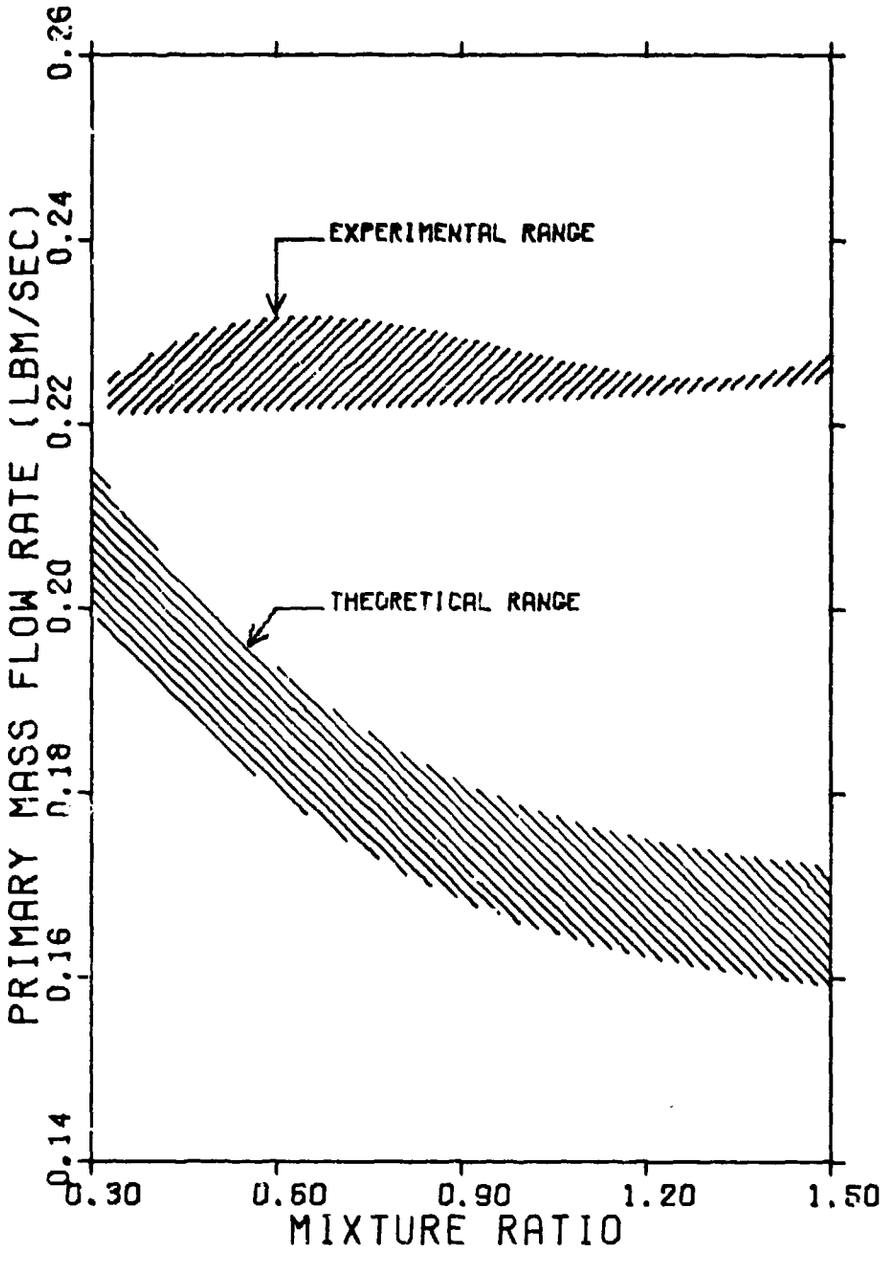

Fig. 35. Theoretical and Experimental Primary Mass Flow Rates

the higher mixture ratios may also partially account for this.

Characteristic Exhaust Velocity

Since characteristic exhaust velocity (C^*) is primarily a function of propellant combination and rocket chamber conditions, there would be no effect on it due to ejector-afterburner operation. Consequently, experimental values from all test firings were taken into account in plotting the range of actual values in Fig 36.

The shape of the experimental band of values in this mixture ratio range agrees favorably with previous experiments performed on this rocket (Ref 4:59; Ref 5:61; Ref 6:41). The magnitudes of C^* found in this study were, on the average, 3.2% to 10.1% lower than those calculated by Nidiffer, using the same nozzle (Ref 5:61). An explanation of this trend is the changing chamber and injector characteristics because of numerous test firings of the rocket between the two studies.

As in the considerations of $\dot{m}_p$, the difference between actual and theoretical performance increases with increasing mixture ratio. Again, this points to decreasing combustion efficiency, as alluded to earlier. Yarborough attributes this decrease in combustion efficiency to the decrease in hydrogen injection velocity as the mixture ratio increases, resulting in less efficient momentum exchange between the oxygen and hydrogen.

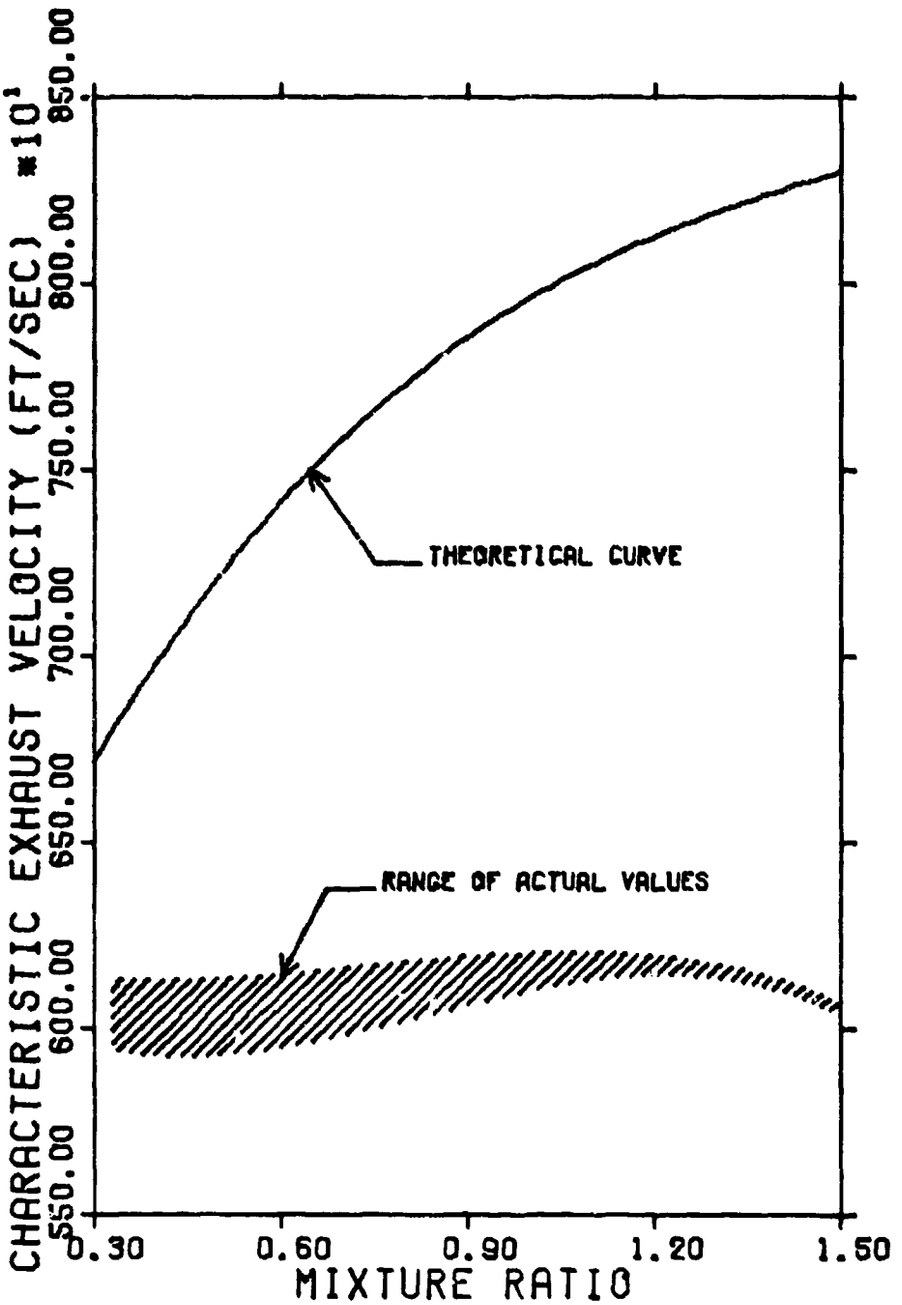

Fig. 36. Theoretical and Experimental Characteristic Exhaust Velocity

Specific Impulse

In comparing the theoretical and experimental values of specific impulse (I_{sp}) in Fig 37, only runs made with the basic rocket are plotted. Theoretical calculations were based on the engine exhausting to an atmospheric pressure of 14.5 psia, a reasonable average value over the period the tests were conducted.

Experimental I_{sp} remained relatively constant over the entire mixture ratio range. The inefficiencies that produced increased propellant mass flow rates account, to a large extent, for deviation from the theoretical curve.

Because I_{sp} is proportional to the rocket exhaust velocity, this parameter provides a good indication of the overall rocket performance. In addition to effects already mentioned in the discussion of $\dot{m}_p$, other loss factors included: friction, flow non-uniformity and maldistribution of the exhaust gases, and real gas effects.

Thrust Coefficient

Due to the fact that thrust coefficient (C_f) is strongly affected by ejector-afterburner characteristics, only experimental values for the basic rocket were included in Fig 38. Agreement between theoretical and experimental results was very good.

Since C_f is a measure of the amplification of thrust due to exhaust gas expansion in the nozzle as compared to if the chamber pressure had acted over the throat area only, one would expect good agreement between theoretical and ex-

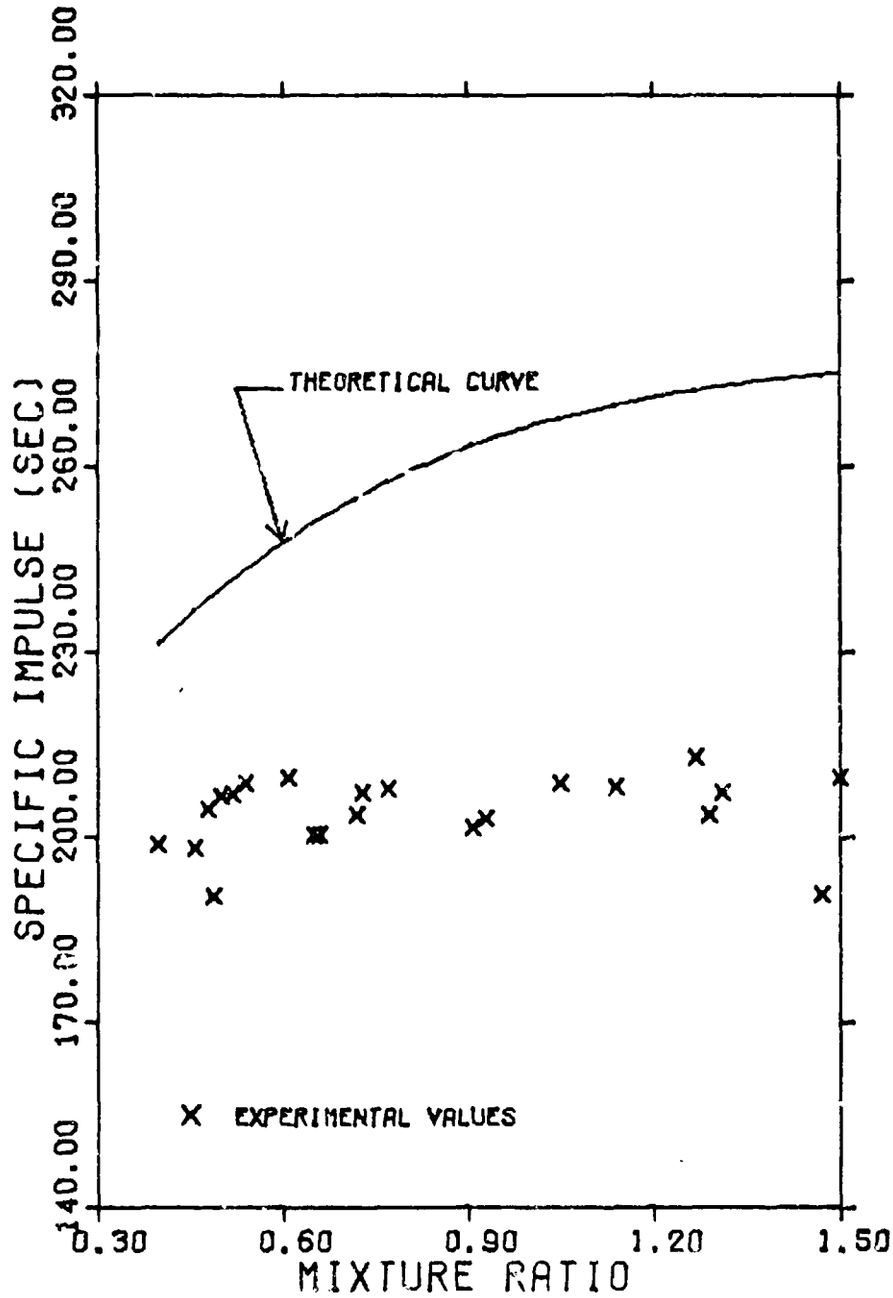

Fig. 37. Theoretical and Experimental Specific Impulse

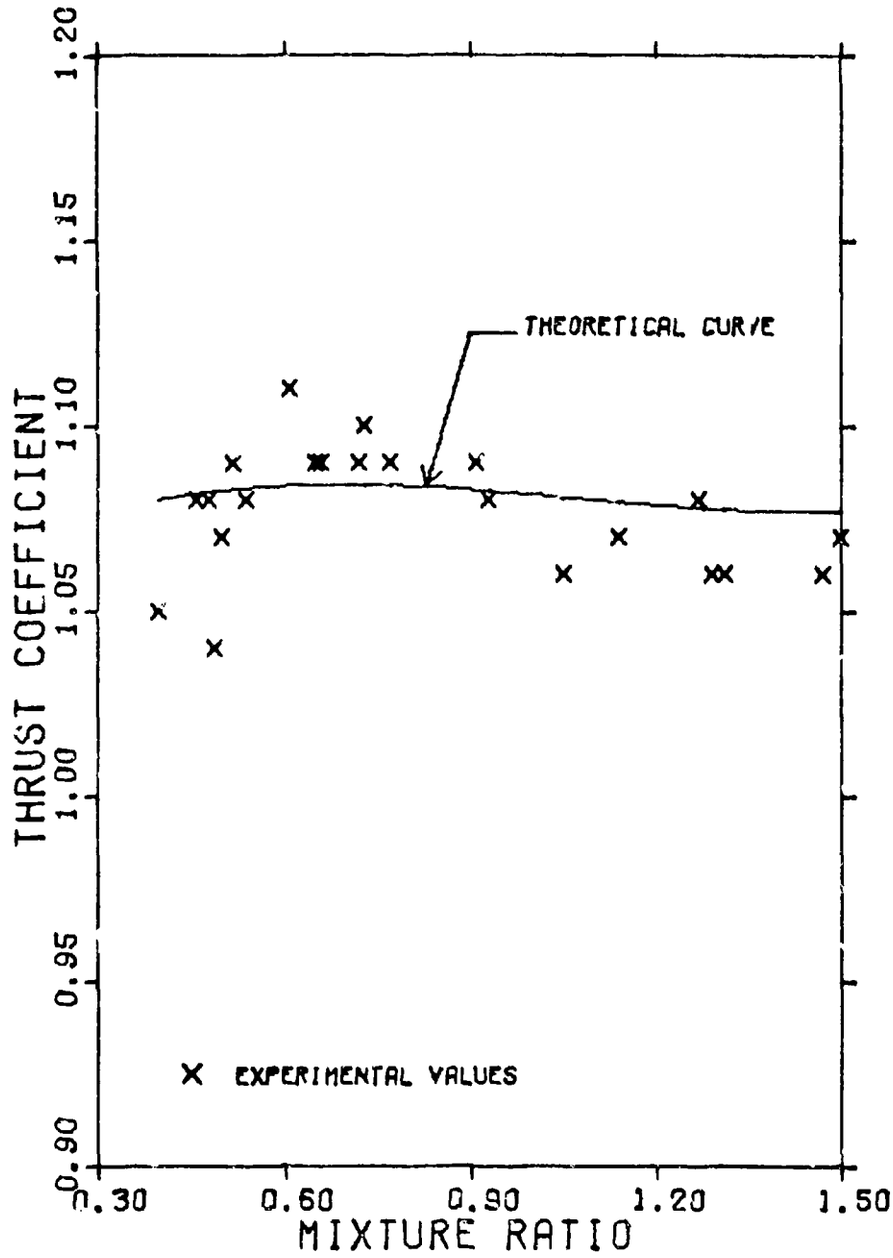

Fig. 38. Theoretical and Experimental Thrust Coefficient

perimental values in the case of a convergent nozzle (Ref 15:56). The losses associated with the divergent section of the Laval nozzle do not enter in. The experimental scatter was likely due to variance in chamber pressure and atmospheric pressure conditions.

Theoretical Temperatures

Figure 39 displays the results of the ideal performance computer program for adiabatic flame temperature and primary nozzle exit temperature. Chemical equilibrium was assumed in the chamber and theoretical exit temperature was computed using frozen flow considerations in the nozzle.

Although not measured experimentally, one can conclude that actual chamber and exit temperatures remained relatively constant as mixture ratio increased. This can be deduced from Fig 36, the plot of characteristic exhaust velocity. C^* is a strong function of the chamber temperature and C^* remains relatively constant throughout the mixture ratio range.

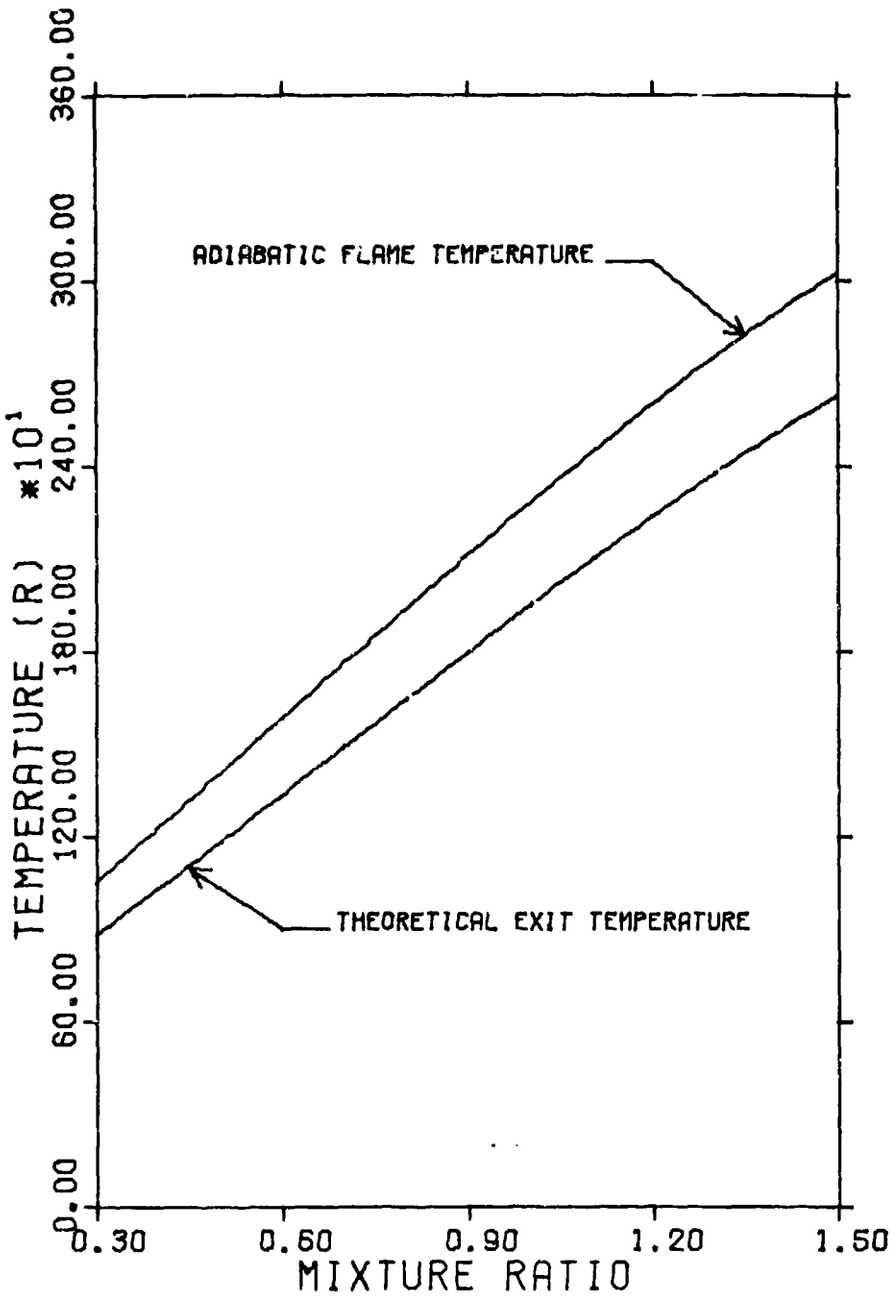

Fig. 39. Theoretical Chamber and Primary Nozzle Exit Temperatures

Appendix D

Tabulated Performance Data

Table IV

Performance Data

Run No.	Config No.	MR	F (lbf)	P_c (psia)	$\dot{m}_{O_2}$ (--lbm/sec---)	$\dot{m}_{H_2}$	$\dot{m}_s$	C^* (ft/sec)	C_f	I_{sp} (sec)	AR	Φ
7701	Rocket	.40	44.1	79.3	.063	.159	0.000	6085	1.05	199	0.00	0.00
903	Rocket	.46	45.8	80.3	.073	.158	0.000	5921	1.08	198	0.00	0.00
905	Rocket	.48	45.8	80.4	.073	.151	0.000	6109	1.08	205	0.00	0.00
7702	Rocket	.49	43.9	79.6	.076	.155	0.000	5875	1.04	190	0.00	0.00
7703	Rocket	.50	45.2	79.8	.073	.146	0.000	6210	1.07	207	0.00	0.00
813	Rocket	.52	47.0	81.4	.078	.149	0.000	6095	1.09	207	0.00	0.00
7704	Rocket	.54	46.0	80.6	.077	.143	0.000	6229	1.08	209	0.00	0.00
908	Rocket	.61	48.7	83.0	.088	.144	0.000	6075	1.11	210	0.00	0.00
909	Rocket	.65	47.2	82.0	.093	.143	0.000	5920	1.09	200	0.00	0.00
812	Rocket	.66	47.8	82.8	.095	.144	0.000	5809	1.09	200	0.00	0.00
7705	Rocket	.72	46.4	80.5	.095	.133	0.000	6018	1.09	204	0.00	0.00
7706	Rocket	.73	47.4	81.1	.097	.132	0.000	6038	1.10	207	0.00	0.00
7707	Rocket	.77	46.8	80.8	.093	.127	0.000	6110	1.09	208	0.00	0.00
7708	Rocket	.91	47.1	81.7	.111	.122	0.000	5951	1.09	202	0.00	0.00
7709	Rocket	.93	45.8	80.3	.109	.117	0.000	6060	1.08	203	0.00	0.00
7710	Rocket	1.05	45.0	80.0	.110	.105	0.000	6320	1.06	209	0.00	0.00
7711	Rocket	1.14	46.5	82.0	.119	.105	0.000	6249	1.07	208	0.00	0.00

Table IV (Continued)

Performance Data

Run No.	Config No.	MR	F (lbf)	P_c (psia)	$\dot{m}_{O_2}$ (--lbm/sec---)	$\dot{m}_{H_2}$	$\dot{m}_s$	C^* (ft/sec)	C_f	I_{sp} (sec)	AR	Φ
802	Rocket	1.27	46.9	82.4	.123	.097	0.000	6368	1.08	213	0.00	0.00
7712	Rocket	1.29	45.4	81.0	.126	.098	0.000	6180	1.06	204	0.00	0.00
7713	Rocket	1.31	45.4	80.6	.124	.095	0.000	6265	1.06	207	0.00	0.00
1310	Rocket	1.47	43.3	77.1	.135	.092	0.000	5770	1.06	191	0.00	0.00
7715	Rocket	1.50	47.1	82.9	.135	.090	0.000	6284	1.07	210	0.00	0.00
1504	1	.39	49.5	81.1	.063	.164	0.886	6074	1.15	218	3.90	1.10
1505	1	.64	50.8	82.5	.090	.141	0.790	6068	1.16	220	3.42	1.06
1506	1	.77	52.9	80.6	.097	.125	1.075	6163	1.24	238	4.83	1.14
1507	1	.91	50.9	79.7	.106	.116	0.915	6107	1.21	229	4.12	1.11
1508	1	1.10	49.9	81.7	.117	.106	0.854	6223	1.15	223	3.82	1.08
1509	1	1.36	49.8	81.2	.129	.095	0.888	6154	1.16	222	3.95	1.09
1601	2	.38	48.7	81.8	.064	.168	1.262	5993	1.12	210	5.43	1.07
1603	2	.42	47.5	81.2	.066	.155	1.240	6248	1.11	215	5.61	1.04
1604	2	.65	49.1	81.8	.092	.140	1.449	6003	1.14	212	6.25	1.04
1606	2	.77	46.0	79.8	.097	.126	1.420	6072	1.09	206	6.35	1.00
1607	2	1.03	46.5	82.7	.118	.114	1.353	6055	1.06	200	5.83	0.98
1611	2	1.27	45.5	82.7	.130	.102	1.420	6060	1.04	196	6.11	0.97

Table IV (Continued)

Performance Data

Run No.	Config No.	MR	F (lbf)	P_c (psia)	$\dot{m}_{O_2}$ (--lbm/sec---)	$\dot{m}_{H_2}$	$\dot{m}_s$	C^* (ft/sec)	C_f	I_{sp} (sec)	AR	Φ
2003	3	.47	46.7	79.4	.073	.157	1.314	5860	1.11	203	5.70	1.04
2004	3	.53	41.5	78.5	.077	.145	1.273	6013	1.00	187	5.73	0.93
2006	3	.60	39.0	79.9	.085	.142	1.259	5991	0.92	172	5.55	0.85
2005	3	.63	40.5	77.2	.085	.135	1.310	5987	0.99	185	5.97	0.92
2007	3	.66	42.5	79.5	.089	.134	1.500	6063	1.01	191	6.72	0.93
2008	3	.78	40.8	79.7	.100	.127	1.455	5987	0.97	180	6.42	0.89
2009	3	1.01	39.7	80.2	.114	.113	1.428	6021	0.94	175	6.30	0.87
2010	3	1.09	40.7	80.6	.113	.104	1.382	6312	0.95	187	6.36	0.89
2202	4	.43	39.4	79.6	.070	.164	1.342	5790	0.94	168	5.73	0.88
2203	4	.44	38.9	79.3	.068	.155	1.306	6048	0.93	174	5.85	0.87
2204	4	.51	40.3	78.7	.073	.143	1.316	6214	0.97	187	6.10	0.90
2205	4	.63	41.6	78.7	.084	.133	1.466	6187	1.00	192	6.77	0.92
2206	4	.71	40.3	80.7	.090	.126	1.421	6362	0.94	187	6.58	0.86
2207	4	.88	39.2	80.1	.101	.114	1.436	6355	0.92	183	6.69	0.85
2208	4	1.25	39.2	81.2	.124	.099	1.375	6176	0.91	175	6.14	0.86
2302	5	.35	48.4	78.8	.054	.156	0.631	6369	1.16	230	2.99	1.12
2304	5	.51	50.2	81.7	.077	.149	0.680	6162	1.16	222	3.01	1.08

Table IV (Continued)

Performance Data

Run No.	Config No.	MR	F (lbf)	P_c (psia)	$\dot{m}_{O_2}$ (--lbm/sec---)	$\dot{m}_{H_2}$	$\dot{m}_s$	C^* (ft/sec)	C_f	I_{sp} (sec)	AR	Φ
2305	5	.64	46.9	81.2	.087	.138	0.746	6145	1.09	208	3.32	1.00
2306	5	.75	46.3	81.3	.098	.131	0.680	6046	1.08	202	2.97	0.98
2307	5	.89	46.6	81.2	.107	.120	0.575	6083	1.08	205	2.53	1.00
2308	5	1.03	46.5	82.5	.116	.112	0.501	6150	1.06	204	2.19	0.99
2309	5	1.26	46.2	81.2	.124	.098	0.631	6220	1.08	208	2.84	1.01
2401	6	.44	50.0	81.0	.073	.166	0.904	5771	1.17	209	3.78	1.10
2402	6	.52	49.4	80.1	.077	.148	0.881	6075	1.17	220	3.93	1.08
2403	6	.63	50.2	81.1	.086	.137	1.060	6191	1.17	225	4.75	1.07
2404	6	.77	47.2	81.2	.099	.128	0.999	6110	1.10	209	4.41	1.01
2405	6	.83	46.9	81.0	.100	.120	0.880	6283	1.09	214	4.01	1.00
2406	6	.99	45.9	81.9	.111	.112	0.847	6249	1.06	206	3.80	0.98
2407	6	1.3[illegible]	47.0	82.6	.129	.098	1.068	6187	1.08	207	4.70	1.01
2702	7	.50	49.1	80.9	.074	.148	0.904	6204	1.15	221	4.07	1.07
2710	7	.51	48.6	81.4	.078	.153	0.840	5995	1.13	210	3.64	1.05
2703	7	.71	47.0	82.1	.098	.138	1.[illegible]5	5932	1.08	200	4.86	0.99
2704	7	[illegible]	43.5	82.6	.111	.126	1.022	5930	1.00	184	4.31	0.91
2705	7	.94	41.7	82.6	.112	.118	0.942	6109	0.95	181	4.09	0.88

Table IV (Continued)

Performance Data

Run No.	Config No.	MR	F (lbf)	P_c (psia)	$\dot{m}_{O_2}$ (--lbm/sec---)	$\dot{m}_{H_2}$	$\dot{m}_s$	C^* (ft/sec)	C_f	I_{sp} (sec)	AR	Φ
2707	7	1.18	43.5	82.5	.124	.105	1.068	6154	1.00	191	4.68	0.93
2709	7	1.43	40.3	81.1	.134	.093	1.063	6090	0.94	178	4.69	0.88
2902	8	.51	50.8	80.2	.075	.148	0.843	6115	1.20	228	3.78	1.11
2904	8	.74	50.7	82.4	.096	.131	1.156	6180	1.16	223	5.09	1.06
2905	8	.78	45.2	80.5	.097	.125	1.100	6173	1.06	204	4.96	0.97
2906	8	.92	43.4	81.5	.108	.117	1.001	6167	1.01	193	4.45	0.93
2907	8	1.06	42.4	82.1	.114	.107	0.946	6332	0.98	192	4.29	0.91
2908	8	1.33	44.7	80.5	.125	.094	1.078	6240	1.05	204	4.91	0.99
3002	9	.45	47.6	82.9	.075	.166	0.931	5856	1.09	198	3.87	1.01
3003	9	.49	45.0	81.0	.076	.156	0.947	5943	1.05	194	4.09	0.98
3004	9	.63	44.6	81.1	.088	.140	0.931	6050	1.04	196	4.08	0.95
3005	9	.74	41.8	81.1	.096	.128	0.870	6166	0.97	187	3.86	0.89
3007	9	.80	39.6	78.3	.098	.123	0.598	6015	0.96	179	2.70	0.88
3008	9	.99	42.2	80.9	.109	.111	0.784	6242	0.99	191	3.55	0.91
3009	9	1.24	41.9	79.8	.122	.098	0.842	6174	0.99	191	3.83	0.94
3402	10	.40	42.8	78.2	.064	.161	1.019	5924	1.03	191	4.53	0.99
3403	10	.44	43.6	78.8	.067	.151	0.975	6148	1.05	200	4.47	0.99

Table IV (Continued)

Performance Data

Run No.	Config No.	MR	F (lbf)	P_c (psia)	$\dot{m}_{O_2}$ (--lbm/sec---)	$\dot{m}_{H_2}$	$\dot{m}_s$	C^* (ft/sec)	C_f	I_{sp} (sec)	AR	Φ
3404	10	.54	43.6	78.4	.074	.136	1.013	6353	1.05	208	4.83	0.98
3405	10	.72	34.7	79.5	.092	.128	0.964	6167	0.83	158	4.39	0.76
3406	10	.79	34.7	79.5	.099	.126	0.816	6021	0.83	154	3.63	0.76
3407	10	1.05	34.6	81.6	.115	.110	0.908	6178	0.80	154	4.04	0.74
3408	10	1.25	35.5	80.1	.123	.098	1.132	6154	0.84	160	5.11	0.79
3601	11	.39	38.9	79.2	.065	.167	1.208	5804	0.93	167	5.20	0.89
3602	11	.45	44.2	78.0	.066	.147	0.781	6240	1.07	208	3.67	1.01
3603	11	.61	43.3	80.9	.084	.137	0.859	6228	1.01	196	3.88	0.93
3604	11	.74	39.1	80.2	.094	.128	0.929	6140	0.92	176	4.18	0.84
3605	11	.86	36.6	80.8	.101	.116	0.751	6339	0.86	169	3.46	0.79
3606	11	1.15	37.9	82.8	.124	.107	0.791	6115	0.87	164	3.43	0.81
3607	11	1.32	37.0	79.1	.126	.096	0.917	6058	0.88	167	4.13	0.84
4101	12	.41	47.7	82.1	.068	.165	0.836	6003	1.10	205	3.59	1.04
4102	12	.45	44.5	80.7	.068	.150	0.694	6316	1.04	205	3.19	0.98
4103	12	.59	45.0	82.5	.084	.142	0.759	6201	1.03	199	3.35	0.95
4104	12	.75	43.4	82.6	.100	.133	0.800	6047	0.99	187	3.44	0.91
4105	12	.89	41.2	81.9	.108	.121	0.712	6087	0.95	180	3.11	0.87

Table IV (Continued)

Performance Data

Run No.	Config No.	MR	F (lbf)	P_c (psia)	$\dot{m}_{O_2}$ (--lbm/sec---)	$\dot{m}_{H_2}$	$\dot{m}_s$	C^* (ft/sec)	C_f	I_{sp} (sec)	AR	Φ
4106	12	1.03	42.6	81.1	.115	.111	0.753	6157	0.98	189	3.33	0.91
4107	12	1.28	41.0	80.0	.125	.098	0.787	6123	0.97	185	3.54	0.91
4303	13	.37	46.7	78.0	.061	.167	0.762	5819	1.13	205	3.34	1.09
4304	13	.48	48.0	79.2	.071	.149	0.785	6106	1.15	218	3.56	1.07
4305	13	.59	48.1	80.5	.082	.139	0.785	6186	1.13	217	3.55	1.04
4306	13	.74	47.3	80.1	.094	.127	0.613	6193	1.12	215	2.79	1.02
4307	13	.91	47.3	81.1	.109	.120	0.546	6031	1.10	207	2.39	1.02
4308	13	1.12	47.9	81.7	.120	.107	0.546	6101	1.11	210	2.40	1.03
4309	13	1.29	46.5	80.5	.126	.098	0.545	6099	1.09	207	2.43	1.03
4310	14	.44	51.7	81.0	.070	.162	1.178	5937	1.21	223	5.08	1.13
4311	14	.51	51.0	80.9	.079	.154	1.178	5920	1.19	219	5.07	1.11
4312	14	.60	49.8	79.7	.085	.141	1.187	6009	1.18	221	5.26	1.09
4313	14	.79	47.3	81.7	.101	.128	0.796	6046	1.09	206	3.46	1.00
4314	14	.90	47.3	81.7	.111	.124	0.784	5912	1.09	201	3.34	1.01
4315	14	1.09	47.3	81.7	.119	.109	0.807	6083	1.09	207	3.53	1.02
4316	14	1.33	46.6	82.5	.129	.097	0.784	6218	1.07	206	3.47	1.00
4408	15	.45	54.4	80.6	.072	.161	1.271	5875	1.28	233	5.44	1.20

Table IV (Continued)

Performance Data

Run No.	Config No.	MR	F (lbf)	P_c (psia)	$\dot{m}_{O_2}$ (--lbm/sec---)	$\dot{m}_{H_2}$	$\dot{m}_s$	C^* (ft/sec)	C_f	I_{sp} (sec)	AR	Φ
4407	15	.46	54.5	79.7	.068	.147	1.280	6314	1.29	254	5.95	1.21
4406	15	.62	52.7	77.7	.083	.134	1.210	6075	1.28	242	5.56	1.[illegible]
4405	15	.77	47.0	78.2	.097	.126	0.848	5948	1.14	210	3.79	1.05
4404	15	.89	49.3	81.3	.109	.122	0.801	6003	1.15	214	3.47	1.05
4403	15	1.14	52.1	82.7	.124	.109	0.853	6038	1.19	223	3.66	1.11
4402	15	1.31	51.8	82.0	.127	.098	0.784	6207	1.19	230	3.48	1.12
5001	16	.45	47.5	82.4	.074	.164	0.869	5885	1.09	199	3.65	1.02
5002	16	.52	46.3	80.5	.076	.148	0.869	6127	1.09	207	3.89	1.01
5003	16	.64	45.7	80.4	.087	.136	0.791	6123	1.07	205	3.54	0.99
5004	16	.75	45.7	80.1	.097	.130	0.608	6019	1.08	202	2.69	0.99
5005	16	.87	46.7	82.4	.110	.126	0.686	5937	1.07	198	2.91	0.98
5006	16	1.11	45.7	81.8	.119	.107	0.584	6154	1.06	203	2.58	0.99
5007	16	1.41	44.2	79.6	.131	.093	0.633	6052	1.05	198	2.83	0.99
5103	17	.47	48.1	81.3	.073	.154	1.033	6079	1.12	211	4.54	1.04
5104	17	.61	48.8	80.9	.086	.141	1.074	6058	1.14	215	4.73	1.05
5105	17	.73	46.8	80.6	.095	.129	0.915	6124	1.10	209	4.09	1.00
5106	17	.87	47.2	81.2	.101	.117	0.942	6327	1.10	216	4.32	1.01

Table IV (Continued)

Run No.	Config No.	MR	F (lbf)	Performance Data P_c (psia)	$\dot{m}_{O_2}$ (--lbm/sec---)	$\dot{m}_{H_2}$	$\dot{m}_s$	C^* (ft/sec)	C_f	I_{sp} (sec)	AR	Φ
5107	17	1.14	49.4	82.9	.121	.106	0.903	6189	1.13	217	3.97	1.05
5108	17	1.33	47.0	81.7	.127	.095	0.958	6263	1.09	212	4.32	1.02
5205	18	.43	42.7	78.7	.070	.161	0.897	5809	1.03	185	3.89	0.97
5203	18	.50	42.6	79.4	.075	.150	0.918	6008	1.01	190	4.09	0.95
5204	18	.64	44.1	80.2	.086	.135	0.940	6189	1.04	200	4.26	0.95
5205	18	.78	42.8	80.3	.097	.125	0.773	6154	1.01	193	3.48	0.92
5206	18	.97	43.2	80.5	.108	.111	0.795	6252	1.01	197	3.63	0.94
5207	18	1.11	44.0	80.5	.115	.103	0.817	6273	1.03	202	3.74	0.97
5208	18	1.35	42.7	80.1	.126	.093	0.783	6227	1.01	195	3.58	0.95
5602	19	.33	49.0	77.9	.055	.164	0.921	6065	1.19	224	4.21	1.16
5603	19	.45	48.6	79.6	.070	.155	0.873	6009	1.15	216	3.88	1.09
5607	19	.64	50.1	79.1	.090	.140	1.007	5848	1.20	218	4.37	1.10
5608	19	.78	47.9	78.8	.098	.126	1.007	5977	1.15	214	4.49	1.06
5609	19	.93	51.8	82.0	.111	.120	0.875	6047	1.19	224	3.79	1.10
5610	19	1.22	52.1	82.3	.128	.105	0.875	6029	1.20	224	3.77	1.12
5708	20	.47	47.0	81.4	.072	.153	1.113	6159	1.09	209	4.98	1.02
5707	20	.63	46.6	81.4	.089	.142	1.089	5997	1.08	202	4.72	0.99

Table IV (Continued)

Performance Data

Run No.	Config No.	MR	F (lbf)	P_c (psia)	$\dot{m}_{O_2}$ (--lbm/sec---)	$\dot{m}_{H_2}$	$\dot{m}_s$	C^* (ft/sec)	C_f	I_{sp} (sec)	AR	Φ
5706	20	.72	41.9	78.5	.092	.128	1.238	6092	1.01	191	5.65	0.93
5705	20	.78	42.0	79.4	.097	.125	1.189	6092	1.00	189	5.36	0.92
5704	20	.92	41.1	79.0	.110	.120	1.091	5855	0.98	179	4.75	0.91
5702	20	1.10	40.8	79.0	.117	.106	1.024	6022	0.98	183	4.59	0.92
5701	20	1.38	46.6	80.2	.129	.093	1.423	6146	1.10	210	6.41	1.03
5901	21	.47	40.9	78.4	.075	.159	1.301	5689	0.99	174	5.55	0.93
5902	21	.52	43.2	81.2	.077	.149	1.263	6112	1.01	191	5.58	0.93
5903	21	.73	45.7	82.7	.098	.134	1.398	6080	1.04	197	6.04	0.95
5904	21	.81	45.3	82.7	.104	.128	1.378	6083	1.04	196	5.95	0.95
5905	21	1.04	41.2	82.8	.117	.113	1.158	6131	0.94	179	5.04	0.87
5906	21	1.16	42.6	82.4	.121	.104	1.139	6241	0.98	190	5.07	0.91
5907	21	1.43	44.1	80.7	.131	.091	1.497	6174	1.03	198	6.73	0.97
6203	22	.46	39.0	77.8	.070	.152	1.252	5963	0.95	176	5.64	0.89
6204	22	.57	43.0	82.6	.086	.150	1.252	5960	0.98	182	5.31	0.90
6205	22	.66	47.1	82.6	.093	.140	1.482	6051	1.08	203	6.38	0.98
6206	22	.79	43.3	81.7	.103	.129	1.467	6004	1.00	187	6.33	0.92
6207	22	.92	43.3	82.0	.112	.122	1.388	5980	1.00	186	5.95	0.92

Table IV (Continued)

Performance Data

Run No.	Config No.	MR	F (lbf)	P_c (psia)	$\dot{m}_{O_2}$ (--lbm/sec---)	$\dot{m}_{H_2}$	$\dot{m}_s$	C^* (ft/sec)	C_f	I_{sp} (sec)	AR	Φ
6208	22	1.07	41.3	81.4	.118	.111	1.200	6045	0.96	180	5.24	0.89
6209	22	1.22	45.1	80.4	.121	.099	1.592	6206	1.06	205	7.22	1.00
6210	22	1.25	44.0	81.7	.123	.098	1.569	6278	1.02	199	7.09	0.96
6407	23	.42	41.8	78.7	.066	.158	1.041	5972	1.00	186	4.64	0.95
6406	23	.49	42.0	78.3	.071	.145	1.041	6171	1.01	195	4.82	0.95
6405	23	.65	40.6	81.0	.089	.137	1.148	6092	0.95	179	5.07	0.87
6404	23	.74	38.9	78.8	.092	.124	1.094	6226	0.93	181	5.08	0.86
6403	23	.91	38.7	79.9	.110	.121	1.079	5865	0.92	167	4.66	0.85
6402	23	1.04	39.1	80.5	.112	.108	1.019	6210	0.92	177	4.62	0.85
6401	23	1.30	39.1	81.0	.129	.099	1.131	6043	0.91	171	4.96	0.86
6609	24	.45	45.6	79.8	.067	.151	1.133	6216	1.08	209	5.18	1.02
6608	24	.48	44.9	78.2	.069	.144	1.183	6242	1.08	211	5.55	1.01
6605	24	.75	33.6	79.1	.095	.127	1.218	6084	0.80	152	5.50	0.73
6606	24	.77	32.5	81.4	.098	.128	1.310	6147	0.75	144	5.81	0.69
6604	24	.88	31.0	78.0	.104	.118	1.310	5990	0.75	140	5.91	0.69
6603	24	1.08	31.3	82.3	.116	.108	1.046	6249	0.72	140	4.66	0.69
6602	24	1.34	33.2	82.9	.130	.097	1.431	6218	0.76	146	6.30	0.71

Table IV (Continued)

Performance Data

Run No.	Config No.	MR	F (lbf)	P_c (psia)	$\dot{m}_{O_2}$ (--lbm/sec---)	$\dot{m}_{H_2}$	$\dot{m}_s$	C^* (ft/sec)	C_f	I_{sp} (sec)	AR	Φ
6901	25	.44	42.5	81.8	.071	.160	1.175	6030	0.98	184	5.09	0.92
6902	25	.59	42.9	81.6	.087	.148	1.141	5907	0.99	183	4.85	0.91
6903	25	.71	45.4	81.8	.097	.137	1.245	5938	1.05	194	5.31	0.96
6905	25	.73	44.6	81.6	.098	.133	1.258	6013	1.03	193	5.45	0.94
6907	25	.90	41.2	81.9	.109	.121	1.178	6056	0.95	179	5.12	0.87
6908	25	1.15	42.1	82.1	.122	.107	1.074	6100	0.97	184	4.69	0.91
6909	25	1.39	43.3	81.2	.133	.096	1.429	6036	1.01	189	6.24	0.95
7009	26	.44	47.0	80.5	.066	.150	0.920	6354	1.10	218	4.27	1.04
7008	26	.48	45.8	78.7	.073	.154	0.931	5902	1.10	202	4.10	1.03
7010	26	.61	43.0	81.4	.085	.140	1.144	6163	1.00	191	5.09	0.92
7007	26	.88	40.8	80.0	.109	.123	1.017	5861	0.96	176	4.38	0.89
7006	26	.89	39.6	79.9	.104	.117	0.931	6138	0.94	179	4.20	0.86
7005	26	1.10	40.1	81.4	.117	.106	0.921	6223	0.93	180	4.14	0.87
7004	26	1.23	41.3	81.1	.122	.099	0.987	6225	0.96	186	4.45	0.90
7802	15	.45	54.0	78.7	.069	.154	1.118	5984	1.30	241	5.00	1.22
7803	15	.47	54.1	79.3	.072	.153	1.133	6015	1.29	241	5.05	1.21
7804	15	.53	53.6	80.9	.077	.145	1.156	6196	1.25	241	5.21	1.16

Table IV (Continued)

Performance Data

Run No.	Config No.	MR	F (lbf)	P_c (psia)	$\dot{m}_{O_2}$ (--lbm/sec---)	$\dot{m}_{H_2}$	$\dot{m}_s$	C^* (ft/sec)	C_f	I_{sp} (sec)	AR	Φ
7805	15	.62	54.6	80.9	.088	.141	1.132	6003	1.28	238	4.94	1.17
7806	15	.66	52.0	79.9	.088	.134	1.009	6117	1.23	234	4.54	1.13
7807	15	.77	49.4	79.3	.098	.126	0.780	6020	1.18	220	3.48	1.08
7808	15	.84	50.3	81.8	.106	.126	0.780	5975	1.16	216	3.35	1.06
7809	15	.93	50.9	82.4	.110	.118	0.792	6127	1.17	222	3.46	1.07
7810	15	.96	50.6	82.2	.111	.115	0.780	6193	1.16	224	3.46	1.07
7811	15	1.05	51.0	81.8	.115	.109	0.825	6224	1.18	228	3.69	1.09
7812	15	1.11	51.0	82.1	.118	.106	0.824	6241	1.17	228	3.68	1.09
7813	15	1.27	49.6	81.5	.125	.098	0.791	6230	1.15	223	3.55	1.08
7814	15	1.30	49.6	81.8	.129	.099	0.780	6121	1.15	218	3.43	1.08
7815	15	1.49	48.6	81.2	.137	.092	0.718	6009	1.13	211	3.12	1.06

Vita

Carl Herman Steiling, Jr. was born 4 February 1946 in St. Louis, Missouri; son of Carl H. Steiling, Sr. and Lottie B. Steiling. After graduation from Christian Brothers High School, he received an appointment to the United States Air Force Academy. He graduated in 1968 with a Bachelor of Science in Engineering Science, and was commissioned a Second Lieutenant in the United States Air Force.

After completion of pilot training in 1969, he was assigned to Charleston Air Force Base, South Carolina, as a C-141 pilot. He spent one year as a Forward Air Controller, flying the O-2 aircraft, at Tan Son Nhut Air Base, Republic of Vietnam, and Nakhon Phanom Royal Thai Air Force Base, Thailand, prior to being assigned to the Air Force Institute of Technology in January 1974.

Permanent address: St. Louis, Missouri 63109

This thesis was typed by the author.